The physics of manganites: Structure and transport

Myron B. Salamon

Department of Physics and Materials Research Laboratory, University of Illinois at Urbana-Champaign, Urbana, Illinois 61801

Marcelo Jaime

MST-NHMFL, MS E536, Los Alamos National Laboratory, Los Alamos, New Mexico 87545

(Published 29 August 2001)

The fundamental physical properties of doped $LaMnO_3$, generically termed "manganites," and much of the underlying physics, were known more than 40 years ago. This article first reviews progress made at that time, the concept of double exchange in particular, and points out the missing elements that have led to a massive resurgence of interest in these and related materials. More recent research is then described, treating first the ground states that emerge as divalent atoms are substituted for trivalent La. A wide range of ground states appear, including ferromagnetic metals, orbital- and charge-ordered antiferromagnets, and more complex stripe and spin-glass states. Because of the interest in so-called colossal magnetoresistance that occurs in the ferromagnetic/metallic composition range, a section is devoted to reviewing the atypical properties of that phase. Next the high-temperature phase is examined, in particular, evidence for the formation of self-trapped small polarons and the importance of Jahn-Teller coupling in this process. The transitions between the high-temperature polaronic phase and the ferromagnetic and charge-ordered states are treated in a fourth section. In each section, the authors stress the competition among charge, spin, and lattice coupling and review the current state of theoretical understanding. They conclude with some comments on the impact that research on these materials has on our understanding of doped oxides and other strongly correlated electronic materials.

CONTENTS

I. INTRODUCTION

Colossal magnetoresistance manganites (i.e., based on $LaMnO_3$ and relatives) are known for the unusually large effect an external magnetic field has on their ability to transport electricity and heat. While many of these effects were known more than 50 years ago (van Santen and Jonker, 1950), an appreciation of the size of these effects is a more recent development (Jin, Tiefel *et al.*, 1994). A sensitivity of this magnitude is not observed in any bulk metallic system where, mostly at low temperatures, magnetoresistance arises from a field dependent electronic mean free path. This effect is measurable only in those metals that have a large mean free path in zero field, i.e., very clean systems, where the magnetic field reduces the mean free path by inducing the electrons to move in orbits. Even then, the resistivity change is usually limited to a few percent in practical magnetic fields. Giant-magnetoresistance multilayer metallic films show a relatively large sensitivity to magnetic fields. The mechanism in these films is largely due to what is known as the spin-valve effect between spin polarized metals. If an electron in a regular metal is forced to move across a spin-polarized metallic layer (or between spin-polarized layers) it will suffer spin-dependent scattering. If the electron was initially polarized parallel to that of the layer the scattering rate is relatively low; if originally polarized antiparallel to that of the layer the scattering is high. (The reverse is also possible.) The effect of an ex-

ternal field is to increase the ratio of the former events, reducing the latter, by aligning the polarization of the magnetic layer along the direction of the external field. This effect is a few tens of percent, and has the very important advantage of not being limited to low temperatures. Spin-valve devices have been used in the magnetic storage industry for several years now, in the form of magnetoresistive read heads. While the physical mechanism that produces the magnetoresistance is well understood, the technological challenges involved in the production of small devices of high sensitivity are the bottleneck of an industry ever hungry for smaller-faster-better sensors.

Magnetic systems of great potential are those with a limited ability to transport electricity in zero field, resulting from competing dissimilar ground states. In these systems, magnetic fields produce truly dramatic effects by inducing phase transitions or increasing the temperature of already existing phase transitions. Examples of this behavior are found in EuO, pyrochlores, and manganites. Also small gap semiconductors like $Ce_3Bi_4Pt_3$ and YbB_{12} can be considered in this category, although a detailed discussion of their ground state is beyond the aim of this review. The limitation of semiconductors in general is that room temperature is a large energy scale. If the gap is large enough to be in the intrinsic conduction limit at room temperature, the magnetic fields required to see changes are unattainable. If the gap is small and magnetic fields within reach, then the effects are limited to very low temperatures (Jaime *et al.*, 2000). In a sense manganites are ideal compounds for magnetic sensor devices, since the two competing ground states are metallic and semiconducting, respectively, and because the energy scale of the phenomenon produces the most interesting effects, i.e., the metal-insulator transition and hence the maximum sensitivity to external fields, at temperatures close to room temperature (Jin, McCormack *et al.*, 1994). See Fig. 1 for recent data on single crystals. It is exactly these features that inspired a tremendous effort from experimentalists and theoreticians to reexamine these materials and to understand the mechanisms involved. Despite this effort neither practical applications nor a satisfactory understanding of the physics of manganites has yet emerged. In the meantime, our perception of the manganites has changed radically. They have been redefined from what seemed a straightforward application in the magnetic-storage industry to a challenge of colossal dimensions from the condensed-matter physics point of view.

Soon after the rediscovery of these materials, theoreticians pointed out that the theoretical framework used in the past to explain their behavior qualitatively does not survive when confronted with a quantitative analysis (Millis *et al.*, 1995). With an understanding of the complexity of the problem came the realization of the uniqueness of manganites as a test field for condensed-matter physics theories. Manganites are prototypical of correlated electron systems where spin, charge, and orbital degrees of freedom are at play simultaneously, and where classical simplifications that neglect some interac-
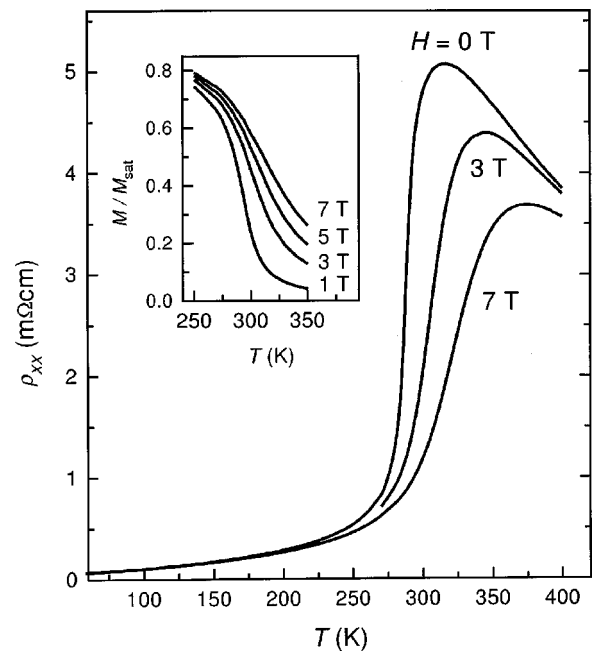

FIG. 1. The temperature dependence of $\rho_{xx}(H,T)$ of a $La_{2/3}(Pb,Ca)_{1/3}MnO_3$ single crystal at various fields H. Inset: $M_H(T)$ in the transition region. From Chun, Salamon, Lyanda-Geller *et al.*, 2000.

tions to study others in detail simply do not work. We are convinced that the comprehension of complex problems posed by the manganites has the potential to produce a substantial advance in the theory of condensed matter, and will eventually shed light into other unsolved problems, for example, high-T_c superconductivity. Several excellent review articles (Ramirez, 1997; Coey *et al.*, 1999; Tokura and Tomioka, 1999; Rao *et al.*, 2000) and edited books (Rao and Raveau, 1998; Tokura, 2000) are available in the literature now which discuss the properties of manganites, mostly from a materials science point of view. A review of the optical properties of manganites and related materials has recently appeared (Cooper, 2001). Our focus is different since we choose to emphasize the physics and mechanisms that determine the properties of manganites in different temperature regions. This approach originated in the realization that the most relevant energy scale in these complex systems is the temperature at which the magnetic ordering is observed, and that the interplay of magnetic, charge, and spin degrees of freedom changes qualitatively and quantitatively depending on whether the temperature is much smaller than, similar to, or much larger than the ordering temperature, irrespective of the chemistry.

In this review we focus on the present understanding of what we think are the most remarkable physical properties of manganites, observed by state of the art experiments and interpreted with modern theories. We have organized the discussion into three main modules: (i) low temperatures, or energy scales much smaller than that responsible for the metal-insulator, magnetic-paramagnetic phase transition, (ii) high temperatures, or

energy scales much bigger than the energy scale of magnetic interactions, and (iii) intermediate temperatures, or energy scales comparable to the interactions where semiconducting and metallic ground states are both highly unstable and susceptible to such external parameters as temperature, magnetic field, electrical field, crystalline disorder, dimensionality, and doping. Before the discussion of the physical properties we introduce the subject with a brief historical summary of both experimental results and theory developments since the discovery of manganites in the early 1950s. We end the review with a discussion of the implications of manganites.

II. BACKGROUND

A. Early experiments

Manganese compounds of composition $A\text{MnO}_3$ (A = La, Ca, Ba, Sr, Pb, Nd, Pr) crystallize in the cubic structure of the perovskite mineral CaTiO_3 (Verwey *et al.*, 1950), and will hereafter be referred to as *manganites*. Depending on the composition they show a variety of magnetic and electric phenomena, including ferromagnetic, antiferromagnetic, charge, and orbital ordering. If the site A is partially occupied by two different atoms, one trivalent as, for example, La and one divalent as Ca, then Mn^{3+} and Mn^{4+} coexist in the samples and the compounds show different behavior as the temperature is changed. The different phase transitions that the mixed manganites display (metal-insulator; charge, orbital, and spin degree of freedom; order-disorder transitions) are sensitive to external parameters such as the pressure and magnetic field. The large sensitivity of the transport properties to external magnetic fields has been optimized recently, and because of this manganites are also known as colossal magnetoresistance (CMR) oxides (Jin *et al.*, 1994). Some manganese compounds crystallize in quasi-two-dimensional (2D) structures (Ganguly, 1984), called *layered manganites*. Their physical properties, also related to the presence of both Mn^{3+} and Mn^{4+} ions placed in the center of an oxygen octahedron in the samples as in the case of the 3D compounds, are in addition anisotropic because the MnO_2 planes, where the magnetic correlations and electrical conductivity take place, are isolated by two $A\text{O}$ planes (Moritomo *et al.*, 1996). Due to these properties manganites and layered manganites have attracted a great deal of attention during the last years. Manganites belong to the group of highly correlated systems where charge, spin, and lattice degrees of freedom are intimately interrelated and have the potential to help us improve our understanding of complex systems.

The study of the properties of manganites started 50 years ago, soon after Jonker and van Santen discovered a striking correlation between the Curie temperature (T_C), saturation magnetization (M_S), and electric resistivity (ρ) in samples of $\text{La}_{1-x}A'_x\text{MnO}_3$, where A' = Ca^{2+}, Sr^{2+}, and Ba^{2+}, when measured as a function of x (Jonker and van Santen, 1950; van Santen and Jonker,

1950). Their polycrystalline samples of composition $\text{La}_{0.7}\text{Sr}_{0.3}\text{MnO}_3$, Fig. 2, showed maximum values $T_C^{\text{max}} \approx 370\,\text{K}$, $M_S^{\text{max}} \approx 90\,\text{G/g}$, corresponding to full polarization of all $3d$ electrons present in the sample, and electrical conductivity $\sigma^{\text{max}} \approx 300\,\Omega^{-1}\,\text{cm}^{-1}$, comparable to single-crystal samples grown more recently (Tokura *et al.*, 1994). A significant research effort followed soon after which included the study of the cobaltites (Jonker and van Santen, 1953) and low-temperature measurements in manganites such as the specific heat, magnetization, dc and ac resistivity, magnetoresistance, magnetostriction, I-V curves, dielectric constant, Seebeck effect, and Hall effect (Volger, 1954; Jonker, 1954). The conclusions arrived at by these early researchers were quite close to those reached by careful examination of results in recent experiments, a surprising fact considering the time elapsed, the progress in sample preparation techniques (direct consequence of more than a decade of high-temperature superconductivity research), and the advances in our understanding of condensed-matter physics.

Some of the most relevant conclusions reached by researchers in the 1950s are the following:

(a) After studying the correlations between crystal structure and the Curie temperature and finding that different samples with the same lattice constant had different Curie temperatures they concluded that a picture of simple exchange interaction could not explain the ferromagnetic transition temperature in manganites (Jonker and van Santen, 1950). We now know that the relevant parameter in determining T_C is not the distance between manganese, but the angle of the Mn-O-Mn bond. This is often characterized by the tolerance factor $f = (\langle r_A \rangle + r_O)/[\sqrt{2}(r_{\text{Mn}} + r_O)]$, which compares the Mn-O separation with the separation of oxygen atom and A-site occupant. These distances are approximated by the ionic radii of the constituent atoms, suitably averaged and $f = 1$ for spherical atoms packed in the perovskite structure.

(b) They found that samples of composition $x \approx 0.3$ showed maximum Curie temperature and minimum electrical resistivity, and uncovered a linear relationship between the magnetoresistance and the magnetization of the specimens, concluding that magnetism and electrical conductivity were definitively correlated, Fig. 3 (Volger, 1954).

(c) They established that both divalent element content and oxygen stoichiometry determined the Mn^{4+} content in the samples.

(d) Their alternating current measurements showed frequency dependence and a magnetoresistance that decreased with the applied voltage. These results clearly pointed to an inhomogeneous phase, and they proposed a model of metallic grains surrounded by a high-resistance intergrain material. We believe today that inhomogeneity is intrinsic to the manganites and may play a very important role in their physics.
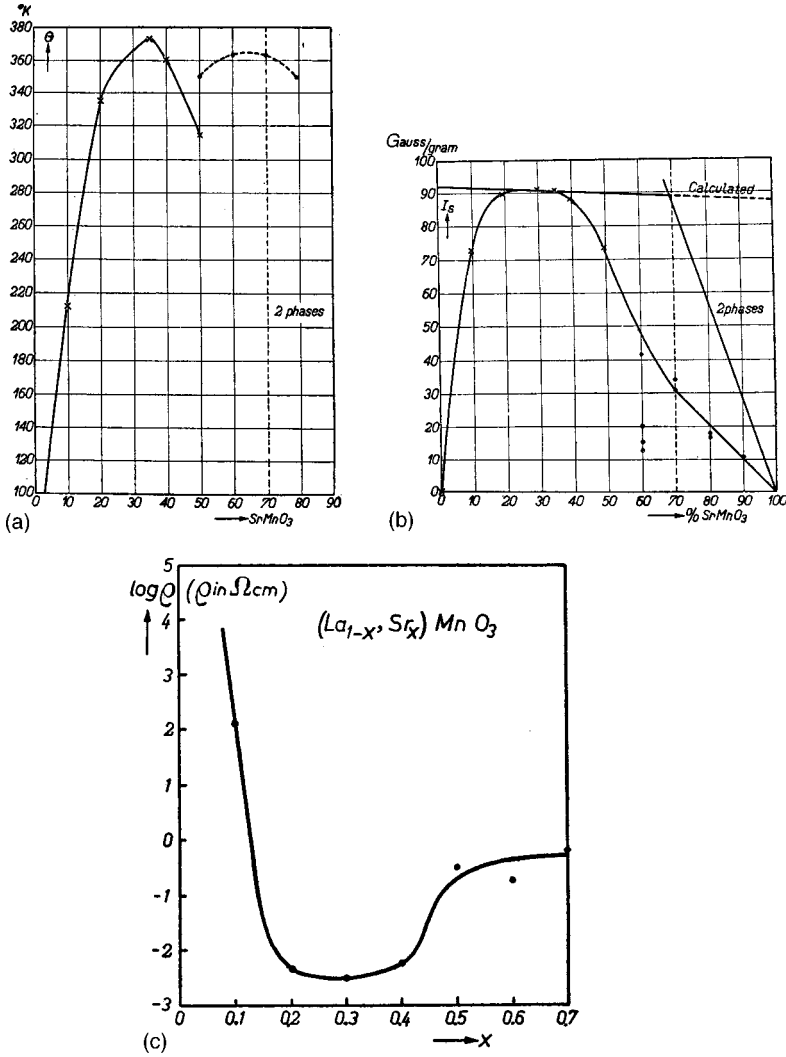
FIG. 2. Magnetic properties of $La_{1-x}Sr_xMnO_3$ vs composition: (a) Curie temperature Θ and (b) saturation magnetization I_S at 90 K vs Sr content in percent. (c) Resistivity ρ vs Sr content x. Crosses in (a) and (b) indicate nominal compositions. From Jonker and van Santen, 1950, and van Santen and Jonker, 1950.

(e) From Seebeck effect measurements they concluded that the ferromagnetic ordering had a rigorous influence upon the band structure.

(f) The Hall effect proved extremely difficult to observe, implying extremely low mobility (mean free path of the order of interatomic distances), and was anomalous in sign. They attributed these to mixed conductivity, but we know today that they are also the signature of charge localization and small polaron conduction.
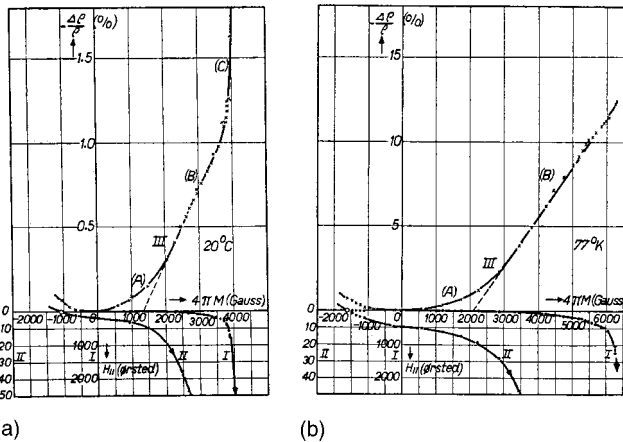
Not long after those pioneering experiments, Wollan and Koehler (1955) published an extensive neutron diffraction study of the series $La_{1-x}Ca_xMnO_3$, identified the type of magnetic order displayed by the end compounds (Fig. 4), and built the first magnetic structure-based phase diagram for the manganites. This early phase diagram closely matches our modern versions (Schiffer *et al.*, 1995). Almost simultaneously (Jonker, 1956) we find the first attempts in the literature to correlate the crystalline structure with the magnetic properties from the point of view of a then-new magnetic interaction proposed by Zener (1951), the so-called double exchange interaction. According to this picture, in the configuration Mn^{3+}–O^{2-}–Mn^{4+}, the easy simultaneous transfer of an electron from Mn^{3+} to O^{2-} to Mn^{4+} causes at the same time a high electrical conductivity and, by the tendency of the traveling electron to retain its spin orientation, a parallel orientation of the mag-
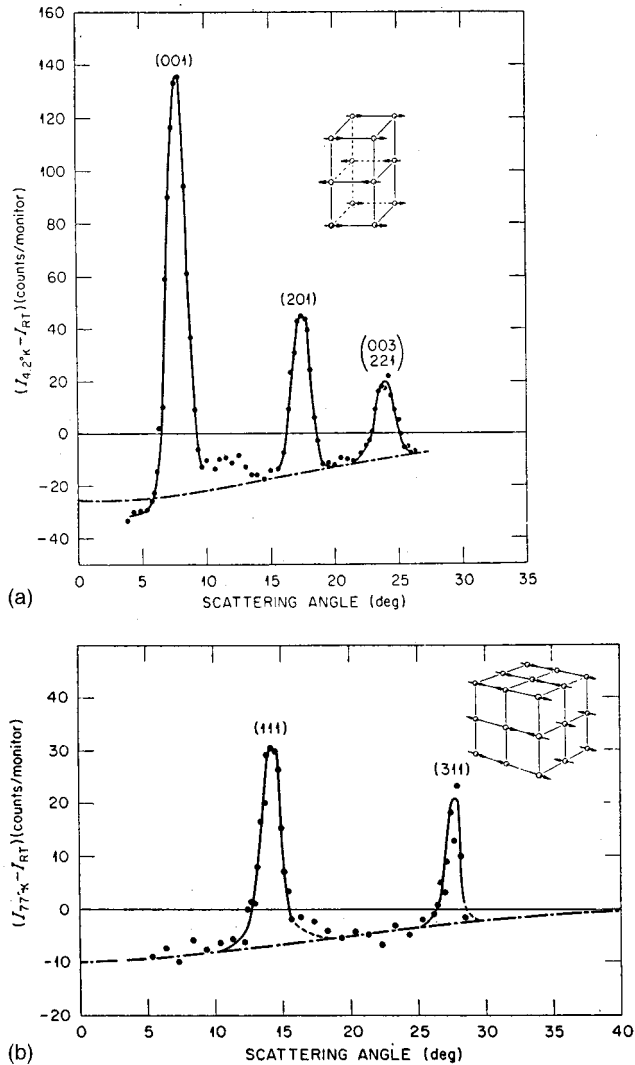

FIG. 3. Early data on the dc magnetoresistance $\Delta\rho/\rho$ of $La_{0.7}Sr_{0.3}MnO_3$ as a function of the magnetization at (a) room temperature and (b) 77 K. From Volger, 1954.

FIG. 4. Difference between neutron-scattering intensity at 4.2 K and room temperature: (a) LaMnO$_3$ showing type-A ordering (inset); (b) CaMnO$_3$, indicating type-G order. From Wollan and Koehler, 1955.
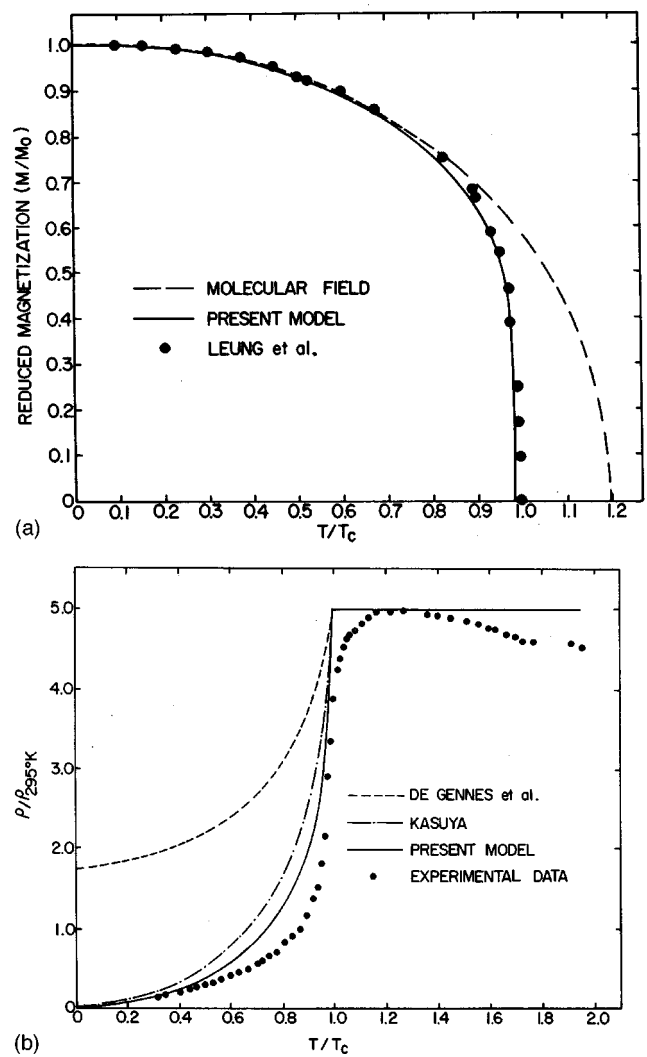

FIG. 5. Comparison of magnetization and resistivity models with experiment: (a) Reduced magnetization $M(T)/M(0)$ as a function of the reduced temperature T/T_C. The experimental points are taken from Leung et al., 1969. The dashed curve is calculated in the molecular-field approximation, while the solid curve is calculated with the Searle and Wang model. (b) Similar comparison for the normalized resistivity vs T/T_C. The solid curve is calculated using the experimental magnetization. From Searle and Wang, 1969.

netic moments of the Mn^{3+} and Mn^{4+} ions. Jonker also found that as the structure of the samples approaches a stable cubic perovskite defined by a tolerance factor f close to unity (Jonker and van Santen, 1950), the saturation magnetization of the specimen approaches the spin only contribution of all Mn ions. Jonker came just short of concluding what these data cry for, i.e., closer to cubic structure⇒closer to colinear Mn^{3+}–O^{2-}–Mn^{4+} bonds⇒stronger double exchange interaction.

Further progress came somewhat later when the group at Manitoba accomplished the first growth of high quality millimeter long single-crystal manganites of composition (La, Pb)MnO$_3$ (Morrish et al., 1969). In a series of five papers they confirmed the results previously obtained in ceramics and improved the understanding of the physics (Leung et al., 1969; Searle and Wang, 1969). By that time the non-Heisenberg nature of the ferromagnetic transition was established and a phenomenological model based on a strongly spin-polarized conduction band was proposed to explain it, with the results

shown in Fig. 5(b) (Searle and Wang, 1969). The one thing that is missing in this whole period is the addition of the electron-phonon interaction. Even though the lattice was clearly linked to the occurrence of ferromagnetism and the metallic phase (Jonker, 1956), a direct attempt to find changes in the rhombohedral Bragg angles at the Curie temperature (Oretzki and Gaunt, 1970) seemed to indicate little lattice involvement. Today we know that hints for the lattice involvement are in fact there, clearly shown by experimental results that reveal the local structure around Mn ions (Louca et al., 1997).

During the 1970s little progress was made in the understanding of the manganites, as attention was focused on studies of other interesting magnetic systems like the Eu chalcogenides (Esaki et al., 1967; von Molnar and

Kasuya, 1968) and EuO (Penney *et al.*, 1972). The extensive study of these compounds drove the development of the concept of localization of charge by magnetic polarons, magnetically ordered clusters originated by exchange between bound carriers, and localized spins (Kasuya and Yanase, 1968; Kasuya *et al.*, 1970; Kasuya, 1970a, 1970b). Other key developments include the work by Mott and Davis (1971) on amorphous conductors and charge localization by crystalline defects. Dormant manganites reappear in the 1980s in a study by a Japanese team (Tanaka *et al.*, 1982), where oxygen stoichiometry and transport properties were revisited. In spite of the huge effort and remarkable theoretical advances of the 1970s a convincing explanation for the behavior of manganites remained elusive. Tanaka *et al.* could not arrive at a unique interpretation of their results, in part because of what resulted in a second failed attempt to measure the Hall effect. They proposed for the first time a plausible interpretation based on charge localization into a small magnetic or lattice polaron that conducts by hopping in the paramagnetic region above T_C, but the mechanism producing such localization was still unknown. They found the resistivity to have a thermally activated form and the Seebeck coefficient to vary inversely with temperature. The activation energy and the energy scale associated with the Seebeck coefficient differ significantly which, as we note below, is a signature of polaronic behavior.

The 3D manganites are the end ($n=\infty$) members of the Ruddlesden-Popper series $(A, A')_{n+1}Mn_nO_{3n+1}$ (Ruddlesden and Popper, 1958). Interest in the properties of small n members was also triggered by the discovery of the behavior of the $n=\infty$ compounds described previously (Gorter, 1963; Bouloux *et al.*, 1981). Similar to the $n=\infty$ case, intense and systematic research was renewed only after the discovery of large magnetoresistance (Moritomo *et al.*, 1996; Battle, 1996) in the $n=2$ member. In these compounds the MnO_6 octahedra are arranged in n planes, separated by two $(Ln, A)O$ layers. Electrical conduction, magnetic correlation, and orbital ordering take place in the MnO_2 planes, and their number and separation determine physical properties.

Even though many of the experimental data have been available for a long time, one cannot help but notice some lack of perspective in the early interpretations, characterized by the emphasis on only certain of the physical mechanisms. In order to improve the understanding of the manganites a much broader point of view is necessary, one that is able to put together the whole body of experimental data, including precise crystallographic details, in addition to the double exchange ideas of Zener (1951), Anderson and Hasegawa (1955), Goodenough (1955), and de Gennes (1960). The magnetic and lattice polaron ideas of Kasuya (1959), Kasuya and Yanase (1968), and Mott and Davis (1971), the developments in the theory of small lattice polarons by Holstein (1959), the narrow-band model of Kubo and Ohata (1972), and the concept of Jahn-Teller distortion of the oxygen octahedra surrounding each Mn ion

(Reinen, 1979) are essential ingredients. To these we must add ideas about phase segregation and intrinsic inhomogeneous behavior explored recently by Moreo *et al.* (1999). In what follows we shall try to summarize the present situation and discuss why the understanding of the physics of manganites is still incomplete and challenging.

B. Early theoretical ideas

1. Double exchange

Soon after Jonker and Van Santen (1950; van Santen and Jonker, 1950) discovered the strong correlation between ferromagnetism and metallic conductivity in doped manganites, Zener (1951) offered an explanation that remains at the core of our understanding of magnetic oxides. Zener noted that, in doped manganese oxides, the two configurations

$$\psi_1 : Mn^{3+}O^{2-}Mn^{4+} \quad \text{and} \quad \psi_2 : Mn^{4+}O^{2-}Mn^{3+} \tag{1}$$

are degenerate and are connected by the so-called double-exchange matrix element. This matrix element arises via the transfer of an electron from Mn^{3+} to the central O^{2-} *simultaneous* with transfer from O^{2-} to Mn^{4+}. Zener points out that the degeneracy of ψ_1 and ψ_2, a consequence of the two valencies of the Mn ions, makes this process fundamentally different from conventional superexchange. Because of strong Hund's coupling, the transfer-matrix element has finite value only when the core spins of the Mn ions are aligned ferromagnetically, again distinguished from superexchange which favors antiferromagnetism. As usual, the coupling of degenerate states lifts the degeneracy, and the system resonates between ψ_1 and ψ_2 if the core spins are parallel, leading to a ferromagnetic, conducting ground state. Zener estimates the splitting of the degenerate levels to be given by the ferromagnetic transition temperature $k_B T_C$ and, using classical arguments, predicts the electrical conductivity to be

$$\sigma \approx \frac{xe^2}{ah} \frac{T_C}{T}, \tag{2}$$

where a is the Mn-Mn distance and x, the Mn^{4+} fraction. This provided a qualitative description of the data then available.

Anderson and Hasegawa (1955) revisited Zener's argument, treating the core spin of each Mn ion classically, but the mobile electron quantum mechanically. Designating the intra-atomic (Hund's) exchange energy by J and the transfer matrix element by b, Anderson and Hasegawa found that Zener's level splitting is proportional to $\cos(\theta/2)$, where θ is the classical angle between the core spins. The fundamental result, which has remained a cornerstone of double exchange theory, is that the effective transfer integral becomes $t_{eff} = b \cos(\theta/2)$. The energy is lower when the itinerant electron's spin is parallel to the total spin of the Mn cores. They also show that the assumption of classical spins can be avoided if one replaces $\cos(\theta/2)$ by $(S_0 + 1/2)/(2S + 1)$, where S_0 is

the total spin of the two Mn ions and the mobile electron and S is the core spin. Anderson and Hasegawa made the interesting conjecture that a plot of the inverse susceptibility versus temperature would exhibit pure Curie-law behavior at high temperatures (effective $T_C = 0$), curving downward as the actual ferromagnetic transition is approached, lying between that of an ordinary ferromagnet and a ferrimagnet. As we will see, the observed behavior is somewhat more complicated.

After a gap of some years, de Gennes (1960) revisited this problem, treating the effect of double exchange in the presence of an antiferromagnetic background. He considered a layered material with N magnetic ions per unit volume, each spin S coupled ferromagnetically to its z' neighbors on the same layer with exchange energy J' and antiferromagnetically to z neighbors on adjacent layers with energy J. When the angle between the magnetization of successive layers is Θ, the exchange energy can be written as

$$E_{ex}/N = -z'J'S^2 + zJS^2 \cos \Theta. \tag{3}$$

The double exchange contribution is calculated in the tight-binding approximation, using the Anderson-Hasegawa effective transfer integral, to be

$$E_m/N = -xb'\gamma_k' + b\gamma_k \cos \Theta/2, \tag{4}$$

where γ_k and γ_k' are, as usual, the sum of phase factors over the z and z' nearest neighbors, and x is the Mn^{4+} concentration. The ferromagnetic state is stable at all temperatures only if the concentration $x \geq 4JS^2/b$. At lower concentrations, there is a low-temperature transition to a canted state that extends to $x=0$; the canting angle between successive planes is given by $\Theta_0 = 2\cos^{-1}(bx/4JS^2)$, reaching π as $x \to 0$. When $x < 2.5JS^2/b$, the canted state gives way to antiferromagnetic alignment along a critical line, while for $2.5JS^2/b \leq x \leq 4JS^2/b$ the intermediate state is ferromagnetic. The boundary between ferromagnetic and antiferromagnetic intermediate states occurs when the canting angle is $\Theta_0 = 2\cos^{-1}(2.5/4) = 103°$. In a concluding section, de Gennes anticipates current research by considering self-trapping of a carrier by distortion of the spin lattice, an entity we would now refer to as a magnetic polaron. He demonstrates that at small values of x, local distortions of the antiferromagnetic structure always tend to trap the doped-in charge carrier.

In a remarkably complete treatment, Kubo and Ohata (1972) considered a fully quantum mechanical version of a double exchange magnet. They introduced the now-standard Hamiltonian

$$\mathcal{H} = -J \sum_{i,\sigma,\sigma'} (\mathbf{S}_i \cdot \sigma_{\sigma,\sigma'}) c_{i\sigma}^\dagger c_{i\sigma'} + \sum_{i,j,\sigma} t_{ij} c_{i\sigma}^\dagger c_{j\sigma}, \tag{5}$$

where $c_{i\sigma}^\dagger$, and $c_{i\sigma}$ are creation and annihilation operators for an e_g electron with spin σ on a Mn site and t_{ij} is the transfer-matrix element. The spin due to t_{2g} electrons is $\mathbf{S}_i$; σ is the Pauli matrix, and J is the intra-atomic exchange energy, typically referred to as the Hund's-rule exchange energy. Kubo and Ohata argue
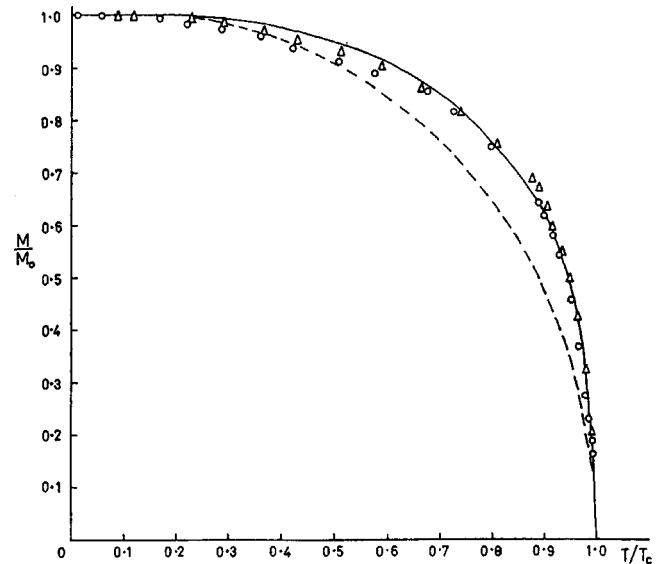
FIG. 6. Reduced magnetization M/M_0 vs the reduced temperature T/T_C: $\bigcirc$, for La$_{0.62}$Pb$_{0.38}$MnO$_3$; $\triangle$, La$_{0.69}$Pb$_{0.31}$MnO$_3$; dashed curve, unmodified, reduced molecular-field curve for $S=1.81$; solid curve, modified curve for a quartic term coefficient of 0.125. From Oretzki and Gaunt, 1970.

that it is preferable to calculate the motion of a spin-down hole moving in a background of spin $S+1/2$ ions. They transform to a hole version of the Hamiltonian and use a projection-operator method to consider only the lowest-energy Hund's-rule states. Consider two sites containing a single hole. If both core spins are up, the hole spin must be down, giving a total spin of $2S-1/2$. On the other hand, if the core spins are oppositely aligned, the configuration belongs to a manifold of total spin 1/2. The corresponding effective transfer-matrix element ranges between $4t/5$ for the aligned case and $t/5$ in the antiparallel configuration for $t_{ij}=t$ for next neighbors. These may be considered to be the average values of $\cos \theta/2$ for the quantum version of the problem. The net result is that the width of the down-spin hole band broadens in the ferromagnetic limit, while that of the up-spin hole band narrows, leading to the expected half metallic ferromagnetic ground state (Irkhin and Katsnel'son, 1994), in which the Fermi surface lies entirely within one spin subband.

2. Magnetic and transport properties

As a result of the change in bandwidth, the Curie temperature increases as the system magnetizes. Kubo and Ohata (1972) carried out a mean-field calculation that takes into account the change in effective Curie temperature, finding that the magnetization increases more rapidly than it would if it followed the usual Brillouin function. Figure 5(a) compares the calculated magnetization with that for a conventional mean-field model with $S=2$; the experimental data shown in the plot are from Leung et al. (1969) Similar data for other materials are shown in Fig. 6.

In addition to the band structure and magnetic properties of the double exchange model, Kubo and Ohata considered the spin-wave spectrum and the resistivity in the low-temperature limit. The double exchange mechanism broadens the down-spin hole band, the bottom of which is at an energy $W/2$ below the (narrow) up-spin band, where W is the $T=0$ width of the down-spin band. If the hole band is filled to a Fermi level ϵ_F, down-spin states are $\mu = W/2 - \epsilon_F$ below any up-spin state. As a consequence, processes that involve the emission or absorption of a single magnon, and therefore scatter a down-spin hole into an up-spin state, are suppressed exponentially as $\exp[-(\mu/k_B T)]$. Kubo and Ohata considered two-magnon processes that do not require a spin flip, and predicted that the resistivity will vary as $T^{9/2}$ at low temperatures. As we shall see, the T^2 temperature dependence expected for single-magnon processes is exponentially suppressed at low temperatures in double exchange magnets.

Polaron transport. More or less concurrent with the development of double exchange theory, Holstein (1959) and collaborators studied the properties of charge carriers that are "clothed" in a distortion of the embedding crystal lattice: the polaron problem. When the hopping probability is large, the charge carrier hops each time a neighboring site acquires, via thermal motion, the necessary lattice distortion. In this case, the polaron is said to be in the adiabatic limit. A characteristic property is that the electrical conductivity is activated and has the form

$$\sigma(T) \propto T^{-1} \exp(-E_\rho/k_B T), \tag{6}$$

where E_ρ is approximately half of the polaron binding energy. The thermoelectric power, as in a semiconductor, is inversely proportional to temperature, but the characteristic energy is much smaller than E_ρ. The simple explanation is that the polaron carries with it only its own chemical potential, but not the energy associated with its accompanying lattice distortion.

Much discussion has centered on the existence of a Hall effect in the hopping regime (Entin-Wohlman *et al.*, 1995). The "drift velocity" in this case is the hopping distance divided by the time between successive hops (dwell time). This cannot be construed as a velocity with which to calculate a Lorentz force. Rather, as Holstein and collaborators (Friedman and Holstein, 1963; Emin and Holstein, 1969) demonstrated, the Hall effect arises through the interference effects induced by the Aharonov-Bohm phase produced when magnetic flux threads the loops defined by distinct hopping paths between two sites. The smallest such loop involves one intermediate site and always gives rise to a negative Hall coefficient (Holstein, 1973). The resulting Hall coefficient is also activated but, when the elemental hopping trajectory involves three sites, has an activation energy $E_H \approx 2E_\rho/3$. These characteristics of polaron transport were noted above, and will be discussed below, as determinants of polaron-dominated transport.

A particular aspect of the electron-lattice coupling in the manganites is the existence of a singly occupied e_g level in Mn^{3+} and its absence in Mn^{4+}. The doubly degenerate e_g level is split if the local symmetry is lower than octahedral, and such a distortion will be expected to occur, lowering the energy of the occupied state, but at a cost in lattice energy. Such effects are generally termed Jahn-Teller distortions (Ashcroft and Mermin, 1976). Indeed as we shall see, the crystal structure of the parent compound $LaMnO_3$ is orthorhombic as a consequence of a collective distortion of the structure and gives rise to a Jahn-Teller splitting of the e_g orbitals by 1.5 eV (Satpathy *et al.*, 1996b). An Mn^{4+} site, however, does not contribute to this lattice distortion, and should be "more cubic" than its Mn^{3+} neighbors. It is generally agreed that the net energy gain due to the Jahn-Teller distortion can bind a charge carrier to its site, creating a small polaron. Many authors refer to the charge carrier in the activated regime as a "Jahn-Teller polaron."

III. LOW-TEMPERATURE STATES

A major motivation for the study of the manganites is the richness of the low-temperature phases that emerge upon doping. The end members of the series, $RMnO_3$ and $DMnO_3$, where R is a rare-earth atom and D is a divalent substituent such as Ca or Sr, are antiferromagnetic insulators. Mixtures of the two exhibit various magnetic and charge-ordered ground states, which are reviewed in this section.

A. Parent compounds

Two of the end-members of the series, $LaMnO_3$ and $CaMnO_3$, were studied in some detail by Wollan and Koehler (1955) more than 40 years ago. The subject has recently been revisited by Huang *et al.* (1997) in a detailed neutron scattering study of $LaMnO_3$. The x-ray-diffraction work of Yakel (1955) showed that stoichiometric $LaMnO_3$ is orthorhombic, belonging to space group $Pnma$, while $CaMnO_3$ is cubic, space group $Pm3m$. The magnetic ground state of $LaMnO_3$ is antiferromagnetic and was labeled A type by Wollan and Koehler. As confirmed by later workers, the magnetic moments lie in the a-c plane and are ferromagnetically aligned along the a axis. Successive planes along b are aligned antiparallel, as sketched in the inset of Fig. 4(a). In this orthorhombic setting of the crystal, the a and c axes are along Mn-Mn directions, with $a=11.439$ Å and $c=11.072$ Å (Yakel, 1955). It is also convenient to use a monoclinic cell with $a_m = c_m = 7.960$ Å because of its close correspondence to the underlying cubic perovskite cell. $CaMnO_3$ also orders antiferromagnetically, and may be considered as two interpenetrating face-centered lattices with opposite spin. This C-type order, in the language of Wollan and Koehler, is sketched in Fig. 4(b).

The magnetic phases of $LaMnO_3$ and $CaMnO_3$ were explained by Goodenough (1955) in terms of covalent bonding between oxygen and Mn^{3+} and Mn^{4+} ions, respectively. In the case of $LaMnO_3$, the degeneracy of the single e_g orbital favors a cooperative Jahn-Teller dis-
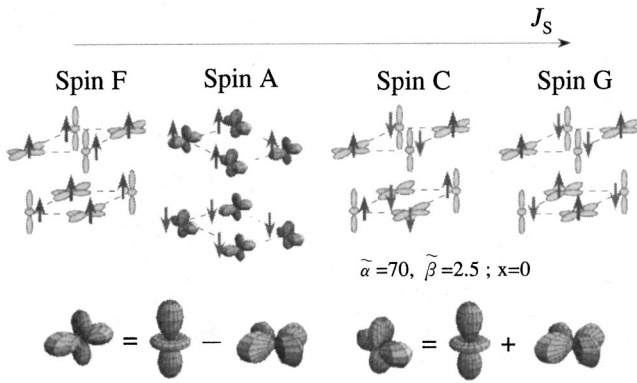
FIG. 7. Orbital structures at $x=0$ as a function of the antiferromagnetic interaction J_S between the t_{2g} spins. The energy parameters are chosen to be $\tilde{\alpha}=70$ and $\tilde{\beta}=2.5$ [case (A)]. The lower sketches demonstrate how the x^2-z^2 and y^2-z^2 orbitals are related to more common representations of d orbitals. From Maezono et al., 1998b.

tortion (Kanamori, 1960), and the appearance of orbital order. The issue of orbital and spin ordering has been examined more recently by Maezono et al. (1998b). For the undoped case (all sites occupied by Mn^{3+} ions), Maezono et al. obtain a mean-field phase diagram for spin/orbital ordering as a function of the antiferromagnetic interaction J_s between t_{2g} core spins. The sequence of phases is sketched in Fig. 7. For intermediate values of J_s the A-type antiferromagnetic phase is stabilized with what is termed G-type orbital order. Linear combinations of e_g orbitals in this state are in the form $d_{z^2-x^2}$ and $d_{z^2-y^2}$, with lobes along Mn-O-Mn directions; i.e., the diagonals of the orthorhombic basal plane. The orbital state alternates between neighboring Mn^{3+} ions; the relative orientation of the spin and orbital order are shown in Fig. 8. Inoue and Maekawa (1995) have suggested, recalling earlier work by de Gennes, that the ground state at low doping would exhibit spiral magnetic order. Mishra et al. (1997), to the contrary, have demonstrated that canted (and presumably spiral) states depend on electronic parameters and are not necessarily the ground state of a double exchange model. More recently, an *ab initio* density-functional calculation (Popovic and Satpathy, 2000) has shown that the orbital and structural order arise simultaneously, driven by band-structure energy contributions.

Detection of orbital ordering requires sensitivity to the asphericity of the electronic charge density in the orbitally ordered state, which leads to intensity at Bragg peaks indexed as $(h00)$ and $(0k0)$, with h,k odd, that are nominally extinct. In this case, Murakami, Hill et al. (1998) observed resonant intensity at the (300) reflection, peaking at an x-ray energy 3 eV above the manganese K absorption edge. The resonant signal at the K edge arises from splitting Δ among unoccupied $4p$ levels via, perhaps, Coulomb interaction between $4p$ and polarized $3d$ levels, as sketched in Fig. 8. With the incident radiation polarized normal to the scattering plane (σ)
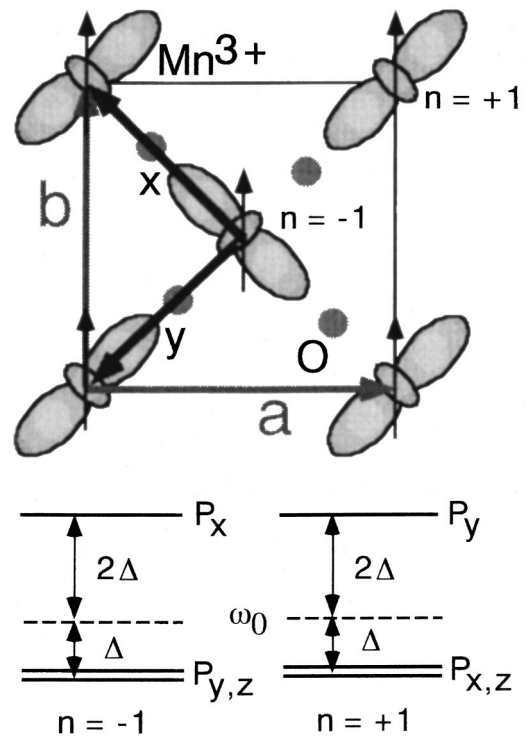

FIG. 8. Schematic view of the orbital and spin ordering in the a-b plane of the perovskite manganite $LaMnO_3$. This is the orbital G spin A state shown in Fig. 7. The schematic energy-level diagram of Mn $4p_{x,y,z}$ in the orbitally ordered state is shown below. From Murakami, Hill et al., 1998.

and with frequency ω, the cross section is zero unless the scattered x rays are polarized (π) in the scattering plane, in which case

$$I_{\sigma,\pi}^{res} \approx \frac{A^4 \sin^2 \psi}{\{1+4[(\omega-\omega_0)/\Gamma]^2\}^2} \frac{\Delta^2}{\Gamma^2}. \qquad (7)$$

Here ω_0 is the resonant energy and Γ^{-1} is the lifetime of the excited state. The angle ψ is zero when the crystal c
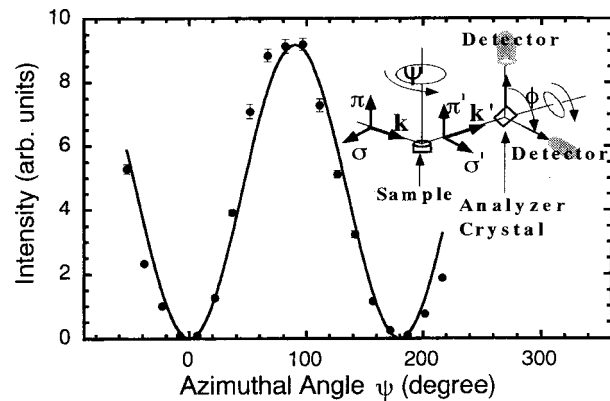

FIG. 9. Azimuthal-angle dependence of the intensity of the orbital ordering reflection (3, 0, 0) normalized by the fundamental reflections (2,0,0) and (4,0,0) at $E=6.555\,keV$ and at room temperature. The solid curve is the calculated intensity. Inset: Schematic view of the experimental configuration and definition of the polarization directions. From Murakami, Hill et al., 1998.
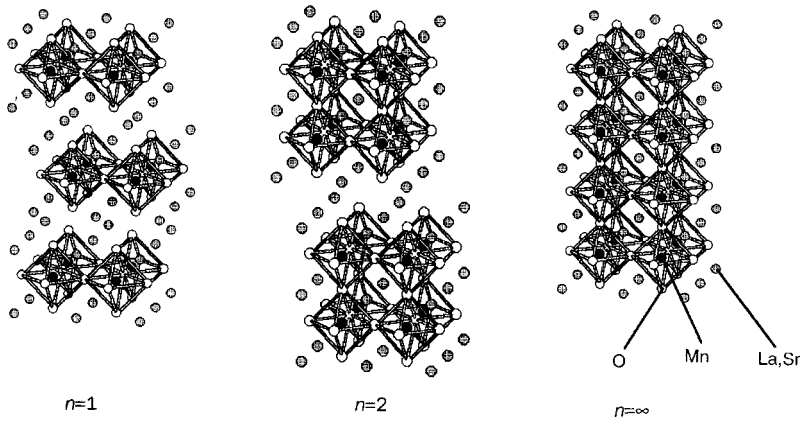
FIG. 10. Structures of the $n=1$, $n=2$, and $n=\infty$ members of the Ruddlesden-Popper series of lanthanum manganites. From Moritomo et al., 1996.

axis is normal to the scattering plane and 90° when in the scattering plane. A key test that the observed intensity arises from orbital ordering is found in the dependence of the (300) intensity on ψ, as shown in Fig. 9. Some questions (Benfatto et al., 1999) have been raised as to whether the observed signal is directly attributable to orbital ordering or to Jahn-Teller distortions of the same symmetry.

Materials of the type AMnO$_3$ are the end ($n=\infty$) members of so-called Ruddlesden-Popper series A_{n+1}Mn$_n$O$_{3n+1}$. The $n=2$ members of the series also show dramatic magnetoresistive effects, and have been widely studied. This compound has space group $I4/mmm$ and, as seen in Fig. 10, consists of square MnO planes arranged in pairs, spaced from each other by AO planes, and from adjacent pairs, by double AO planes. The "parent" compound in this series, corresponding to all manganese atoms nominally in the Mn^{3+} state, is R_2SrMn$_2$O$_7$. Almost all work reported has been done on samples doped to have the formula R_{2-2x}Sr$_{1+2x}$Mn$_2$O$_7$ with $x\geq0.3$. These will be discussed in the next section.

B. Doped compounds

1. Charge ordering at half filling: $n=\infty$

Upon doping, the manganites exhibit a wide variety of ordered states, including ferromagnetic and charge-ordered phases, in addition to the antiferromagnetism and orbital ordering described above. In those compounds in which the proportions of Mn^{3+} and Mn^{4+} ions are rational fractions, charge- and orbital-ordering effects are particularly pronounced. Charge ordering might be expected as a consequence of nearest-neighbor Coulomb repulsion V_{NN}. However, the observed ordered structure in the 3D materials suggests a more complicated explanation. The first clear evidence for charge ordering was found in La$_{0.5}$Ca$_{0.5}$MnO$_3$ by Chen and Cheong using electron microscopy (Chen and Cheong, 1996). Electron-diffraction images exhibit commensurate superlattice peaks at low temperature, consistent with alternation of Mn^{3+} and Mn^{4+}, as expected for dominance of Coulomb repulsion. The crystal structure of this phase can be indexed in space group $Pbnm$, with

the b and c axes in the parent compound interchanged. The magnetic order is antiferromagnetic of the charge-exchange (CE) type described by Wollan and Koehler (1955). A sketch of the complex orbital, charge, and spin order is shown (Tokura and Tomioka, 1999) in Fig. 11. While the spins are purely antiferromagnetic, the charge and orbital ordering occurs in alternate b-c planes, contrary to expectations for large V_{NN}, giving rise to charge-stacked order. A Monte Carlo simulation carried out recently (Hotta et al., 1999) considered Hund's rule J_H, Jahn-Teller λ, and antiferromagnetic J_{AF} interactions. Using either a $4\times4\times2$ bilayer or a $4\times4\times4$ cube, they find that the observed c axis charge-stacked state has lowest energy at intermediate values of J_{AF} so long as V_{NN} does not exceed $\simeq0.2$ eV. The bare value $V_{NN}\simeq3.6$ eV is reduced below this critical value by the large dielectric constant of the manganites. Stabilization of this state requires the assistance of cooperative Jahn-Teller phonons. At larger and smaller values of J_{AF}, the
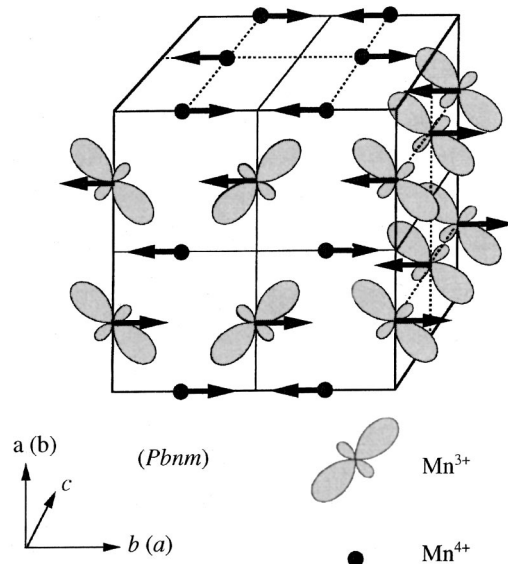

FIG. 11. Spin, charge, and orbital ordering pattern of the CE antiferromagnetic type observed for most of the $x\approx1/2$ manganites. The e_g-orbital ordering on Mn^{3+} sites is also shown. The Mn^{4+} sites are indicated by closed circles. Note that Mn^{3+} sites form chains along a, contrary to expectations from Coulomb considerations. From Tokura and Tomioka, 1999.
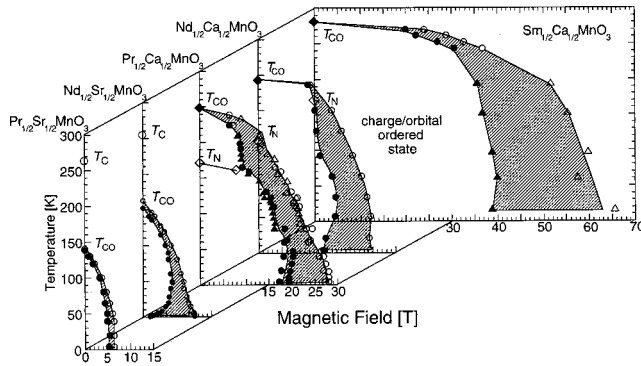
FIG. 12. Charge/orbital-ordered phase diagrams of various $RE_{1/2}Sr_{1/2}MnO_3$ and $RE_{1/2}Ca_{1/2}MnO_3$ (RE=Pr, Nd, and Sm) plotted in the magnetic field-temperature plane. The phase boundaries have been determined by measurements of the magnetic-field dependence of resistivity and magnetization at fixed temperatures. Low-temperature data were obtained utilizing pulsed magnetic fields up to 40 T. From Tokura and Tomioka, 1999.

stable states of the system are G-type antiferromagnetic (neighboring Mn spins antiparallel) and ferromagnetic states, respectively. This close relationship among various phases is observed experimentally.

Substitution of Nd for La narrows the bandwidth and destabilizes the ferromagnetic state. $Nd_{0.5}Sr_{0.5}MnO_3$ exhibits a narrow CE-type, charge ordered state (Kajimoto *et al.*, 1999), while $Pr_{0.5}Sr_{0.5}MnO_3$, with a still narrower band exhibits A-type antiferromagnetic order and remains conductive (Kawano *et al.*, 1997). Indicative of the delicate balance among charge, spin, and orbital ordering, $Pr_{0.5}Ca_{0.5}MnO_3$ is reported to order in the charge-ordered, CE antiferromagnetic phase (Tokura and Tomioka, 1999). Another manifestation of this balance is found in the field-induced melting of the charge ordered state. This was first reported by Kuwahara *et al.* (1995) for $Nd_{0.5}Sr_{0.5}MnO_3$ and subsequently to occur in Pr-Ca, Nd-Ca (Tokunaga *et al.*, 1998), Pr-Sr (Tomioka *et al.*, 1995), and Sm-Ca analogs, as seen in Fig. 12. The transition is, as seen, highly hysteretic and accompanied by drop in resistivity by as much as four orders of magni-

tude at low temperatures, as seen in Fig. 13. The sequence of phases with various combinations of trivalent and divalent ions in equal proportion has been reviewed in detail recently by Tokura and Tomioka (1999).

A related compound, $La_{0.5}Sr_{1.5}MnO_4$, similar to the 214 family of cuprate superconductors and having equal numbers of Mn^{3+} and Mn^{4+} ions, was found by Moritomo *et al.* (1995) and Bao *et al.* (1996), using transport and electron diffraction, to exhibit charge and magnetic order. These results were confirmed by neutron diffraction (Sternlieb *et al.*, 1996) and by x-ray diffraction at the (3/2, 3/2, 0) superlattice position, making use of anomalous dispersion terms for Mn^{3+} and Mn^{4+} ions at the K edge (Murakami *et al.*, 1998). The latter result was part of a path-breaking experiment by Murakami *et al.* in which orbital ordering, which doubles the charge ordered cell, was detected. The combined magnetic, orbital, and charge structure is shown in Fig. 14. Due to the anisotropy of the e_g wave functions, the atomic scattering factors must be treated as tensors near an absorption edge. These give measurable intensity at the K edge at the otherwise forbidden (3/4, 3/4, 0) position. The intensity varies with azimuthal angle as in $La_{0.5}Ca_{0.5}MnO_3$ and shows the required change in polarization. This work represented one of the first direct observations of orbital ordering, although earlier reports of (1/4, 1/4, 0) reflections in electron diffraction (Moritomo *et al.*, 1995; Bao *et al.*, 1996) may also have been due to orbital ordering.

2. Charge ordering at half filling: $n=2$

In the $n=2$ bilayer compounds, equal numbers of Mn^{3+} and Mn^{4+} ions are expected for the composition $RSr_2Mn_2O_7$. Here, however, charge ordering is less prevalent. Using electron diffraction, Li *et al.* (1997) and Kimura *et al.* (1998) detected the presence of charge order in $LaSr_2Mn_2O_7$ at 110 K via an increase in resistivity and the appearance of superlattice peaks in x-ray diffraction. The additional peaks have the wave vector $q = (1/4, 1/4, 0)$, and are consistent with charge/orbital ordering. However, recent neutron-diffraction results (Kubota, Fujioka *et al.*, 1999) find that it does not persist
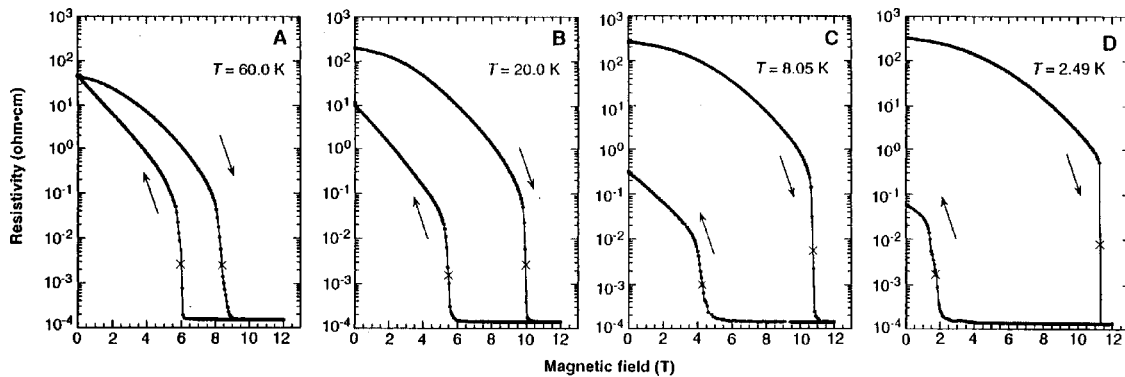

FIG. 13. Changes in the resistivity of a $Nd_{1/2}Sr_{1/2}MnO_3$ crystal after cooling to $T=2.49$ K in zero field. The resistivity shows jumps with increasing and decreasing fields at lower and upper critical fields, respectively, as indicated by crosses. From Kuwahara *et al.*, 1995.
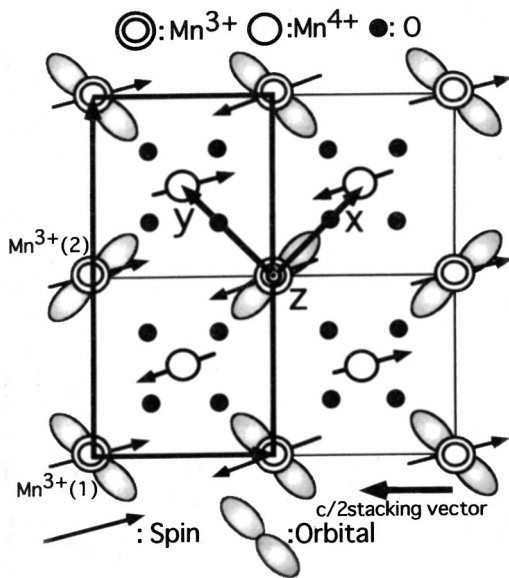
FIG. 14. Schematic view of the charge, spin, and orbital ordering in a layered perovskite manganite, $La_{0.5}Sr_{1.5}MnO_4$. The stacking vector along the c axis, shown in the figure, means that the second layer is shifted by one unit cell in this direction. From Murakami, Kawada et al., 1998.

at 80 K. They indicate that the magnetic order is predominantly A type, with some admixture of CE antiferromagnetic order and suggest a competition between $d_{x^2-y^2}$ orbital order and charge localized $d_{3x^2-r^2}/d_{3y^2-r^2}$ charge order. This result is not surprising, as the Monte Carlo results (Hotta et al., 1999) for bilayers suggest that the charge ordered state is stable only over a very narrow part of the phase diagram without cooperative Jahn-Teller distortions. The series from $R=$ Nd to $R=$ La has been studied in some detail by Moritomo and co-workers (1999). At low temperatures ($T \lesssim 20$ K) the Nd compound has been found to order in a complicated antiferromagnetic state, in which both Mn and Nd moments are canted (Battle et al., 1996). Substi-

tution of La for Nd reduces this lower Néel temperature, leaving antiferromagnetic order of the Mn ions in which the Mn bilayers form ferromagnetic sheets with the moments aligned and antialigned with Mn-O-Mn bond directions. Below the Néel temperature $T_N \approx 150$ K of the Mn spins in $NdSr_2Mn_2O_7$, Maezono et al. (2000) predicted ordering of $d_{x^2-y^2}$ orbitals concurrent with A-type antiferromagnetic order. A remarkable study by Takata et al. (1999) combined Rietveld analysis of powder-diffraction data with the maximum-entropy method. In this method, all deformations of the electron density allowed by symmetry are considered, and result in electron density maps which, as shown in Fig. 15, clearly demonstrate the ordering of orbitals into the expected $d_{x^2-y^2}$ configuration.

3. Other fractional doping levels

It is natural to expect that charge ordering phenomena might appear at other rational values of doping level. Indeed, Cheong and Chen (1998) have suggested that carrier concentrations of $x = N/8$ per Mn atom characterize special points on the phase diagram. It is somewhat difficult to make this case apart from the $x = 4/8$ materials discussed in the previous section. There appears to be a boundary between CE- and C-type antiferromagnetic order in the $La_{1-x}Ca_xMnO_3$ system near $x = 7/8$. When Mn^{3+} and Mn^{4+} are in the ratio 1:2, as they are in $La_{1/3}Ca_{2/3}MnO_3$, the system was thought to order into diagonal charge stripes (Cheong and Hwang, 2000). The stripe order is closely related to the $x = 1/2$ charge ordering, with an extra stripe of Mn^{4+} inserted between diagonal Mn^{3+}-Mn^{4+} rows. The original interpretation, based on electron diffraction and termed the bistripe mode, has been shown to be inconsistent with more recent x-ray and neutron data (Radaelli et al., 1999). The two structures are compared in Fig. 16.

In many of these materials, a ferromagnetic phase appears in a range of compositions, optimized for a wide range of materials when the Mn^{4+}/Mn^{3+} ions are in the
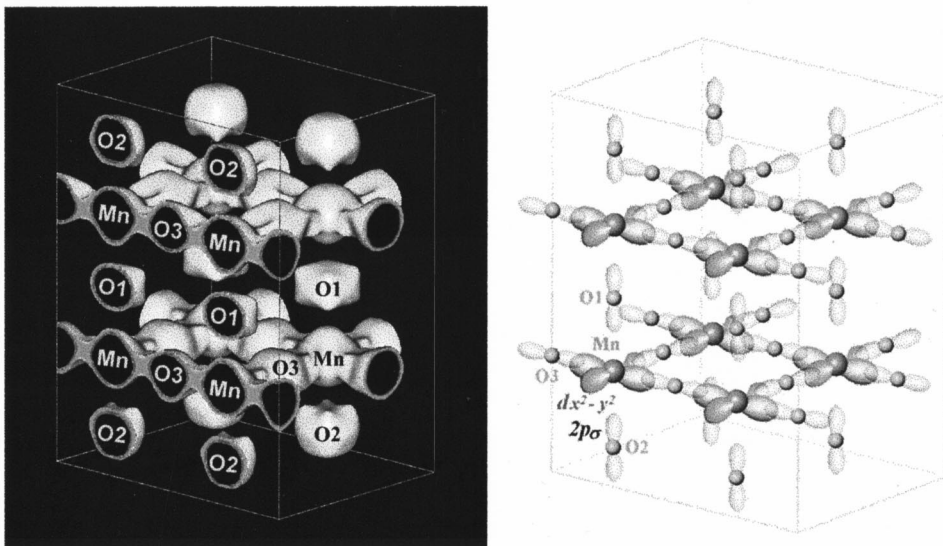

FIG. 15. Contours containing a charge density of $0.4\,e$ Å^{-3}, obtained by maximum-entropy analysis of synchrotron-x-ray powder-diffraction data for $NdSr_2Mn_2O_7$ at 19 K, showing the MnO_6 double layers. The schematic orbital structure is also shown. From Takata et al., 1999.

"Wigner-crystal" model
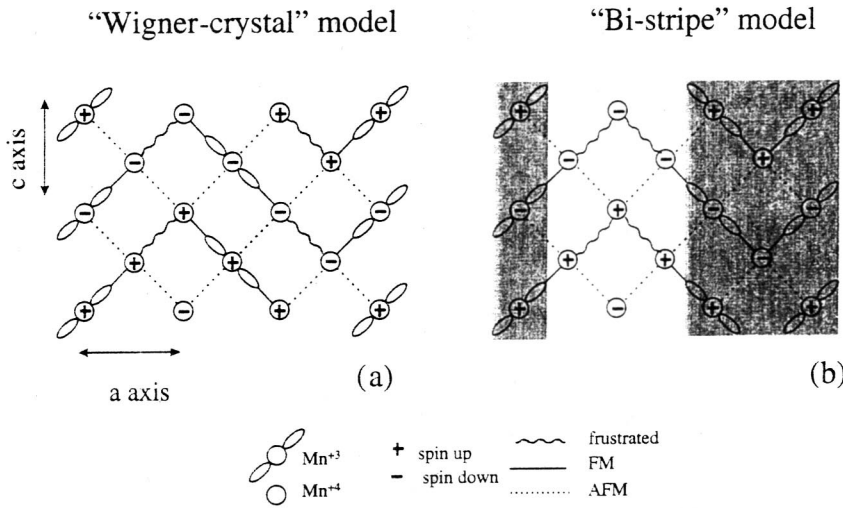
"Bi-stripe" model

(a)

(b)

a axis

FIG. 16. Schematic diagram of charge ordering patterns in $La_{1/3}Ca_{2/3}MnO_3$ showing alternating chains of Mn^{4+} (open circles) and Mn^{3+} (orbitals) separated by double chains of Mn^{4+} sites (bistripe model). The Wigner-crystal model is in better agreement with observations. From Radaelli *et al.*, 1999.

ratio 3:5 ($x=3/8$) (Cheong and Hwang, 2000). It is, of course, this range of compositions that is of the most interest, as these are the most metallic compounds. We defer a discussion of the low-temperature properties of the ferromagnetic composition range to the next section. Figure 17 shows the sequence of phases for $Nd_{1-x}Sr_xMnO_3$. The sequence A-type antiferromagnetic to ferromagnetic to A-type antiferromagnetic to C-type antiferromagnetic is typical of all the 3D perovskites. The intermediate CE phase at $x=1/2$ is not universally present. The surrounding diagrams in the figure sketch the orbital ordering deduced from the x-ray studies described above.

The $n=2$ compounds have been studied over a narrower composition range, but also show a variety of low-temperature phases (Kubota, Fujioka *et al.*, 1999; Argy-

riou *et al.*, 1999). In $La_{2-2x}Sr_{1+2x}Mn_2O_7$, the ferromagnetic order below $x=0.32$ has all spins normal to the double MnO planes, designated in Fig. 18 as FM-II. Between $x=0.3$ and $x=0.4$, the spins lie in the plane (FM-I). Beyond $x=0.4$, there is canting, or else an admixture of FM-I and AFM-II, with spins in the double planes parallel, but antiparallel stacking of successive double planes.

4. Theoretical situation

Since Goodenough's early work (Goodenough, 1955) on covalence effects, the sequence of phases as a function of doping has remained a topic of considerable interest. Semicovalency, a term coined by Goodenough, arises when the overlap of spin-polarized sp orbitals of manganese ions with unoccupied orbitals of the oxygen allow only covalent bonds involving electrons of one spin direction. Four possible Mn-O-Mn configurations
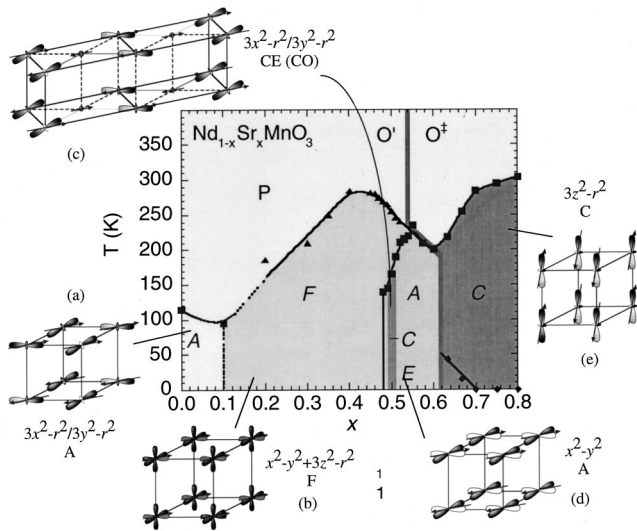

FIG. 17. Phase diagram of $Nd_{1-x}Sr_xMnO_3$ crystals. The sketches illustrate the orbital structure types associated with each phase. The letters within the phase diagram refer to paramagnetic (P), ferromagnetic (F), A-type antiferromagnetic (A), CE-type antiferromagnetic (CE), and C-type antiferromagnetic (C) spin ordering. From Okuda *et al.*, 1999.
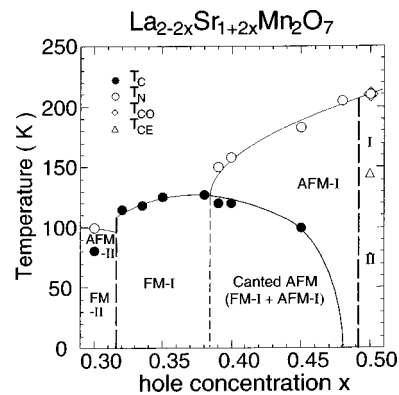
FIG. 18. Magnetic phase diagram of layered $La_{2-2x}Sr_{1+2x}Mn_2O_7$ ($0.30 \leq x \leq 0.50$). AFM-I (AFM-II) indicates the planar A-type AFM structure with AFM (FM) intrabilayer coupling and FM (AFM) interbilayer coupling. FM-I and FM-II stand for the ferromagnetic structures with spin within the ab plane and along the c axis, respectively. As for $x=0.50$, only AFM-I exists in phase I, while AFM-I and CE-type AFM coexist in phase II. From Kubota, Fujioka *et al.*, 1999.

TABLE I. The sequence of phases as the fraction x of divalent substituents is increased. The magnetic and orbital states are indicated (Goodenough, 1955).

x range	Type	Transport	Magnetic order	Orbital order
$0 \leqslant x \leqslant 0.1$	α	insulating	A-type antiferromagnetic	normal to ferromagnetic sheets
$0.2 \leqslant x \leqslant 0.4$	β	conducting	ferromagnetic	disordered
$0.5 \leqslant x \leqslant 0.75$	δ	insulating	CE-type antiferromagnetic	charge ordered
$0.75 \leqslant x \leqslant 0.85$	γ	insulating	C-type antiferromagnetic	
$0.9 \leqslant x \leqslant 1.0$	ϵ	insulating	G-type antiferromagnetic	none

are possible: antiferromagnetic if both empty Mn bonds point toward the bridging oxygen; ferromagnetic if one such bond connects to the oxygen, the other Mn-O bond being essentially ionic; paramagnetic in the absence of covalency; and ferromagnetic and conducting if there is disorder that allows double exchange coupling. In this scheme, the end points can be explained, as noted above. At $x=1$ all six Mn-O-Mn bonds are antiferromagnetic giving rise to G-type order, while at $x=0$, only four bonds can be covalent, leading to A-type antiferromagnetic order. Table I summarizes the sequence of phases predicted by Goodenough. At intermediate concentrations, there is an admixture of adjacent phases.

A more recent study of the doping phase diagram has been carried out by Maezono *et al.* (1998a, 1998b), using a double exchange model in which the orbital degeneracy of the e_g levels is included by means of an isospin $\vec{T}_i$. The mean-field energy associated with orbital order has the form $-\beta\Sigma_i\langle\vec{T}_i\rangle\vec{T}_i$, which is solved along with spin ordering. For $\beta=0$ and reasonable values of the underlying antiferromagnetic superexchange interaction J_s, the ferromagnetic state is stable from $x=0$ to $x \approx 0.6$ at $T=0$. When β is sufficiently large, the model predicts the progression $A \rightarrow F \rightarrow A \rightarrow C \rightarrow G$. The CE phase is not found. The phase diagram, along with spin/orbital ordering patterns, is shown in Fig. 19. The model leading to Fig. 19 does not include Jahn-Teller coupling, and predicts, as seen, that the orbital state at $x=0$ is G-type ordering of y^2-z^2 and z^2-x^2 orbitals. This differs from the experimentally deduced model shown in Fig. 8. Maezono *et al.* considered the addition of Jahn-Teller coupling and find that it tends to suppress the ferromagnetic spin arrangement and to favor the $3x^2-r^2/3y^2-r^2$ ordering found experimentally. The calculated ferromagnetic region is less robust than is observed; cf. Fig. 17. Maezono *et al.* suggest that increasing the bandwidth $\propto t_0$ and the antiferromagnetic exchange $J_s \propto t_o^2$, while keeping the other parameters constant, moves the ferromagnetic/antiferromagnetic boundary to larger values of x. Maezono *et al.* (2000) have also extended their calculations to the layered manganites, including orbital ordering, spin canting, and c-axis lattice deformation. The results are in qualitative agreement with experiment. This model includes on-site Coulomb interactions, but ignores intrasite repulsion. A calculation by Mishra *et al.* (1997) suggests such terms favor the antiferromagnetic phase near $x=1/2$.

A quite different approach has been taken by Yunoki and co-workers (Yunoki, Hu *et al.*, 1998; Yunoki, Moreo *et al.*, 1998) via Monte Carlo simulation. The model includes two e_g orbitals, the usual Kondo Hamiltonian for the double exchange model, and Jahn-Teller coupling to classical phonons. The core spins are assumed to be classical. In chains up to 18 sites in length, the carrier density is found to be a discontinuous function of the chemical potential, suggesting phase separation. Extended to clusters of 4^2 sites, the system still exhibits phase separation. Above a critical value of the Jahn-Teller coupling λ, there is separation between a hole-rich ferromagnetic phase and hole-poor antiferromagnet, as shown in Fig. 20; note that $\langle n \rangle$ here is $1-x$ in our notation. This model does not include long-range Coulomb interactions which should prevent macroscopic separation between doped-in holes and their Ca^{2+} or Sr^{2+} donor sites. This point is discussed in a review article by Moreo *et al.* (1999), where it is suggested that either droplets or polarons may be the most likely configuration. It is not clear the degree to which these 2D Monte Carlo results carry over to 3D manganites.

Density-functional methods have been applied to $LaMnO_3$ and $CaMnO_3$ by Satpathy *et al.* (1996a, 1996b). For $LaMnO_3$ the splitting between t_{2g} and singly occupied e_g levels is found to be 2.0 eV, with a 1.5 eV Jahn-Teller splitting between $d_{3z^2-r^2}$ (lower) and $d_{x^2-y^2}$ orbitals. Both the experimental results and the calculations of Maezono suggest that a linear combination of these is required in the ground state. The bandwidth is found to
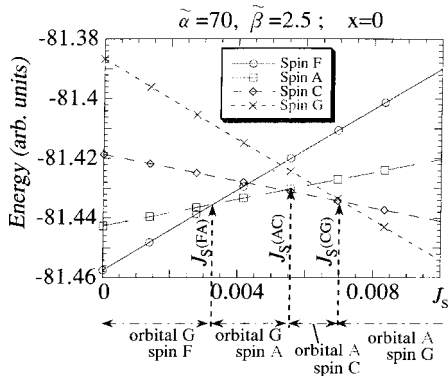

FIG. 19. Free energies for each spin alignment as a function of the antiferromagnetic interaction J_S between t_{2g} spins at $x=0$. The energy parameters are chosen to be $\tilde{\alpha}=70$ and $\tilde{\beta}=2.5$ [case (A)]. These correspond to the orbital structures shown in Fig. 7. From Maezono *et al.*, 1998b.
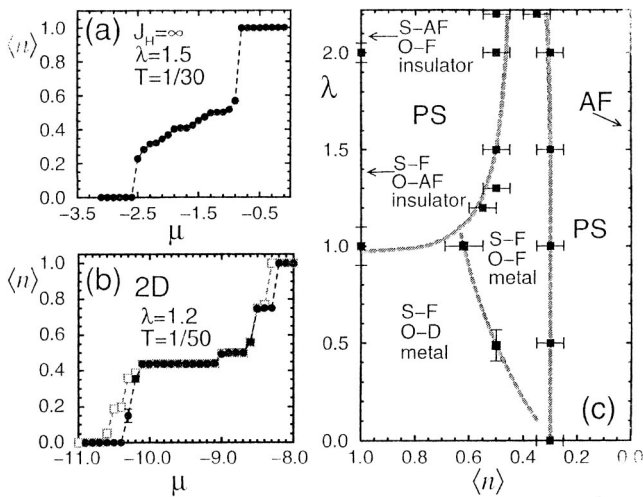
FIG. 20. Monte Carlo simulations of double exchange models with scaled Jahn-Teller interaction parameter λ: (a) Charge per site $\langle n \rangle$ vs chemical potential μ in the limit that the Hunds' exchange $J_H = \infty$, using $\lambda = 1.5$, antiferromagnetic coupling $J' = 0.05$; (b) μ at $\lambda = 1.2$ using a 42-site cluster and at $T = 1/50$. The two sets of points that produce the hysteresis loops are obtained by increasing and decreasing μ using $\sim 10^4$ sweeps at each μ; (c) phase diagram of the 2D model at $J_H = 8.0$, $J' = 0.05$. Jumps that appear in (b) are signatures of phase separation (PS). The phases are denoted S-F and S-AF (FM- and AFM-spin order, respectively) and O-D, O-F, and O-AF (disordered, uniform, and staggered orbital order, respectively). From Yunoki, Moreo, and Dogotto, 1998.

be approximately 1.5 eV, with a small gap at the Fermi energy. On doping, the $3z^2 - r^2$ band is emptied, leading to the metallic state. Similar results have been reported by Pickett and Singh (1996, 1997a, 1997b).

There remain doubts as to which aspects—double exchange, Jahn-Teller effects, polarons, phase separation, among others—are essential to produce a minimal theoretical picture of the manganites. The different contributions are discussed in a recent survey by Loktev and Pogorelov in which they search for common elements needed to produce a strongly field-sensitive metal-insulator transition (Loktov and Pogoretov, 2000). They conclude that the coexistence of various spatial scales, a strong competition between magnetic, orbital, and lattice ordering, and the tendency toward the formation of domains with sharply contrasting properties must remain central factors in any eventual theory.

## C. Ferromagnetic regime, 3D materials

By far, the most attention has been directed to those compositions that have a low-temperature, metallic, ferromagnetic state. Such a phase is a common feature in the phase diagram of the mixed manganites $A_{1-x}A'_x MnO_3$, where $(A, A') = (La, Ca)$, (La, Sr), (La, Ba), (La, Pb), (Sm, Sr), and (Nd, Sr) to mention some of them, for values of x close to 3/8 and extending from 0.2 to 0.5. The metallic state was studied to some extent in the past but not until recently were the intrinsic properties identified and separated from sample-dependent

ones. At low temperatures, the metallic state is characterized by almost fully spin-polarized bands (Park et al., 1998) and a relatively high residual electrical resistivity in the range 50–80 $\mu\Omega$ cm.

1. Magnetic properties

Perhaps the simplest question about the ferromagnetic regime in manganites, and one we should be able to answer, is to what extent are manganites standard Heisenberg-like ferromagnets? Magnetization vs magnetic field results in films of $(La, Ca)MnO_3$ reveal typical hysteresis loops with coercivity H_c of about 30–50 Oe and a saturation field H_S close to 1/2 T (McCormack et al., 1994). The saturation magnetization at $T \approx 0$ matches well the spin only value expected from all $3d$ electrons present in manganese ions: $M_S = x \times Mn^{3+}(S = 4/2) + (1-x) \times Mn^{4+}(S = 3/2) = 4x\mu_B + 3(1-x)\mu_B$ for concentrations $x \approx 0.3$. When doping is lower than 0.2 or larger than 0.5, the saturation magnetization vanishes very quickly, Fig. 2 (Jonker and van Santen, 1950). Measurements in $La_{0.67}(Pb, Ca)_{0.33}MnO_3$ single crystals performed by the authors (Jaime et al., 1998) reveal that the magnetization decreases when the temperature is increased as expected for spin-wave excitations, i.e., $M(T) = M(0) - BT^{3/2} - CT^{5/2} \cdots$ where $B = 0.0587g\mu_B(k_B/D)^{3/2}$ and D is the spin-wave stiffness constant. At temperatures one order of magnitude lower than the Curie temperature the $T^{3/2}$ term dominates the temperature dependence of M, but at $T_C/2$ higher power terms take over, and at T_C the magnetization vanishes abruptly deviating from Heisenberg-like behavior, similar to data obtained in Ca-free single crystals [Fig. 5(a)]. The stiffness constant determined from the magnetization measured in a field of 10 kG is $D = 165$ meV Å^2 in very good agreement with neutron-diffraction data.

Neutron-diffraction studies in the manganites started with the work by Wollan and Koehler (1955) who measured $La_{1-x}Ca_x MnO_3$ for various compositions. They found pure ferromagnetic behavior only in the narrow composition range $0.25 < x < 0.4$, confirming Jonker's results on the composition dependent magnitude of the saturation moments. They did not study the temperature dependence in detail. During the last five years, neutron-scattering techniques were exploited to study the manganites in greater detail, and proved to be both extremely interesting and highly nontrivial. At low temperatures and in all compositions, the magnetic inelastic spectra, i.e., energy scans at constant momentum transfer Q, show typically ferromagnetic spin-wave peaks with essentially zero gap and a quadratic dependence on Q at small Q (Lynn et al., 1996; Fernandez-Baca et al., 1998). Well below T_C the spin-wave excitations decrease in energy and increase in amplitude when the temperature is increased as expected, Fig. 21. However, as the temperature approaches T_C, a new feature develops in the spectrum, consisting of a zero energy quasielastic component also known as the central component. The

La$_{0.67}$Ca$_{0.33}$MnO$_3$
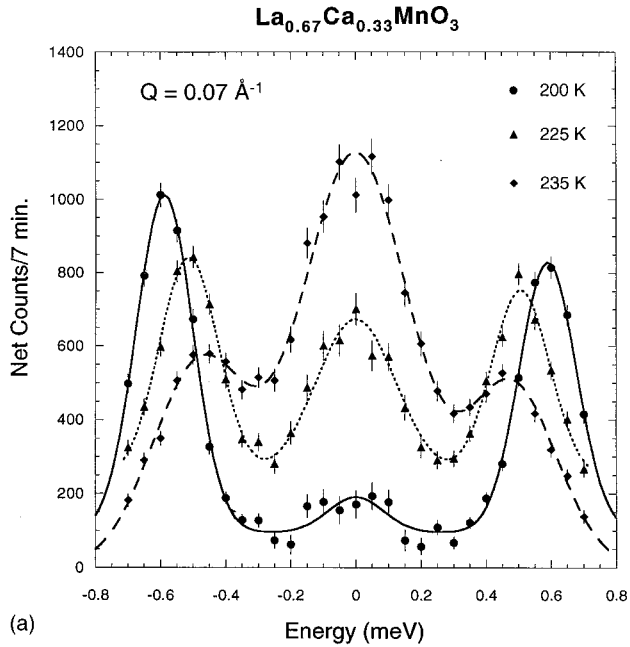
(a)
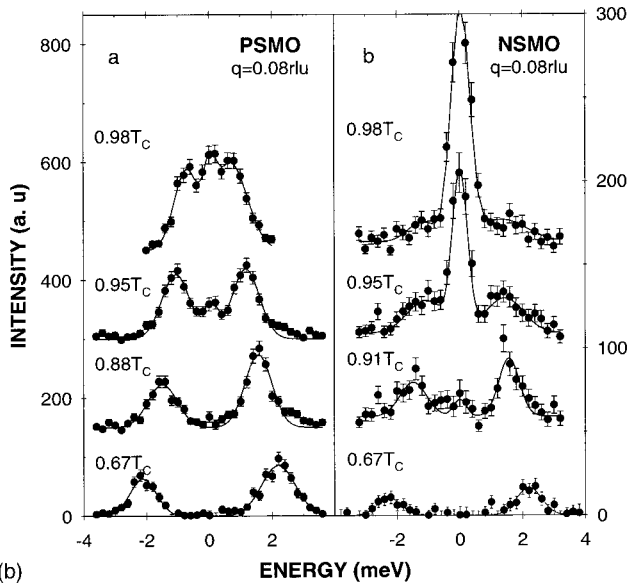
(b)

FIG. 21. Magnetic inelastic neutron scattering below T_C (a) La$_{1-x}$Ca$_x$MnO$_3$ for $x=1/3$ at a momentum transfer $Q=0.07\,\text{Å}^{-1}$. At 200 K the spectrum is dominated by the spin waves in both energy gain and loss. However, as $T \rightarrow T_C$, a quasielastic (near $E=0$) component develops and grows to dominate the spectrum (Lynn *et al.*, 1997). (b) Similar energy scans for Pr$_{2/3}$Sr$_{1/3}$MnO$_3$ (PSMO) and Nd$_{2/3}$Sr$_{1/3}$MnO$_3$ (NSMO) at momentum transfer $q=0.08$ (in reciprocal-lattice units). From Fernandez-Baca *et al.*, 1998.

central component, more notorious in those compositions with lower T_C, persists at least up to $1.25T_C$ with little T dependence above T_C and follows the quadratic dependence in Q expected for spin diffusion. The magnetic nature of the central mode has been verified with measurements in magnetic fields. As the magnetic field is increased at constant temperature, the central mode is suppressed and the spin-wave components sharpen as they increase in energy and intensity, Fig. 22 (Lynn *et al.*, 1997). The temperature dependence of the quasielastic
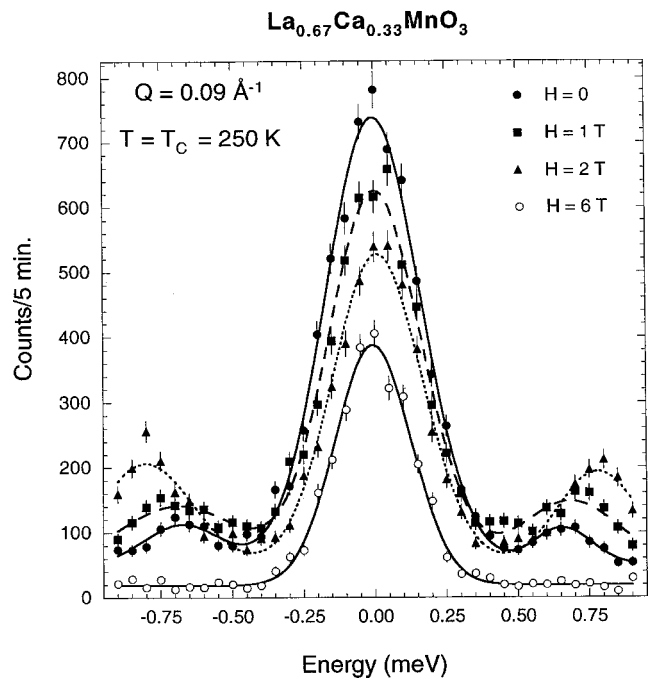
La$_{0.67}$Ca$_{0.33}$MnO$_3$

FIG. 22. Inelastic neutron-scattering spectra at 250 K (T_C) and $Q=0.09\,\text{Å}^{-1}$ as a function of applied field H. At this temperature there are still spin waves present, but the spectrum is dominated by the quasielastic scattering. In a field of 2 T, the spin-wave signal increases in intensity and sharpens, while the quasielastic response decreases. At 6 T, the spin-wave peaks have moved out of the range of the energy scan. From Lynn *et al.*, 1997.

peak is anomalous. For typical isotropic ferromagnets, such as Ni, Co, Fe any quasielastic scattering below T_C is too weak to be observed directly in the raw data (Vasiliu-Doloc *et al.*, 1998), while in some manganites this feature starts to dominate at temperatures well below T_C. These results together suggest a correlation between two mechanisms (spin waves on one side and quasielastic neutron-scattering centers, possibly small polarons, on the other) that dominate different temperature, ranges (low and high temperatures, respectively) and coexist in an extended region around T_C. We shall discuss both the high-temperature regime and the coexistence region in detail later.

The energy dispersion for spin waves has also been measured in detail, and from it the spin-wave stiffness constant was calculated by fitting the low-Q region to the expression $E=\Delta+D(T)Q^2$ for a number of compounds (Fernandez-Baca *et al.*, 1998). Neutrons do not detect a measurable energy gap Δ in the spin-wave dispersion relation; based on the experimental errors an upper limit has been estimated not to exceed 0.05 meV, which indicates that manganites are soft isotropic ferromagnets, comparable to very soft amorphous ferromagnets. As the temperature is increased and the spin-wave energy renormalizes, the stiffness constant decreases following a law expected for two-magnon processes (Mattis, 1981),

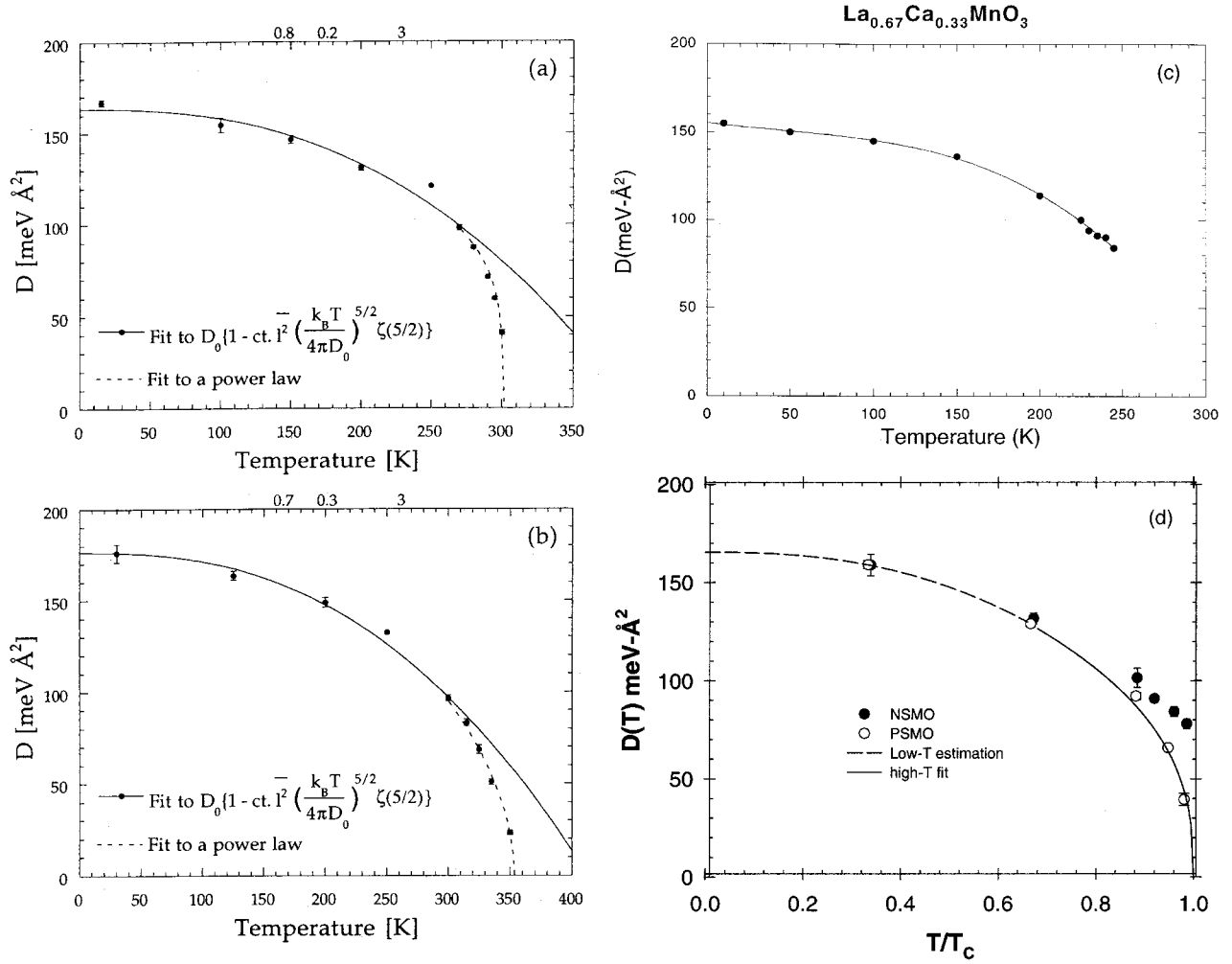$$D(T)=D(0)(1-A\,T^{5/2}),\qquad(8)$$

FIG. 23. Spin-wave stiffness coefficient D in $E = E_0 + Dq^2$ as a function of temperature: (a) in $La_{0.8}Sr_{0.2}MnO_3$; (b) in $La_{0.7}Sr_{0.3}MnO_3$. (c) in $La_{0.67}Ca_{0.33}MnO_3$ (d) in $Nd_{0.7}Sr_{0.3}MnO_3$ (NSMO) and $Pr_{0.63}Sr_{0.37}MnO_3$ (PSMO). In (a) and (b), the solid curves are fits to the usual Bloch law. D appears to vanish at the ferromagnetic transition temperature, as expected for a conventional ferromagnet; the dashed curves are fits to a power law in $(1 - T/T_C)$. In (c) D does not vanish at the ferromagnetic transition temperature, in contrast to the behavior of conventional ferromagnets (Lynn *et al.*, 1996). In (d) the spin-wave stiffness coefficient vs T/T_C vanishes at T_C for PSMO (open circles), but not for NSMO (solid circles). The solid line is the fit to the mode-mode coupling and hydrodynamic theories at high temperatures. The dashed line is an extrapolation to $T=0$ from the low-temperature mode-mode coupling theory. From Fernandez-Baca *et al.*, 1998.

where

$$A = (v_0 \overline{l^2} \pi/S)(k_B/4\pi D_0)^{5/2} \zeta(\tfrac{5}{2}), \tag{9}$$

v_0 is the unit-cell volume, S is the manganese spin, $\zeta(\tfrac{5}{2})$ is the Riemann zeta integral, and $\overline{l^2}$ is a parameter which gives the mean-square range of the exchange interaction, usually comparable to the square of the lattice parameter a^2. As a rule the stiffness constant decreases when the temperature is increased, as predicted by this formalism, only at low temperatures, and deviates from it as the temperature reaches T_C. The temperature dependence in the transition region differs for LaSr and LaCa compounds. For LaSr it is well described by an expression of the form $D(T) \sim [(T - T_C)/T_C]^{\nu - \beta}$ with the critical exponent $(\nu - \beta)$ very close to the value observed in 3D ferromagnets like iron, cobalt, and nickel (Vasiliu-Doloc *et al.*, 1998). For LaCa compounds, the stiffness constant seems to remain finite at T_C, a result that clearly goes beyond standard ferromagnetism, as seen in Fig. 23.

Computation of the spin-correlation length from neutron measurements of the static wave-vector-dependent susceptibility reveals that while the correlation length diverges at $T_C = 300.9$ K for $Pr_{0.63}Sr_{0.37}MnO_3$, it remains finite and around 20 Å down to $0.95 T_C = 0.95 \times 197.9$ K for $Nd_{0.7}Sr_{0.3}MnO_3$. It has been proposed (Fernandez-Baca *et al.*, 1998) that magnetism alone cannot explain the exotic spin dynamical properties of these systems and that the increased electron-lattice coupling plays a role. Support for these claims is found in the energy dispersion relation for spin waves. Indeed, when studied in all the way to the zone boundary an anomalous softening/broadening is found in LaCa compounds while the energy dispersion relation for LaSr compounds is
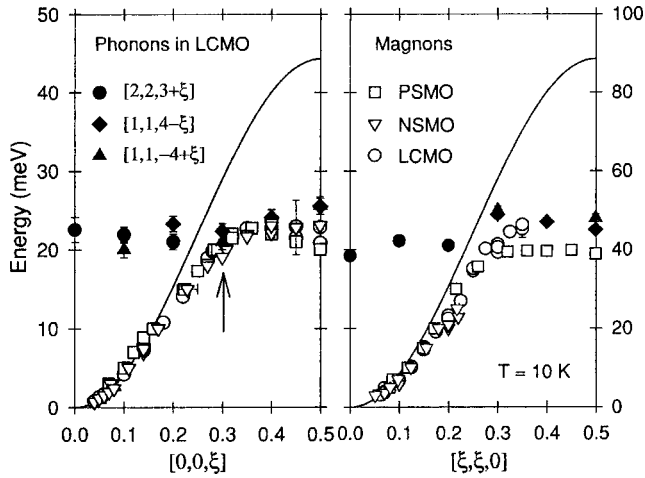
FIG. 24. Magnon dispersion curves open (symbols) along $[0,0,\xi]$ and $[\xi,\xi,0]$ directions for PSMO, NSMO, and LCMO as in Fig. 23 at 10 K. Superposed on these are optical-phonon curves (solid symbols) for LCMO. The solid lines are a fit of a nearest-neighbor spin-wave model to the data for $\xi < 0.1$. The spin waves become strongly damped and nondispersive once their energy intersects the optical-phonon branches. From Dai, Huang *et al.*, 2000.

not anomalous. The softening and broadening cannot be explained by the double exchange mechanism; in fact, no correlation between the Curie temperatures and dispersion relation for LaCa, NdSr, and PrSr compounds is found. On the other hand, a remarkable correlation with optical-phonon modes, as shown in Fig. 24, strongly suggests that magnetoelastic coupling (possibly between magnons and Jahn Teller modes) is responsible for the softening (Dai *et al.*, 2000). A theoretical study shows that in fact phonon-magnon interactions can result in magnon broadening in low-T_C (narrow bandwidth) manganites provided a large enough magnon-phonon interaction is present (Furukawa, 2000), an interaction that could at least in principle originate in the fact that the metallic state in these compounds is in close proximity to the charge ordered insulating state. In conclusion, La-Sr, and perhaps Pr-Sr, manganite can be well described as a Heisenberg ferromagnet, but other manganites cannot. It may be that in those compounds with smaller tolerance factors and correspondingly lower transition temperatures, large phonon-magnon interactions and Jahn-Teller modes begin to play an important role.

2. Electrical transport properties

The low-temperature transport properties of manganites have been studied in some detail only in recent years. Those properties, which require a finite electric current through the sample, have proven to be sensitive to extrinsic effects as grain boundaries and magnetic domain boundaries. These effects are related to grain boundary charge/spin tunneling-limited transport and have attracted a great deal of attention because of the potential applications of manganites as spin-valve-like devices. A large low-field/low-temperature magnetore-
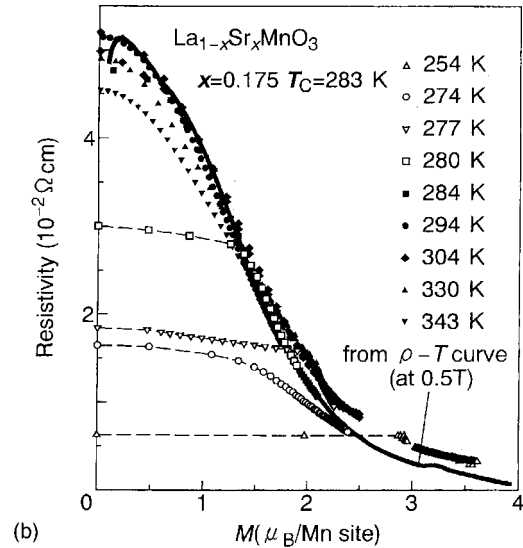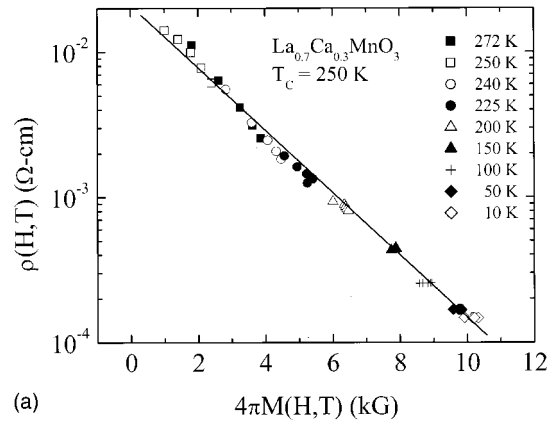

(a)

(b)

FIG. 25. Two different treatments of the dependence of the resistivity $\rho(H,T)$ on the magnetization $M(H,T)$: (a) an exponential dependence in $La_{0.7}Ca_{0.3}MnO_3$, using data taken at $H = 10, 20, 30, 40$, and 50 kOe that progress, respectively, from low to high M values; solid line, a least-squares fit to the data (Hundley *et al.*, 1995); (b) similar analysis for a $La_{1-x}Sr_xMnO_3$ crystal ($x = 0.175$). The points are obtained from the $\rho(B)$ and $M(B)$ curves at respective temperatures. The solid line is obtained using the $\rho(T)$ and $M(T)$ data in a field of 0.5 T. The behavior is quadratic at small values of the magnetization. From Tokura and Tomioka, 1999.

sistance can be obtained when samples are polycrystals prepared with conveniently small crystallographic grains (Schiffer *et al.*, 1995). This spin-tunneling limited magnetoresistance is based on good spin polarization of individual grains or magnetic layers in the system and vanishes as thermal entropy kills intragrain polarization, more or less rapidly as practical temperatures are reached (Hwang *et al.*, 1996). Epitaxial films do not show low-field magnetoresistance (Li, Gupta *et al.*, 1997). There is also a high-field magnetoresistance component associated with the grain boundaries that is essentially temperature independent between 5 and 280 K, and is most likely related to alignment of spins in a magnetically disordered region near the grain boundaries. The low- and high-field magnetoresistance, studied as functions of the grain size by the group in Barcelona

(Balcells *et al.*, 1998), show saturation in low fields and monotonic increase in high fields for grain sizes equal to or smaller than 1 μm, revealing the distinct origin of both contributions. $La_{2/3}Sr_{1/3}MnO_3$ samples, where grain sizes are 30 nm or smaller, do not show a metallic electrical resistivity in any temperature range, not even in the low-temperature ferromagnetic phase. This behavior has been attributed to a Coulomb blockade contribution to the resistivity, similar to that observed in such other half metallic systems as CrO_2 (Coey *et al.*, 1998).

The intrinsic low-temperature transport properties of ferromagnetic manganites are far from trivial, and in fact have proven to be a challenge. The intrinsic magnetoresistance of these compounds vanishes at low temperatures, and correlates well with the magnetization, i.e., saturated magnetization=null magnetoresistance. A detailed study of these correlations indicates that the resistivity and magnetization are related by the empirical expression $\rho(H,T)=\rho_m \exp[-M(H,T)/M_0]$ over a wide temperature range all the way up to the Curie temperature (Hundley *et al.*, 1995), clear evidence of the double exchange interaction at play [Fig. 25(a)]. However, in contradiction to the exponential fit, $\rho(H,T)$ is found to decrease as the square of the magnetization near T_C (Tokura and Tomioka, 1999), as seen in Fig. 25(b).

As a consequence of the double exchange mechanism, charge carriers at low temperatures are spin-down holes moving in an $S=5/2$ background. There are no propagating up-spin hole states in the $S=2$ manifold; they only exist localized on sites at which the t_{2g} core is not ferromagnetically aligned. Therefore single-magnon scattering processes, which cause the resistivity of conventional ferromagnets to vary as T^2, are suppressed. Kubo and Ohata extended the standard perturbation calculation of Mannari (1959) to consider two-magnon processes, predicting a leading $T^{9/2}$ temperature dependence of the resistivity. However, a dominant T^2 contribution is universally observed in the manganites, and has usually been ascribed to electron-electron scattering (Urushibara *et al.*, 1995; Schiffer *et al.*, 1995; Snyder *et al.*, 1996). However, there is a general relationship between the coefficient A of the T^2 contribution to the resistivity and the electronic heat-capacity coefficient γ, pointed out by Kadowaki and Woods (1986). In the manganites, the ratio A/γ^2 is more than an order of magnitude larger (Jaime *et al.*, 1998) than the Kadowaki-Woods ratio for metals in which strong electron-electron interactions are present. This suggests that a different mechanism is involved. In a recent paper (Jaime *et al.*, 1998) resistivity data on single crystals of composition $La_{0.67}(Ca,Pb)_{0.33}MnO_3$ are discussed, demonstrating that the quadratic temperature dependence is rapidly suppressed as the temperature is reduced. They argue that the observed T^2 contribution reflects the reappearance of minority spin states that are accessible to thermally excited magnons. Spin-polarized photoemission data, taken on films exhibiting square hysteresis loops, indicate 100% spin polarization only at low temperatures, decreasing gradually as the temperature is in-
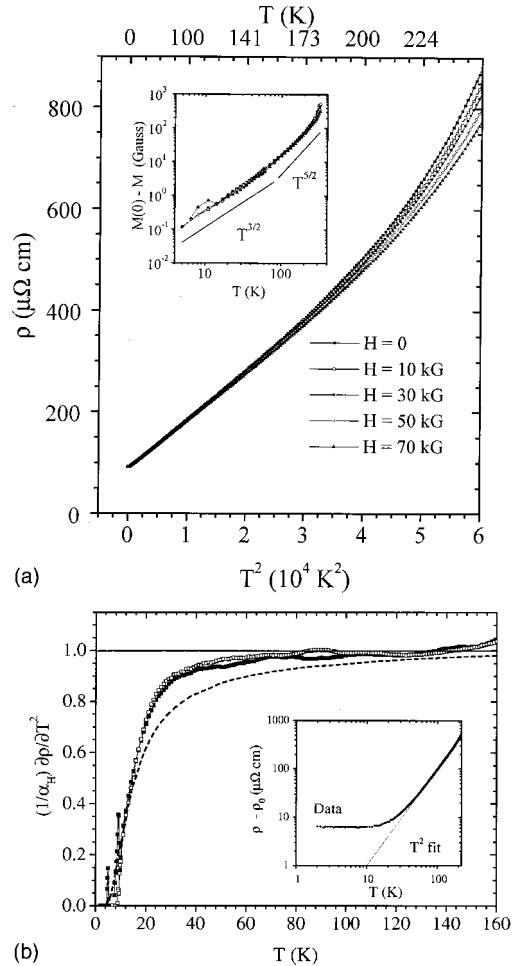

FIG. 26. Low-temperature behavior of the resistivity: (a) resistivity vs T^2 for magnetic fields up to 70 kG in a thin-film sample of $La_{2/3}Ca_{1/3}MnO_3$. (b) Numerical derivative of the data, $\alpha_H^{-1}\partial\rho/\partial T^2$; ■, for zero field; □, for 70 kG dashed curve, the same quantity calculated for the magnon model with $Dq_{min}/k_B=44$ K. Inset: raw data minus calculated residual resistivity (solid squares) and least-squares curve (dotted line) vs temperature. The nonadditivity of the residual resistivity and the quadratic component violate Matthiesson's rule. From Jaime *et al.*, 1998.

creased (Park *et al.*, 1998). Single crystals, which have essentially no hysteresis, would be expected to depolarize more rapidly. Jaime *et al.* have extended Mannari's calculation to the situation in which a minimum magnon energy is required to induce spin-flip transitions. At temperatures well below that energy, single magnon scattering is suppressed exponentially as predicted by Kubo and Ohata. The treatment is in the context of the relaxation time approximation while a proper theory would consider lifetime effects from magnon scattering using Furukawa's many-body approach. Nonetheless, the results are in qualitative agreement with the data. Band-structure calculations (Pickett and Singh, 1996; Singh and Pickett, 1998) also indicate that minority spin states persist at E_F, even at $T=0$ K.

Figure 26(a) shows the resistivity of a single-crystal sample of $La_{0.67}(Ca,Pb)_{0.33}MnO_3$ with $T_C=300$ K, vs the

square of the temperature in fields up to 70 kOe. The data show a dominant T^2 temperature dependence with evidence of a small T^5 contribution (10 $\mu\Omega$ cm at 100 K). A calculation of the $T^{9/2}$ contribution predicted by Kubo and Ohata for two-magnon processes predicts only 0.5 $\mu\Omega$ cm at 100 K with appropriate parameters. It is likely, then, that this is the usual T^5 contribution from electron-phonon processes. The inset to Fig. 26(b) shows that the data do not follow a T^2 dependence to the lowest temperatures. Rather, they deviate gradually from the curve $\rho_0 + \alpha(H)T^2$, fit over the range $60 \lesssim T \lesssim 160$ K, before saturating at an experimental residual resistivity $\rho_0^{\text{exp}} = 91.4$ $\mu\Omega$ cm, comparable to values observed by Urushiba et al. (1995), but $\sim 7\%$ larger than ρ_0. This conclusion is not changed by including the T^5 contribution. Fits to data taken in various fields show that α_H decreases with increasing field and is the source of the small negative magnetoresistance at low temperatures. To quantify the disappearance of the T^2 contribution, Jaime et al. numerically differentiate the data, plotting $\alpha(H)^{-1} d\rho/d(T^2)$ in Fig. 26(b). The T^5 contribution, not subtracted, gives a slight upward curvature to the data at higher temperatures.

The usual calculation of the electron-magnon resistivity (Mannari, 1959) has been extended to allow the minority-spin subband to be shifted upward in energy such that its Fermi momentum differs by an amount $q_{\min}$ from that of the majority subband. This should be a reasonable approximation in the intermediate temperature regime in which both minority and majority bands have substantial densities of states at E_F. The one-magnon contribution can then be written as $\rho_\epsilon(T) = \alpha_\epsilon T^2$, where

$$\alpha_\epsilon = \frac{9\pi^3 N^2 J^2 \hbar^5}{8 e^2 E_F^4 k_F} \left(\frac{k_B}{m^* D}\right)^2 I(\epsilon). \tag{10}$$

In this equation, NJ is the electron-magnon coupling energy which is large and equal to $\mu = W - E_F$ in the double exchange Hamiltonian of Kubo and Ohata; $2W$ is the bandwidth. The magnon energy is given by Dq^2, and we have defined

$$I(\epsilon) = \int_\epsilon^\infty \frac{x^2}{\sinh^2 x} dx. \tag{11}$$

The lower limit is $\epsilon = Dq_{\min}^2/2k_B T$, where $Dq_{\min}^2$ is the minimum magnon energy that connects up- and down-spin bands; this result reproduces Mannari's calculation in the limit $\epsilon \to 0$, and Kubo and Ohata's exponential cutoff for large ϵ. At high temperatures, the lower limit of the integral in Eq. (10) can be set equal to zero, leaving only the coupling energy $NJ = W - E_F$ as a parameter. Equating the calculated value to the experimental α fixes the coupling to be $W - E_F \approx 1.0$ eV or $W \approx 1.5$ eV, in good agreement with a virtual crystal estimate of the bandwidth (Pickett and Singh, 1997a). Figure 26(b) shows the experimental data $(1/\alpha_H)\partial\rho/dT^2$, and $\alpha_0^{-1} d(\alpha_\epsilon T^2)/d(T^2)$ assuming $D(0)q_{\min}^2 = 4$ meV and including the temperature dependence observed experimentally, $D(T)/D(0) = (1 - T/T_C)^{0.38}$ (Fernandez-Baca et al., 1998) which is important only at higher tem-

peratures. While the curve follows the data qualitatively, it is clear that the minimum magnon energy is substantially larger than 4 meV at low temperatures, and decreases with increasing temperature.

This extension of the magnon resistivity calculation to spin-split parabolic bands greatly oversimplifies the changes in the minority-spin band that accompany magnetic ordering. As a consequence, the calculation cannot be expected to represent accurately the cutoff of magnon scattering due to loss of minority-spin phase space. Nonetheless, the rapid suppression of the T^2 contribution to the resistivity and the agreement between its magnitude at higher temperatures with parameters expected for the manganites confirm the basic picture. In the intermediate temperature regime, $0.2 \lesssim T/T_C \lesssim 0.5$ here, the manganites appear to be normal metallic ferromagnets with the resistivity dominated by spin-wave scattering. At lower temperatures, the increasingly half metallic character of the material is manifested by a temperature dependent cutoff of the spin-wave scattering process, leaving in its wake only residual resistivity from the intrinsic doped-in disorder and indistinguishable phonon and two-magnon contributions. As these heavily doped materials have significant disorder and large residual resistivities, we recall that strongly disordered materials also exhibit T^2 regimes below half the Debye temperature (Nagel, 1977). This result, however, an extension of the Ziman theory of liquid metals, sets an upper limit of $\alpha T^2/\rho_0 \simeq 0.03$ before the resistivity changes to a linear temperature dependence; our ratio is unity at 100 K with no evidence for a linear regime. We conclude that the quadratic temperature dependence is not due to phonon scattering in a strongly disordered material.

An alternative explanation of the low-temperature electrical transport is based on an argument by Alexandrov and Bratkovsky that polarons remain the predominant charge carriers even below T_c (Alexandrov and Bratkovsky, 1999), and that transport is dominated by polaron tunneling. As a consequence, the low-temperature resisitivity is predicted to behave as

$$\rho(T) = \rho_0 + E\omega_s/\sinh^2(\hbar\omega_s/2k_B T), \tag{12}$$

where E is a constant and ω_s is the softest optical mode. This expression gives a T^2 contribution above $T = \hbar\omega_s/k_B$, which as been determined to be 86 K from fitting to data on polycrystalline $La_{0.8}Ca_{0.2}MnO_3$ (Zhao et al., 2000). However, as we have seen in Fig. 24, the lowest optical mode has an equivalent temperature of 250 K, considerably higher than the polaron picture would indicate.

In a recent theoretical effort, Furukawa (2000) has discussed the problem of quasiparticle lifetimes due to magnon scattering processes in half metals, taking into account the effects of spin fluctuations. He argues that there is no minority-spin Fermi surface in a half metal at zero temperature but that spin fluctuations induce a minority band at finite temperatures. At low temperatures, then, the one-magnon scattering self-energy depends on spin fluctuations and increases as T departs from zero.

This nonrigid band picture allows unconventional one-magnon scattering processes to arise as the minority band is created and occupied, provided the incoherent limit $\delta m = [(M(0) - M(T))/M(0)] \ll 1$ holds. In this limit the resistivity is expected to be proportional to the cube of the temperature divided by the spin-wave stiffness constant $\rho_{incoherent} \propto (T/D)^3$, where D is defined via $\omega_q = Dq^2$. As the temperature increases, δm cannot be considered small and conventional magnon scattering is recovered (coherent limit), where the usual T^2 dependence in the resistivity is expected. The crossover temperature is estimated by $T^* \simeq [2M(0)/0.06W]^2 D^3$ where W is the bandwidth, $M(0)$ the saturation magnetization, and D the spin-wave stiffness. Reasonable parameters for manganites result in $T^* \approx 50$ K, in good agreement with the temperature where the T^2 regime appears in $La_{0.67}(Ca, Pb)_{0.33}MnO_3$ (Jaime *et al.*, 1998), $La_{1-x}Sr_xMnO_3$ ($0.2 < x < 0.4$) (Furukawa *et al.*, 2000), and bandwidth controlled $La_{0.67}(Ca, Sr)_{0.33}MnO_3$ (Broussard *et al.*, 1999). Similar results have also been observed in a classical half metal, CrO_2 (Watts *et al.*, 2000).

The Hall effect in the ferromagnetic phase of manganites is particularly puzzling, and a relatively large effort has been made to try to understand it. In ferromagnetic metallic systems, the embedded magnetic moments cause asymmetric scattering of current-carrying electrons, producing a voltage that superimposes on the usual Hall voltage, the so-called anomalous Hall voltage. The total Hall resistance ρ_{xy} can be written as

$$\rho_{xy}(B, T) = R_H(T)B + \mu_0 R_S(T) M(B, T), \quad (13)$$

where $R_H(T)$ is the temperature-dependent Hall coefficient, B is the applied magnetic field (unit demagnetization factor assumed), $R_S(T)$ is the temperature-dependent anomalous Hall coefficient, and $M(B, T)$ is the magnetization. Measurements in films of composition $La_{0.67}Ca_{0.33}MnO_3$ (Matl *et al.*, 1998; Jakob *et al.*, 1998) and single crystals of composition $La_{0.67}(Ca, Pb)_{0.33}MnO_3$ (Chun *et al.*, 1999) show an almost temperature-independent Hall coefficient R_H and strongly temperature-dependent anomalous Hall coefficient that peaks above the Curie temperature and is not simply related to the ordinary resistivity. Typical results in single-crystal samples are displayed in Figs. 27(a) and (b). Figure 27(a) shows the measured Hall resistance in magnetic fields up to 7 T, for several temperatures below and above T_C. At low temperatures (solid symbols) two different regimes (low fields≡anomalous, high fields ≡normal) are evident. Figure 27(b) shows in its inset how the two components are separated using the demagnetizing-field-corrected magnetization measured in the same samples. Also in the inset is shown the scaling of the anomalous hall coefficient with the sample resistivity. The body of Fig. 27(b) displays the calculated effective carrier concentration $n_{eff}(T) = 1/eR_H$, which show a monotonic increase as the temperature is reduced and is as large as 2.4 holes/Mn (*almost five times larger than nominal doping level*). These large values
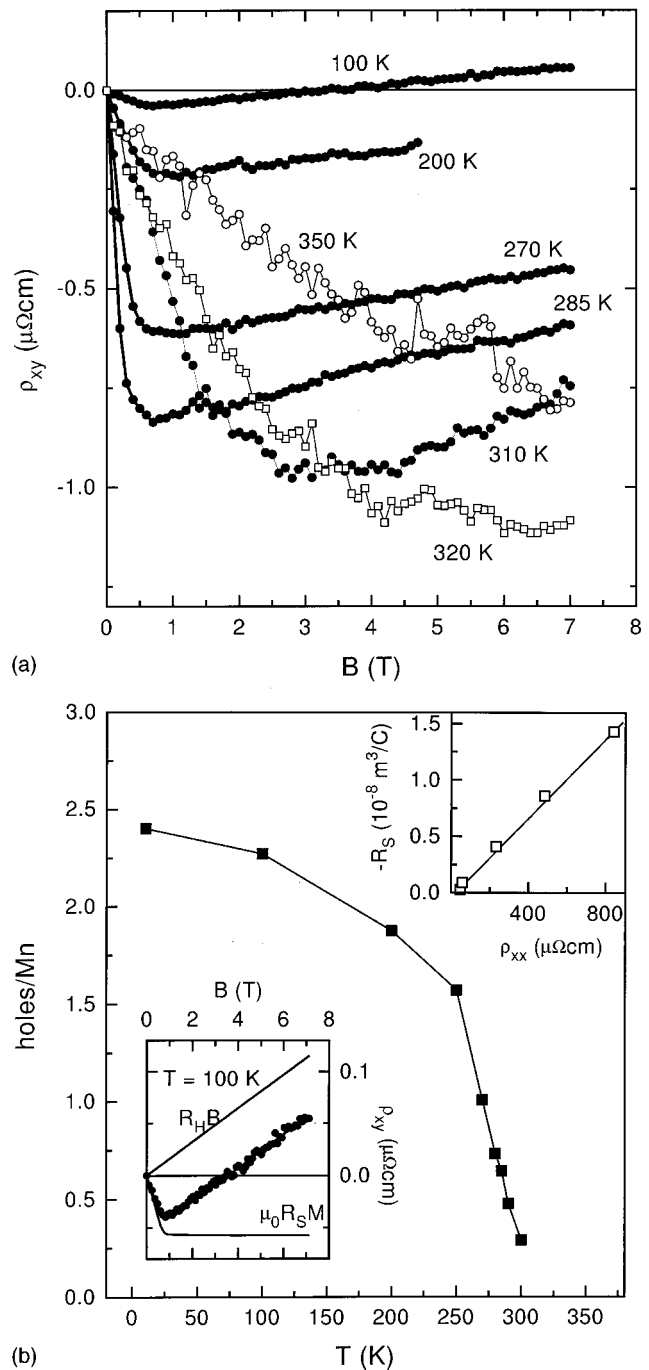

FIG. 27. Hall data taken over a wide range of fields and temperatures: (a) Hall resistivity ρ_{xy} of a $La_{2/3}(Pb, Ca)_{1/3}MnO_3$ single crystal as a function of field; (b) effective number of holes per Mn atom as a function of temperature, calculated from the data of (a), assuming the high-field slope to determine the ordinary coefficient, and $n_{eff} = e/R_0$. The lower inset shows the decomposition of ρ_{xy} into ordinary and anomalous Hall effects below T_C. The upper inset shows the linear relation between the anomalous Hall coefficient R_S and the longitudinal resistivity ρ_{xx}. From Chun *et al.*, 1999.

have been attributed to charge compensation effects. In a two-band model, the Hall coefficient is given by $R_H = (r_h n_h \mu_h^2 - r_e n_e \mu_e^2)/e(n_h \mu_h + n_e \mu_e)^2$ and the experimental values in Fig. 27(b) can be reproduced using

band-structure calculations (Pickett and Singh, 1997b) and a mobility ratio $\mu_e/\mu_h = 1.6$. The anomalous Hall coefficient and its scaling with the sample magnetization will be discussed in detail later, since it is closely related to the physics of the transition between a high-temperature state where charge carriers are localized as small polarons and the low-temperature ferromagnetic state. Interestingly, layered manganites do not show charge compensation effects and the carrier concentration deduced from Hall-effect measurements in single crystals agrees very well with the values expected from the nominal doping level. The anomalous Hall effect in layered manganites seems to scale with the resistivity, exhibiting a minimum at the same temperature where the electrical conductivity is maximal (Chun, Salamon, Jaime *et al.*, 2000), but more work needs to be done extending the measurements above the Curie temperature to be able to compare them to their 3D counterparts.

3. Thermal properties

a. Thermal conductivity of 3D materials

The thermal conductivity κ of ferromagnetic manganites, both in polycrystal (Hejtmanek *et al.*, 1997; Chen *et al.*, 1997; Cohn *et al.*, 1997) and single-crystal samples (Cohn *et al.*, 1997; Visser *et al.*, 1997), is relatively small, with room-temperature values between 1 and $3 \text{ W K}^{-1} \text{m}^{-1}$ and a low-temperature peak that never exceeds $4-5 \text{ W K}^{-1} \text{m}^{-1}$. These conductivities are 5–10 times smaller than those observed in the normal state of high-temperature superconductor single crystals at similar temperatures (Peacor *et al.*, 1991). In both systems electrons contribute a small (20–40 %) fraction of the total observed thermal conductivity κ_{tot} in the high-temperature phase. In high-temperature superconductors the mean free path of unpaired electrons increases dramatically below the superconducting transition, causing κ_e to dominate κ_{tot} somewhat below the transition before dropping at low temperatures. In manganites the transition into the metallic ferromagnetic state shows a similar effect, i.e., the thermal conductivity improves as the electrons (localized in the paramagnetic state) gain mobility in the ferromagnetic phase but κ_e remains a small fraction of κ_{tot}. Figure 28(a) displays the thermal conductivity in $La_{1-x}Ca_xMnO_3$ polycrystals for different κ values, Fig. 28(b) shows the thermal conductivity vs temperature in semilog scale for a number of polycrystal and single-crystal samples. In the low-temperature region (the high-temperature paramagnetic region will be discussed later) we notice an appreciable enhancement of the thermal conductivity in ferromagnetic compounds. The Wiedemanz-Franz law can be used to estimate the electronic contribution to the thermal conductivity κ_e in the metallic state. Such an estimate in Cohn's samples results in an electric contribution no larger than 20% of the total thermal conductivity. A similar estimate for single crystals and films of different Curie temperatures is displayed in Fig. 29(a), where it can be seen that $\kappa_e(T)$ can only qualitatively explain the low-temperature increase in κ. In order to make a quantita-
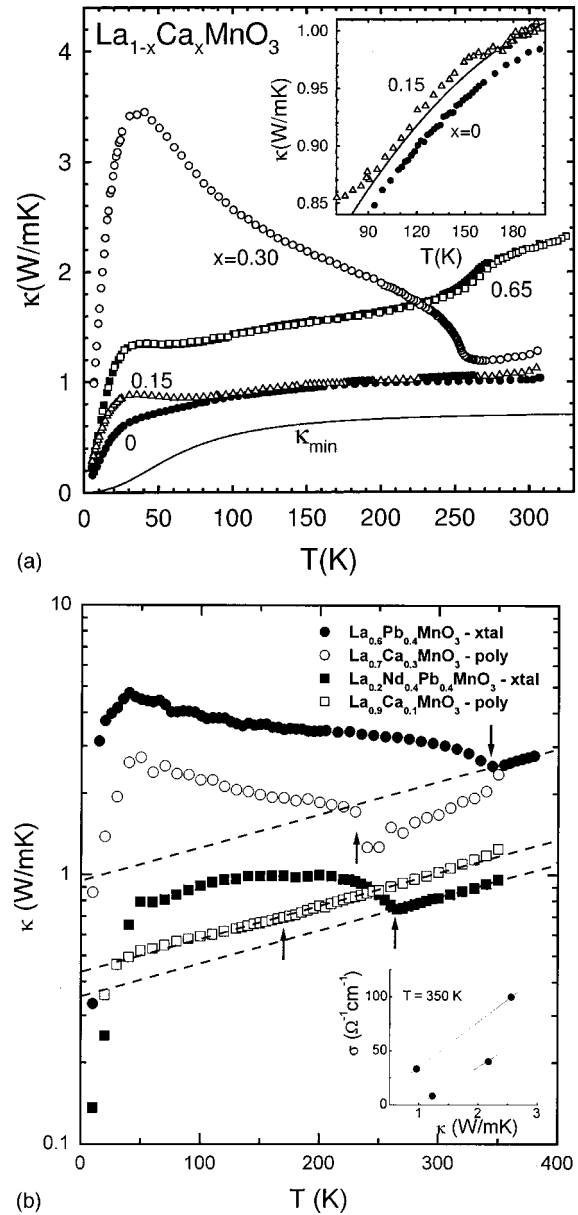

FIG. 28. Comparison of thermal conductivity for various samples: (a) thermal conductivity vs temperature for $La_{1-x}Ca_xMnO_3$ polycrystals. The inset is a magnified view of the data for $x=0$ and 0.15, showing the anomaly observed near $T_C = 170$ K for $x=0.15$. The solid line represents the data for $x=0$ shifted upward by 0.02 W/mK (Cohn *et al.*, 1997). (b) Thermal conductivity κ for four different manganite perovskite samples. The arrows denote the ferromagnetic transition temperature. The three samples possessing a sharp change in $\kappa(T)$ at T_C also undergo a metal-insulator transition. The dashed lines represent an exponential temperature dependence $\kappa = \kappa_0 \exp(T/350)$, with κ_0 values described in the text. The inset shows the electrical conductivity σ versus κ, at 350 K for the four samples. From Visser *et al.*, 1997.

tive analysis, we have taken data from Visser's report and plotted them together with the result of a Wiedeman-Franz estimate and an extrapolation of the high-temperature phonon contribution in Fig. 29(b). Here we can see that $\kappa_e(T)$ can only account for 40% of the low-temperature value by itself and about 80% of
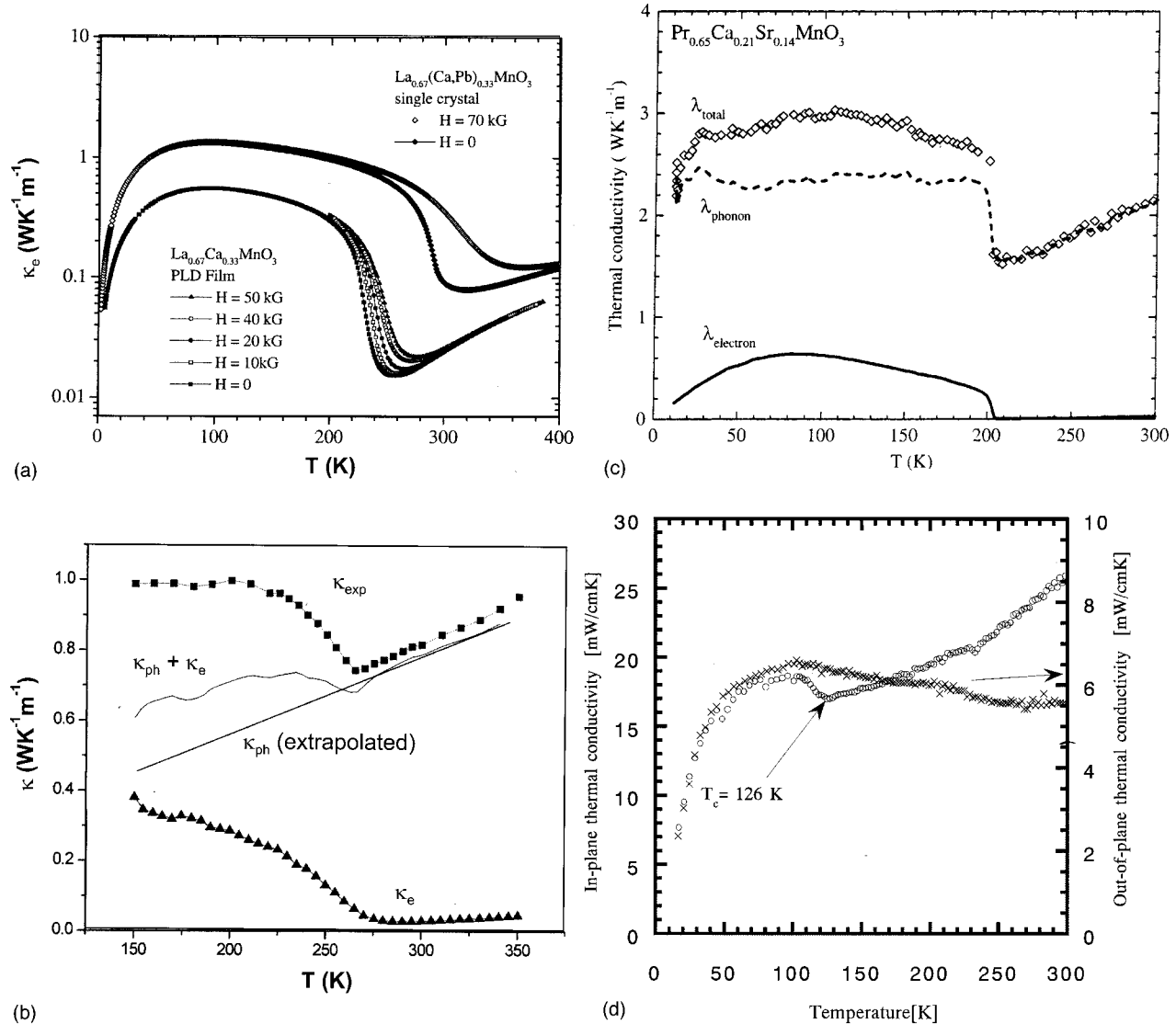
FIG. 29. Separation of thermal conductivity into electron and phonon contributions: (a) Electronic thermal conductivity calculated from electrical resistivity in a $La_{0.67}(Ca,Pb)_{0.33}MnO_3$ single crystal using the Wiedemann-Franz law. (b) Total thermal conductivity κ_{exp} for $La_{0.2}Nd_{0.4}Pb_{0.4}MnO_3$ single crystal (from Visser *et al.*, 1997), high-temperature phonon contribution κ_{ph} and electronic contribution κ_e calculated using the electrical resistivity and Wiedemann-Franz law. (c) Temperature dependence of the total thermal conductivity $\lambda_{total} = \lambda_{electron} + \lambda_{phonon}$ for a ferromagnetic ($T_C = 205$ K) $Pr_{0.6}Ca_{0.2}Sr_{0.14}MnO_3$ single crystal. For the separation of phonon and electron parts of thermal conductivity the electronic contribution was estimated using the experimental resistivity data, corrected for sample porosity and assuming the validity of Wiedemann-Franz law. (d) Similar data for a layered compound. Note different scales for in-plane and out-of-plane curves. From Hejtmanek *et al.*, 1999.

the total when added to a simple extrapolation of the high-temperature lattice contribution κ_{ph}. In Fig. 29(c) we see data for a single crystal of composition $Pr_{0.65}Ca_{0.21}Sr_{0.14}MnO_3$ (Hejtmanek *et al.*, 1999) from which it is clear that an extra contribution is missing from the picture. Two conclusions can be derived from this behavior. In the first place, the lattice thermal conductivity in the ferromagnetic manganites is lower than in the cuprates and is not limited by electron-phonon scattering. This conclusion finds support in the absence of a linear term in the low-temperature electrical conductivity. Consequently we believe that the observed κ_{ph} is small due to the presence of large cationic disorder and to the scattering of phonons against Jahn-Teller

modes (an estimate by Cohn *et al.* found that the phononic mean free path is comparable to the Mn-Mn distance ~ 4 Å). Second, because of the very nature of small magnetoelastic polarons in the paramagnetic phase, as the temperature is reduced and the charge carriers delocalize, the effective electron-phonon scattering rate decreases and both thermal conductivities (κ_e and κ_{ph}) increase in the metallic state.

b. Thermal conductivity of layered materials

The thermal conductivity of single crystal samples of the layered manganite $La_{1.2}Sr_{1.8}Mn_2O_7$ is anisotropic, as expected from the structure and the behavior of other
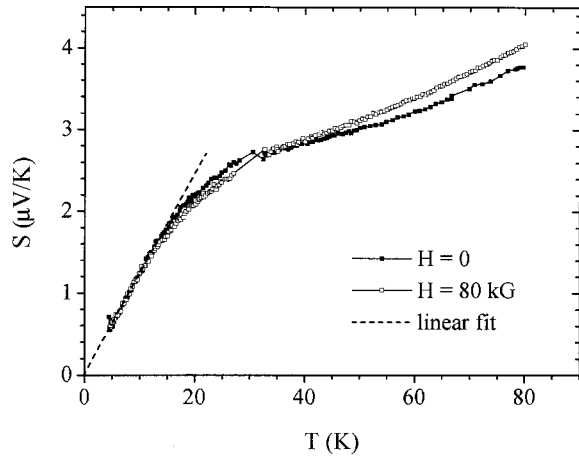
FIG. 30. The Seebeck coefficient S vs temperature for a mixed Pb-Ca-doped sample. It is positive and metal-like at low temperature, has an anomalous kink near 30 K, and develops a positive field dependence above 40 K. The dashed line is a linear fit in the low-temperature regime. From Jaime *et al.*, 1998.

transport properties (Matsukawa *et al.*, 2000). The component along the *ab* crystallographic direction increases in the ferromagnetic state as in the 3D compounds, while the component along the *c* axis shows no change. Another contribution to κ_{tot} in manganites should come from spin waves (κ_m), however, an estimate using the specific-heat anomaly ΔC at T_C results in a very small value, $\kappa_m \simeq 0.1 \, \mathrm{W\,K^{-1}\,m^{-1}}$ for polycrystal $La_{0.7}Ca_{0.3}MnO_3$ (Cohn *et al.*, 1997). Detailed measurements of the very low-temperature thermal conductivity in good single crystals should tell us more about the relative contribution from spin waves, and could help to better understand the transport properties of manganites. A discussion of the high-temperature thermal conductivity in manganites is presented in Sec. IV.

c. Thermoelectric properties and heat capacity

The Seebeck coefficient $S(T)$ provides additional information on the nature of transport at low temperatures. Figure 30 shows $S(T)$, measured on the same sample as in Fig. 26 at $H=0$ and 80 kOe. At the lowest temperatures, $S(T)$ is positive, linear in temperature, and extrapolates to zero as $T \to 0$. The field dependence is small and negative. The large slope suggests, from the Mott formula, that the resistivity is a strong function of energy at E_F. There is a sharp deviation from linear behavior in the temperature range in which the T^2 dependence of the resistivity becomes dominant and the field dependence changes sign and becomes larger. We note that the peak in the low-temperature thermopower that is regularly seen in thin-film samples is absent here, and is therefore not intrinsic to these materials. If we take the scattering to be independent of energy, which is the case below 20 K, the Seebeck coefficient can be expressed as $S(T) = (\pi^2/2e)(k_B^2 T/E_F)$ (Ashcroft and Mermin, 1976). Using the simplistic approximation of a parabolic band $E_F = \hbar^2 k_F^2/2m^*$, and spherical Fermi sur-
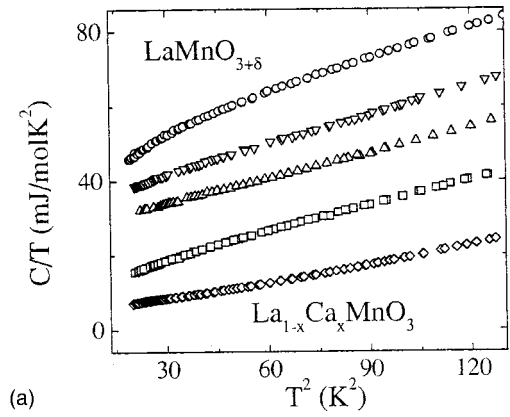
(a)
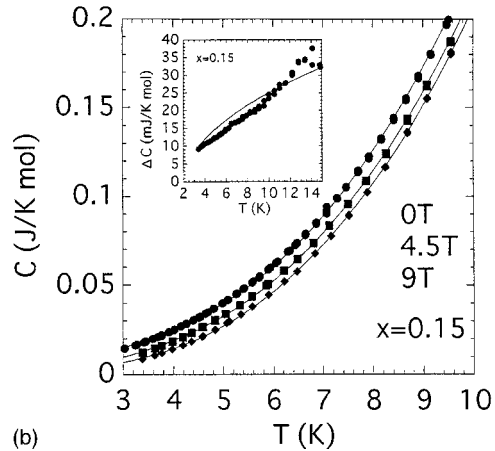
(b)

FIG. 31. Composition dependence of the heat capacity: (a) From top to bottom, low-temperature specific heat, plotted as C/T vs T^2, for $LaMnO_{3+\delta}$: $\bigcirc$, with $\delta = 0.26$; $\triangledown$, $\delta = 0.15$; $\triangle$, $\delta = 0.11$; for $La_{1-x}Ca_xMnO_3$ $\square$, $x = 0.11$ $\diamondsuit$, $x = 0.33$ Ghivelder *et al.*, 1999. (b) Specific heat C for $La_{1-x}Sr_xMnO_3$, $x = 0.15$ under magnetic fields. The inset shows reduction of C upon application of 9 T for $x = 0.15$. From Okuda *et al.*, 1998.

face $k_F^3 = 3n\pi^2$, the effective mass turns out to be $m^*/m \approx 3.7$, comparable to the value obtained from specific-heat measurements. The sharp deviation from linear behavior in the temperature range 20–40 K correlates with the onset of electron-magnon scattering which, being a spin-flip process, must involve the minority spin band, and which therefore has a different dependence on energy near E_F. Comparable behavior has been observed in CrO_2 films (Watts, 2000).

The specific heat in the ferromagnetic phase of manganites has received a great deal of attention recently. Measurements at low temperatures in $La_{1-x}Ca_xMnO_3$ have been done in polycrystalline samples (Coey *et al.*, 1995; Hamilton *et al.*, 1996; Ghivelder *et al.*, 1998). Results for $x = 0.1$, 0.33, and 0.62 are displayed in Fig. 31(a) between 4 and 10 K. Both experimental groups have attempted to fit the data using three-parameter fits of the form

$$C = C_e + C_l + C_m,$$

where C_e is the electronic contribution γT, C_l is the lattice contribution $\beta T^3 + \alpha T^5$, and C_m is the magnetic

contribution, $\delta T^{3/2}$ in the case of a ferromagnet, $\delta_2 T^2$ in the case of a standard Néel antiferromagnet. A fit to the experimental results for metallic $La_{0.67}Ca_{0.33}MnO_3$ gives $\gamma = 4.7$ mJ/mol K^2, $\beta = 0.12$ mJ/mol K^4, and $\delta = 0$ indicating the absence of a spin-wave contribution. The electronic density of states at the Fermi energy determined from the measured γ is $N(E_F) = 3\gamma/(\pi k_B)^2 = 2.0$ eV^{-1} Mn^{-1}. The lattice contribution indicates a Debye temperature $\theta_D = 430$ K. Neutron-scattering measurements (Lynn *et al.*, 1996) provide a direct measurement of the spin-wave stiffness constant $D = 170$ meV Å^2, which would yield a specific-heat magnetic term $\delta = 0.62$ mJ/mol K$^{5/2}$, equivalent to 20% of the experimental value at 5 K and above the scatter of the data. The absence of a spin-wave component in the low-temperature specific heat is not understood at present. On the other hand, measurements in the system $La_{0.7}Sr_{0.3}MnO_3$ do show a spin-wave component, see Fig. 31(b) (Coey *et al.*, 1995; Woodfield *et al.*, 1997). The stiffness constant deduced from it is $D = 130$ meV Å^2 in rough agreement with the neutron-scattering results $D = 188$ meV Å^2 (Martin *et al.*, 1996) and $D = 154$ meV Å^2 (Smolyaninova *et al.*, 1997), with no indication of a spin-wave energy gap. The electronic component in this material is $\gamma = 3-7$ mJ/mol K^2 implying a density of states at the Fermi energy $N(E_F) = 1.3-2.7$ eV^{-1} Mn^{-1}, close to the value found in $La_{0.33}Ca_{0.67}MnO_3$ and roughly a factor 2–3 larger than the band-structure estimate (Pickett and Singh, 1996) $N(E_F) = 0.8$ eV^{-1} Mn^{-1}, implying some mass renormalization effect is present. The study of the doping dependence of the Sommerfeld coefficient γ in $La_{1-x}Sr_xMnO_3$ (Okuda *et al.*, 1998) reveals a behavior not typical for a filling-controlled metal-insulator transition. Results for $La_{1-x}Sr_xTiO_3$ and $La_{1-x}Sr_xMnO_3$ are displayed in Fig. 32. The critical mass enhancement near the metal-insulator phase boundary (vertical hatching), indicating a canonical Mott transition, in $La_{1-x}Sr_xTiO_3$ is absent in $La_{1-x}Sr_xMnO_3$.

A recent heat-capacity study of other compounds reveals more about the manganites behavior. Measurements in $Nd_{0.67}Sr_{0.33}MnO_3$ ($T_C \approx 200$ K) show no spin-wave contribution as in the case of $La_{0.33}Ca_{0.67}MnO_3$, but contain a hyperfine contribution $\sim T^{-2}$, a broadened Schottky-like anomaly originating in the Nd spin system and excess entropy attributed to Nd-Mn exchange interaction and responsible for a temperature-dependent "linear" term $\gamma(T)T$ (Gordon *et al.*, 1999). Oxygen deficient samples of $LaMnO_3$ have been measured by the group in Brazil (Ghivelder *et al.*, 1999), in samples with insulating, ferromagnetic, low-temperature phases [Fig. 31(a)]. These compounds, as in the case of $La_{0.7}Ca_{0.3}MnO_3$, do not show a spin-wave contribution. The most surprising feature in both $Nd_{0.67}Sr_{0.33}MnO_3$ and $LaMnO_{3-\delta}$ is an unexpectedly large zero-temperature linear term, even in the case of insulating compounds. Ghivelder *et al.* (1999) propose that the spin-wave component and the large electronic component have their origin in ferromagnetic clusters, where mass-enhancement mechanisms (magnetic polarons, lat-
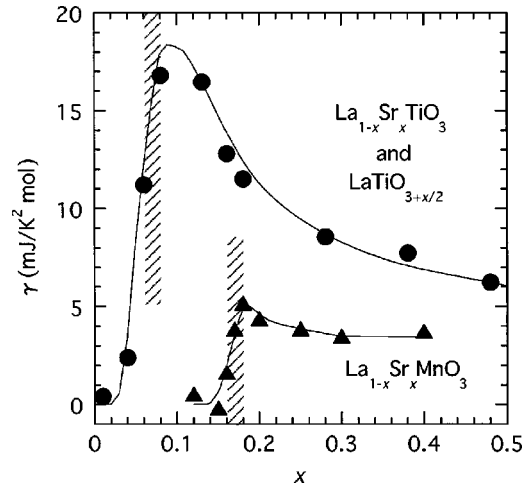

FIG. 32. Doping level (x) dependence of the electronic specific-heat coefficient γ for $La_{1-x}Sr_xMnO_3$ compared with that for $La_{1-x}Sr_xTiO_3$ ($LaTiO_{3+x/2}$). The hatched vertical bar for $La_{1-x}Sr_xTiO_3$ ($LaTiO_{3+x/2}$) indicates an antiferromagnetic metallic region sandwiched by AF insulating ($x < 0.05$) and PM metallic ($x > 0.08$). The hatched region for $La_{1-x}Sr_xMnO_3$ is the metal-insulator transitional region. From Okuda *et al.*, 1998.

tice polarons, Jahn-Teller effect, or Coulomb interactions) are at play. It seems strange though that mass enhancement mechanisms have no effect in Ca or Sr compounds, nor in layered manganites as discussed below.

Heat-capacity experiments have also been performed in layered manganite $La_{1.3}Sr_{1.7}Mn_2O_7$ (Okuda *et al.*, 1999). In this system spin-wave excitations contribute to the specific heat and can be suppressed by a 9-T magnetic field, which results in a 12-K energy gap in the spin-wave spectrum as shown in Fig. 33. The effect is larger than in the case of 3D compounds, but not as large as expected for an ideal 2D system. The authors claim that a finite dispersion of the spin wave along the c axis will explain the results. The zero-field linear term is $\gamma = 3 \pm 1$ mJ/mol K^2, comparable to values in the 3D counterpart $La_{0.7}Sr_{0.3}MnO_3$. The lack of mass enhancement effects in the linear term may imply the presence of an anomalous carrier scattering process or dynamical phase separation (Yunoki, Moreo, and Dagotto, 1998). A relatively large low-temperature magnetoresistance indicates that transport is somewhat limited by electron-magnon scattering, but spin-valve effects and field-dependent localization also play a role.

In conclusion, the low-temperature thermal properties of manganites and layered manganites are still far from being completely understood, especially in what concerns spin-wave contributions and mass enhancement effects. More detailed quantitative studies are in order, to test the spin-wave excitation spectrum in those compounds that show the contribution, in single-crystal samples that reveal intrinsic as opposed to sample-dependent effects. A summary of heat-capacity results is shown in Table II.
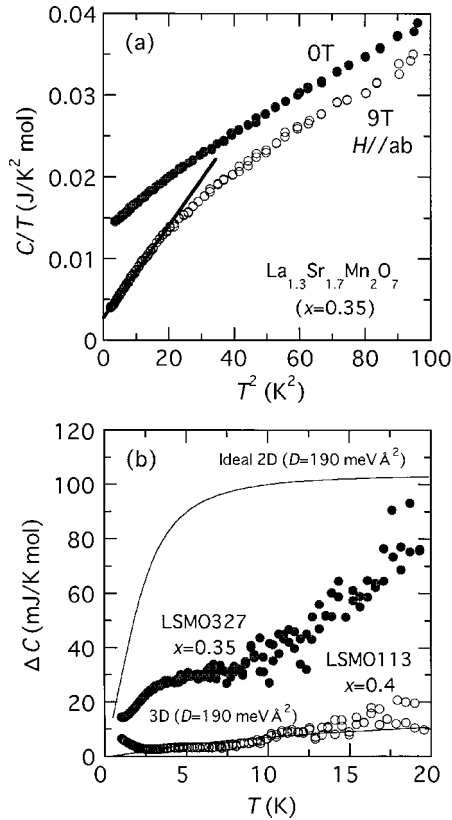
FIG. 33. Heat capacity of layered manganites: (a) temperature dependence of specific heat (C) as shown in a C/T vs T^2 plot in 0 and 9 T for a layered ($n=2$) manganite; solid line the extrapolated C/T value at 0 K, which expresses the γ value; (b) reductions of C upon the application of a field of 9 T for La$_{1.3}$Sr$_{1.7}$Mn$_2$O$_7$ (LSMO327, $x=0.35$), compared with La$_{0.6}$Sr$_{0.4}$MnO$_3$ (LSMOI13, $x=0.4$) along with the calculated results (solid lines) for the simple-square 2D lattice and simple-cubic 3D lattice with an appropriate spin-wave stiffness constant ($D=190\,\mathrm{meV\,Å^2}$). From Okuda, Kimura, and Tokura, 1999.

IV. HIGH-TEMPERATURE BEHAVIOR

A. Polaron effects—3D materials

In the early experimental study of manganites unexpected high-temperature transport properties were believed to be dominated by nonintrinsic effects like defects, crystalline disorder, grain boundaries, and impurities. Years later, with the preparation of good quality films by laser ablation on lattice-matched substrates and the growth of large single crystals, it became evident that the observed behavior is intrinsic and due to localization of charge carriers in small polarons (Ohtaki *et al.*, 1995; Jaime, Salamon, Pettit *et al.*, 1996; Jaime *et al.*, 1997; Palstra *et al.*, 1997; Chun *et al.*, 1999). The localization is a consequence of a large electron-phonon interaction, enhanced by the Jahn-Teller activity of Mn^{3+} in the manganites, and has an impact on the electric and thermal transport properties as well as on the lattice properties. We will see in what follows that the high-temperature regime is where magnetic correla-

tions become negligible and electric charge/lattice interplay is dominant (Jaime and Salamon, 1999).

As noted in Sec. II.B.2, the formation and transport properties of small lattice polarons in strong electron-phonon coupled systems, in which charge carriers are susceptible to self-localization in energetically favorable lattice distortions, were first discussed in disordered materials (Holstein, 1959) and later extended to crystals (Mott and Davis, 1971). Emin (1973) and Hillery *et al.* (1988) considered the nature of lattice polarons in magnetic semiconductors, where magnetic polarons are carriers, self-localized by lattice distortions but also dressed with a magnetic cloud. A transition from large to small polaron occurs as the ferromagnet disorders, successfully explaining the metal-insulator transition observed experimentally in EuO. If the carrier, together with its associated crystalline distortion, is comparable in size to the cell parameter, the object is called a small, or Holstein, polaron. Because a number of sites in the crystal lattice can be energetically equivalent, a band of localized states can form. These energy bands are extremely narrow, and the carrier mobility associated with them is predominant only at very low temperatures. At high temperatures the dominant transport mechanism is thermally activated hopping, with an activated mobility $\mu_p = [x(x-1)ea^2/h](T_0/T)^s \exp[-(W_H-J^{3-2s})/k_BT]$ with a the hopping distance, J the transfer integral, x the polaron concentration, and W_H one-half of the polaron formation energy. There are two physical limits for these hopping processes, depending on the magnitude of the optical phonon frequency. If lattice distortions are slow compared to the charge carrier hopping frequencies, the hopping is adiabatic, otherwise it is nonadiabatic. In the adiabatic limit, $s=1$ and $k_BT_0=h\omega_0$, where ω_0 is the optical phonon frequency and in the nonadiabatic limit, we have $s=3/2$ and $k_BT_0=(pJ^4/4W_H)^{1/3}$. The polaronic transport in manganites is usually considered adiabatic, in this case the conductivity is given by

$$\sigma = \frac{x(1-x)e^2T_0}{\hbar aT}\exp\left(-\frac{\epsilon_0+W_H-J}{k_BT}\right)$$

$$= \frac{\sigma_0T_0}{T}\exp\left(-\frac{E_\sigma}{k_BT}\right). \quad (14)$$

The temperature dependence observed in the high-temperature resistivity of manganites follows this adiabatic prediction very well, as seen in Fig. 34, from temperatures close to T_C up to 1200 K (Jaime, Salamon, Rubinstein *et al.*, 1996; Worledge *et al.*, 1996; De Teresa *et al.*, 1998). At high enough temperature magnetic correlations can be completely ignored, since charge/lattice and charge/charge interactions dominate. In this regime on-site Coulomb repulsion (Worledge *et al.*, 1998) has been observed in support of the small polaron picture. Small grain polycrystalline samples, very thin and unannealed films, on the other hand, have been reported to show variable-range-hopping-type localization (Coey *et al.*, 1995; Ziese and Srinitiwarawong, 1998) and nonadiabatic small polaron transport (Jakob, Westerburg *et al.*, 1998).

TABLE II. Results from fits to the low-temperature specific heat in manganite compounds. Units are mJ/mol K^2 for γ, K for θ_D, meV Å^2 for D_{sw}, mJ/mol K^3 for δ_2, and J K/mol for A. The cases where a contribution from spin waves is observed, but its magnitude not reported, are indicated by *. The cases where a spin wave contribution is not observed are indicated by -.

Composition	Order/T_C	γ	θ_D	D_{sw}	δ_2	A	sample	Reference
La$_{0.85}$Sr$_{0.15}$MnO$_3$	FM/230	0	386	*			SC	Okuda et al., 1998
La$_{0.84}$Sr$_{0.16}$MnO$_3$	FM/250	1.5	390	*			SC	Okuda et al., 1998
La$_{0.83}$Sr$_{0.17}$MnO$_3$	FM/260	4.0	388	*			SC	Okuda et al., 1998
La$_{0.82}$Sr$_{0.18}$MnO$_3$	FM/290	5.2	395	*			SC	Okuda et al., 1998
La$_{0.80}$Sr$_{0.20}$MnO$_3$	FM	4.5	398	*			SC	Okuda et al., 1998
La$_{0.75}$Sr$_{0.25}$MnO$_3$	FM	4.0	420	*			SC	Okuda et al., 1998
La$_{0.70}$Sr$_{0.30}$MnO$_3$	FM	3.5	450	*			SC	Okuda et al., 1998
La$_{0.60}$Sr$_{0.40}$MnO$_3$	FM	3.7	438	*			SC	Okuda et al., 1998
La$_{0.90}$Sr$_{0.10}$MnO$_3$	FM	0	255	*		9.20	PCC	Woodfield et al., 1997
La$_{0.80}$Sr$_{0.20}$MnO$_3$	FM/320	3.34	270	*		9.30	PCC	Woodfield et al., 1997
La$_{0.70}$Sr$_{0.30}$MnO$_3$	FM/375	3.29	285	130		8.69	PCC	Woodfield et al., 1997
La$_{0.70}$Sr$_{0.30}$MnO$_3$	FM/370	6.0	353	-			PCC	Coey et al., 1995
La$_{0.67}$Ba$_{0.33}$MnO$_3$	FM/330	4.4	383	-			PCC	Hamilton et al., 1996
La$_{0.67}$Ba$_{0.33}$MnO$_3$	FM/340	5.6	416	-			PCC	Hamilton et al., 1996
La$_{0.70}$Ba$_{0.30}$MnO$_3$	FM/220	6.1	333	-			PCC	Coey et al., 1995
La$_{0.90}$Ca$_{0.10}$MnO$_3$	FMI/140	0	368	40			PCC	Ghivelder et al., 1998
La$_{0.67}$Ca$_{0.33}$MnO$_3$	FM/250	4.7	430	-			PCC	Ghivelder et al., 1998
La$_{0.38}$Ca$_{0.62}$MnO$_3$	A-AFM	0	490	162	1.3		PCC	Ghivelder et al., 1998
La$_{0.53}$Ca$_{0.47}$MnO$_3$	FM/255	8					PCC	Smolyaninova et al., 1997
La$_{0.50}$Ca$_{0.50}$MnO$_3$	CO-AFM	0					PCC	Smolyaninova et al., 1997
La$_{0.47}$Ca$_{0.53}$MnO$_3$	FM-AFM	0					PCC	Smolyaninova et al., 1997
La$_{0.80}$Ca$_{0.20}$MnO$_3$	FM/250	7.8	390	-			PCC	Hamilton et al., 1996
La$_{0.70}$Ca$_{0.30}$MnO$_3$	FM/260	5.2					PCC	Coey et al., 1995
LaMnO$_3$	AFM	0	302	55	3.80	8.03	PCC	Woodfield et al., 1997
LaMnO$_{3.11}$	FM-CG/154	23	369	75			PCC	Ghivelder et al., 1999
LaMnO$_{3.15}$	FM-CG/142	19	387	32			PCC	Ghivelder et al., 1999
LaMnO$_{3.26}$	SG/48	0	498	16.1			PCC	Ghivelder et al., 1999
Nd$_{0.67}$Sr$_{0.33}$MnO$_3$	FM/280	25					PCC	Gordon et al., 1999
Pr$_{0.60}$Ca$_{0.40}$MnO$_3$	CO-AFM/230-160	0	433		1.89	28.0	PCC	Lees et al., 1999
Pr$_{0.6}$Ca$_{0.3}$Sr$_{0.1}$MnO$_3$	FM/196	4.72	344	-		59.1	PCC	Lees et al., 1999
Pr$_{0.6}$Ca$_{0.2}$Sr$_{0.2}$MnO$_3$	FM/235	4.51	342	-		57.34	PCC	Lees et al., 1999
Pr$_{0.6}$Ca$_{0.1}$Sr$_{0.3}$MnO$_3$	FM/262	5.77	333	-		40.82	PCC	Lees et al., 1999
Pr$_{0.6}$Sr$_{0.4}$MnO$_3$	FM/305	5.40	339	-		33.3	PCC	Lees et al., 1999
Pr$_{0.50}$Ca$_{0.50}$MnO$_3$	CO-AFM/230-180	2.4				23.7	PCC	Smolyaninova et al., 2000
Pr$_{0.55}$Ca$_{0.45}$MnO$_3$	CO-AFM/230-170	3.1				24.2	PCC	Smolyaninova et al., 2000
Pr$_{0.65}$Ca$_{0.35}$MnO$_3$	CO-AFM/230-160	15.7				20.7	PCC	Smolyaninova et al., 2000
Pr$_{0.65}$Ca$_{0.35}$MnO$_3$ ($H=8.5$ T)	CO-FM/200-140	7.0				7.6	PCC	Smolyaninova et al., 2000
Pr$_{0.7}$Ca$_{0.3}$MnO$_3$	CO-AFM/230-140	30.6				12.2	PCC	Smolyaninova et al., 2000
La$_{2.3}$Ca$_{0.7}$Mn$_2$O$_7$		41					PCC	Raychaudhuri et al., 1998
La$_{1.3}$Sr$_{1.7}$Mn$_2$O$_7$	FM/120	3		190			SC	Okuda et al., 1999

The thermopower of small polaronic systems is similar to that of band semiconductors, governed by thermal activation of carriers across a small barrier and thus a function of the inverse temperature:

$$S = \frac{k_B}{e}\left(\frac{E_S}{k_B T} + b\right). \tag{15}$$

Contrary to the case of band semiconductors, where

the chemical potential determines the temperature dependence of both the conductivity and the thermoelectric properties and $\epsilon_0 = E_\sigma = E_S$, small polaronic conduction results in very different characteristic energies, i.e., $E_S = \epsilon_0 \ll E_\sigma$ because E_σ includes W_H, which implies that for the charge carrier to be able to hop from one site to another, a lattice distortion of energy $2W_H$ needs to be provided. In a band semiconductor the strongest
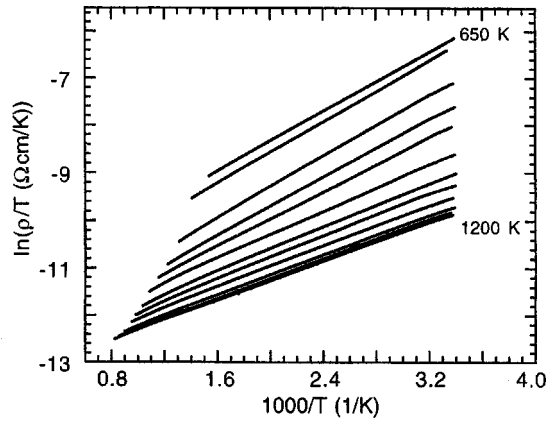
FIG. 34. The resistivity of an $n=\infty$ manganite, following the adiabatic, small-polaron hopping model at all stages of annealing. Each line is the cooling curve after being held at T_h for 10 h. $T_h=650$ K for the top curve, and increases by 50 K for each successive run, up to $T_h=1200$ K for the bottom curve. From Worledge *et al.*, 1996.

temperature dependence comes from the availability of carriers in the conduction band; in a small polaron system the limiting factor is the number of available sites that the charge carriers can hop to. For the manganites high-temperature transport measurements reveal $E_S \approx$ few meV $\ll E_\sigma \approx 100$–200 meV, the signature of small polarons (Fig. 35). The independent term $k_B b/e$ in the thermopower is given by the configurational entropy of, in the case of the manganites, placing a hole with spin 3/2 ($S_h=3/2$) moving in a spin-2 background ($S_b=2$), namely, $-(k_B/e)\ln\{[2S_h+1]/[2S_b+1]\}=-(k_B/e)\ln(4/5)$ $=-19\,\mu$V/K plus the mixing entropy term that counts in how many different ways x holes can be distributed between n Mn sites. The mixing term in the case of correlated 1D hoping with weak near-neighbor repulsion is given by $\ln[x(1-x)/(1-2x)^2]$ (Chaikin and Beni, 1976). Alternative models were discussed by Heikes (1965), giving in the correlated limit $\ln[(1+x)/(1-x)]$ and in the uncorrelated limit (where double occupancy is allowed) $\ln[x/(1-x)]$. None of these models can explain quantitatively the experimental results, and only the uncorrelated limit by Heikes predicts the right qualitative dependence on the carrier concentration x. There are three proposed explanations for this behavior. The first is a disproportionation model, where two Mn^{3+} atoms generate Mn^{2+} and Mn^{4+} sites with the transference of one electron. The disproportionation density is related to oxygen nonstoichiometry (Hundley and Neumeier, 1997). Another possibility is that small polarons move by hopping between divalent atoms in real space due to the elastic stress introduced in the lattice by atomic size mismatch (Jaime *et al.*, 1997). This is a type of impurity conduction where the number of available sites for hopping increases with the carrier concentration x and as a consequence the mixing entropy remains unchanged. Finally, the Heikes uncorrelated limit also suggests that multiple occupancy or collective behavior is possible for small polarons.

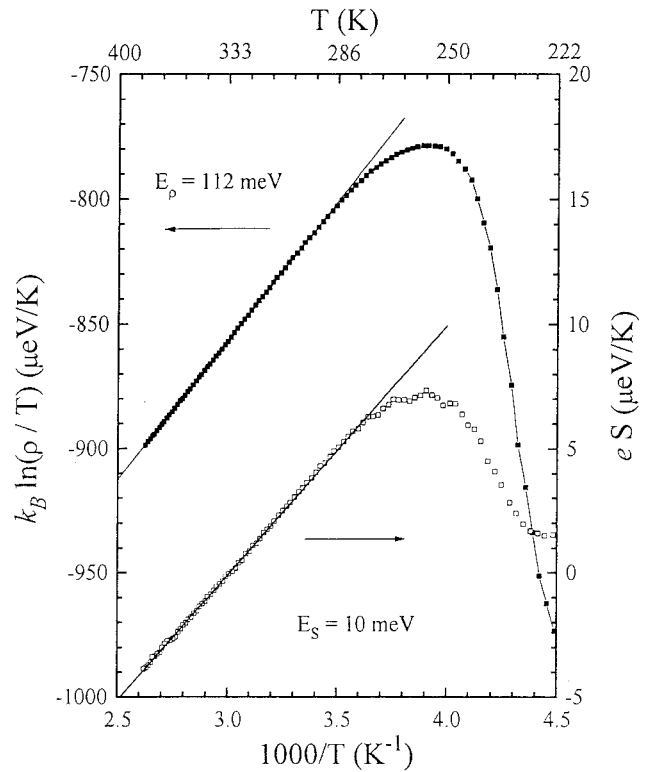One of the most distinctive properties of small po-

FIG. 35. The resistivity in the adiabatic limit and thermopower vs 1000/temperature. Lines are fits in the high-temperature regime, and $E_\rho=\epsilon_0+W_H$ and $E_S=\epsilon_0$. As in Fig. 6, there is a large difference in these two energy scales. From Jaime, Salamon, Pettit *et al.*, 1996.

laronic transport is the magnitude and temperature dependence of its Hall mobility $\mu_H(T)$. The Hall mobility is not a power law of the temperature as in band semiconductors but thermally activated, with an activation energy E_μ calculated to be always less that for the drift mobility E_d. The simplest model predicts $E_\mu \approx E_\sigma/3$, experimentally observed in oxygen-deficient $LiNbO_3$ (Nagels, 1980). As first pointed out by Friedman and Holstein (Friedman and Holstein, 1963) the Hall effect in hopping conduction arises from interference effects of nearest-neighbor hops along paths that define an Aharonov-Bohm loop. When the loops involve an odd number of sites sign anomalies arise in the Hall effect and the Hall coefficient is activated with a characteristic energy $E_H=2E_\sigma/3$:

$$R_H=R_H^0 \exp\left(\frac{2E_\sigma}{3k_BT}\right), \tag{16}$$

where

$$R_H^0=\frac{g_H}{g_d}\frac{F(|J|/k_BT)}{ne}\exp\left\{-\frac{\epsilon_0+\dfrac{4|J|-E_S}{3}}{k_BT}\right\}. \tag{17}$$

At sufficiently high temperatures, the contribution from the anomalous Hall effect is sufficiently small to allow a measurement of the polaronic contribution. Figure 36 (Jaime *et al.*, 1997) shows both the sign anomaly (negative Hall effect for hole transport) and activated
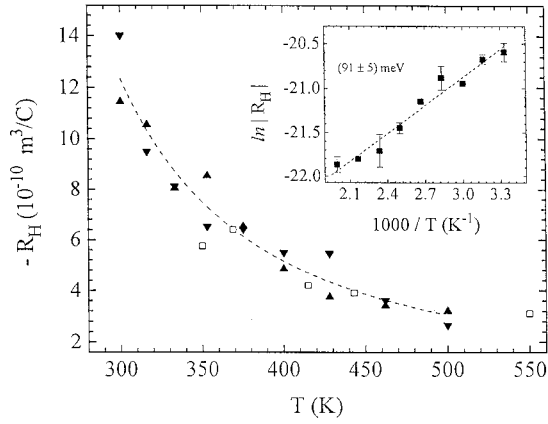
FIG. 36. The magnitude of the Hall coefficient $-R_H$ vs temperature showing the values obtained by ▲, ramping the magnetic field up and ▼, ramping; down in a thin-film sample; ■, from a single-crystal sample with a higher transition temperature; dashed line, Arrhenius fit Inset: The natural logarithm of the averaged Hall coefficient for the thin film. The solid line is a linear fit giving 91 meV for the activation energy. From Jaime et al., 1997.
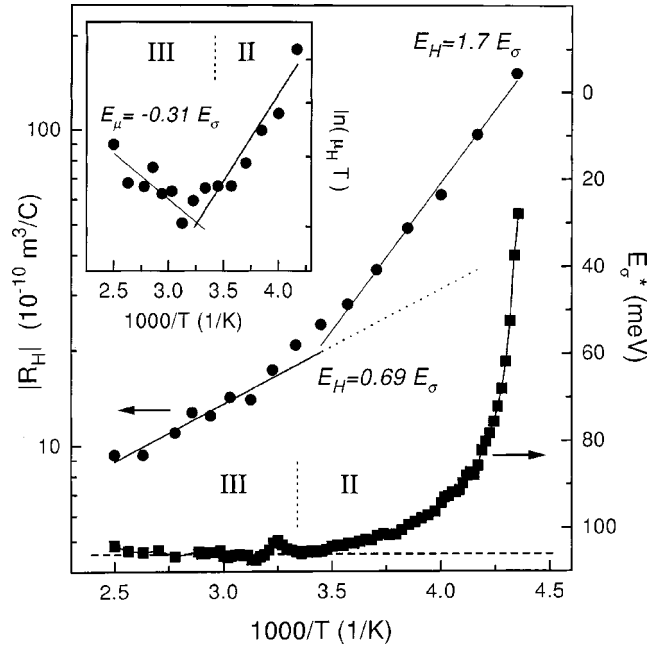

FIG. 37. The activated behavior of Hall coefficient R_H (main panel) and Hall mobility μ_H (inset) above $T_C = 220$ K for a single crystal of $La_{0.7}Ca_{0.3}MnO_3$. Above 300 K, the slopes are in accord with small-polaron hopping theory. Also shown in the main panel is the effective activation energy of the conductivity, E_σ^*. The Hall and resistivity data deviate from polaronic behavior at the same temperature. From Chun, Salamon, Tomioka et al., 2000.

behavior of the Hall coefficient expected from the Friedman-Holstein picture in a film sample of $(La_{0.75}Gd_{0.25})_{2/3}Ca_{1/3}MnO_3$. Indeed, the energy characterizing the exponential rise of the Hall coefficient, $E_H = 91 \pm 5$ meV is about 2/3 the measured conductivity activation energy, $E_H/E_\sigma = 0.64 \pm 0.03$ in excellent agreement with theory.

In order to compare the prefactor R_H^0 with the experimental results some assumptions need to be made. The geometrical factor g_d depends on the ratio of the probability P_{nnn} of next-near-neighbor (nnn) hops to P_{nn}, that of near-neighbor (nn) hops, through $g_d = (1 + 4P_{nnn}/P_{nn})$. If these probabilities are comparable, i.e., if diagonal hopping is allowed in the Mn square sublattice, $g_d = 5$, $g_H = 5/2$, and the exponential factor in Eq. (17) becomes $\exp[(E_S - |J|)/3k_BT] \approx 1$. In the regime $|J| \geq k_BT$, the function $F(|J|/k_BT)$ is relatively constant with a value ≈ 0.2, leading to $R_H^0 = -0.02/ne = -3.8 \times 10^{-11}$ m³/C. This yields an estimated carrier density $n = 3.3 \times 10^{27}$ m⁻³, quite close to the nominal level of 5.6×10^{27} m⁻³.

The main effect of Gd, trivalent as La, is to reduce the Curie temperature by further reducing the Mn-O-Mn bond angle (and hence reducing the bandwidth) without changing the doping level. This trick made the Hall effect measurement possible to temperatures as high as four times T_C allowing the observation of the small polaron regime for the first time. Chun et al. have confirmed the picture with recent measurements in slightly underdoped single crystals and show (Fig. 37) how the small polaron picture breaks down as the Curie temperature is approached from above, a remarkable accomplishment given the small size of the samples and the intrinsic experimental difficulties (Chun, Salamon, Tomioka et al., 2000).

Note that diagonal hopping is *not* disallowed by symmetry considerations in manganites because the Mn-

O-Mn bond angle is smaller than 180° (regardless of Gd content). Diagonal hopping successfully explains the sign anomaly in the Hall effect, which requires small polarons traversing Hall-effect loops with odd number of legs, predicts correctly the carrier concentration in the sample and also reduces the value of the hopping attempt frequency required to fit the electrical conductivity prefactor (Jaime et al., 1997). Worledge et al. studied the electrical resistivity of (Gd free) $La_{1-x}Ca_xMnO_3$ films in the full composition range $0 \leq x \leq 1$ (Worledge et al., 1998). They find that a model for small polarons that hop adiabatically between nn sites and experience Coulomb repulsion reproduces well the results but underestimates the total conductivity, and propose that considering hopping to more than nearest neighbors (nnn) could fix the problem. Interestingly, a theoretical study based on *ab initio* density-functional calculations, showing how cooperative Jahn-Teller coupling between individual MnO_6 centers in manganites leads to the simultaneous ordering of the octahedral distortion and the electronic orbitals, has found that a nnn hoping integral $V_\sigma' = -0.42$ eV comparable to the nn hoping integral $V_\sigma = -0.52$ eV together with a small but finite third neighbor hopping V_σ'' are necessary to fit the e_g bands in the linear muffin-tin orbital theory (Popovic and Satpathy, 2000).

The thermal transport of manganites in the paramagnetic state is particularly puzzling because, besides its magnitude being very close to the theoretical minimum value (Cohn, 2000) [see Fig. 28(a)], it does not show the
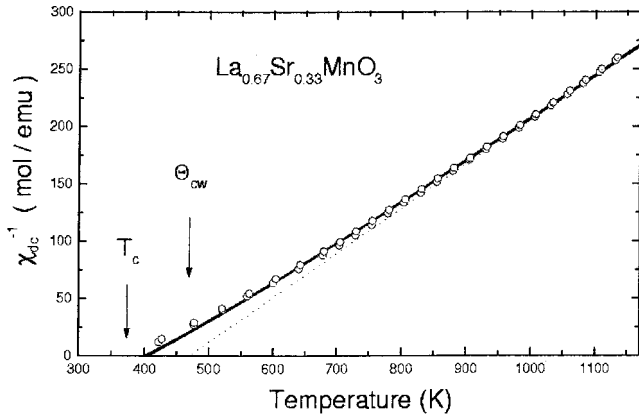
FIG. 38. The inverse of the dc susceptibility for $La_{0.67}Sr_{0.33}MnO_3$: $\bigcirc$, experimental data. Solid and dotted lines are fits to the constant-coupling and Curie-Weiss models, respectively. From Causa *et al.*, 1998.

FIG. 39. Peak-to-peak magnetic resonance linewidth ΔH_{pp} vs temperature, showing a universal behavior for the perovskites $La_{0.67}A'_{0.33}MnO_3$ with $A' = $Ca, Sr, and Pb. Different symbols refer to X-, L-, and Q-band data. The inset shows similar data for the Pr-Sr analog. From Causa *et al.*, 1998.

characteristic $1/T$ temperature dependence for heat carried by phonons with a mean free path limited by anharmonic decay (Berman, 1976). Instead $\kappa(T)$ increases with temperature. An exponential increase with equal temperature parameters, found in samples with very different compositions, has been interpreted as due to dynamical lattice distortions, a consequence of T-dependent Debye-Waller factors (Visser *et al.*, 1997). These results however have not been reproduced by other groups (Hejtmanek *et al.*, 1999; Cohn, 2000) and a definitive explanation is still missing. One possibility is that the very moderate increase in κ with temperature is due to the increase of a relatively small electronic component added to a saturated and temperature-independent phonon component. Such an increase of the electronic component with temperature could be due to the increase in thermally activated small polaron mobility with temperature. Indeed, in Fig. 29(b) we can see a small but distinguishable increase in the high-temperature electronic component κ_e calculated using the Wiedemann-Franz relation.

Electron-spin-resonance (ESR) studies in the paramagnetic phase reveal the nature and interaction properties of Mn^{3+}-Mn^{4+} spin pairs. High-temperature ESR experiments were performed by Causa *et al.* (1998) together with magnetic susceptibility experiments up to 1200 K in $La_{0.67}Ca_{0.33}MnO_3$, $La_{0.67}Sr_{0.33}MnO_3$, $Pr_{0.67}Sr_{0.33}MnO_3$, and $La_{0.67}Pb_{0.33}MnO_3$. $\chi_{dc}(T)$ follows, in all cases, a ferromagnetic Curie-Weiss temperature dependence $\chi_{dc}(T) = C/(T-\Theta)$, at high enough temperatures ($T > 2\Theta$). For temperatures below 1.5Θ the curve for the inverse susceptibility vs T (Fig. 38) shows a positive curvature suggesting spin clustering effects. In the paramagnetic regime the ESR spectrum consists of a single line, with g values that go from 1.992 for Ca compound to 2.00 for Pr-Sr compound, with a linewidth that deviates from linearity and a tendency to saturation with the temperature (Fig. 39). The computation for χ_{ESR} performed by Causa *et al.* demonstrates that both χ_{ESR} and χ_{dc} have the same temperature dependence clearly indicating that all the Mn ions contribute to the ob-
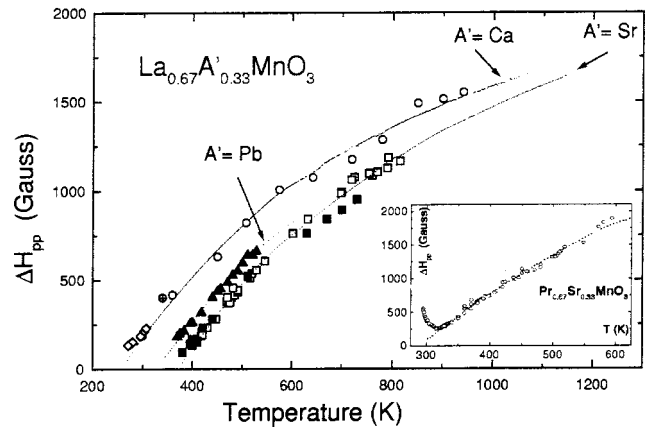
served ESR spectra and that the ESR linewidth should be related to the relaxation mechanism of the coupled magnetic system. The authors also claim that the temperature dependence of the ESR linewidth may be described by a universal curve, whose temperature scale is associated with T_C. The behavior above T_C is determined solely by the temperature dependence of $\chi_{ESR}(T)$ and the infinite temperature linewidth kept as an adjustable parameter. No evidence is found of a spin-phonon contribution to the experimental linewidth in this regime. These results agree with previously discussed transport experiments that show evidence for decoupling of small polarons from spins above $T = 2T_C$.

Additional evidence for polaron formation is found from structural and optical studies. Pair-distribution analysis of neutron powder-diffraction data, the width of EXAFS features, and Raman data all find evidence for structural features consistent with polaron formation well above T_c. A surprising aspect of these results is that such evidence persists well into the ferromagnetic regime. We will return to the question of admixtures of polaronic and metallic phases in Sec. V. Perhaps the strongest evidence that polaron effects are important is found in the isotope effect. Substitution of ^{16}O by ^{18}O lowers the transition temperature by 21 K for $La_{0.8}Ca_{0.2}MnO_3$ (Zhao *et al.*, 1996) and lesser amounts for $x = 0.3$ (Babushkina *et al.*, 1999). The shift is attributed to the mass dependence of the polaron bandwidth, and provides strong evidence that oxygen motions play a central role in controlling the ferromagnetic transition.

B. Polaron effects—layered manganites

The paramagnetic state of layered manganites [small n members of the Ruddlesden-Popper series $(La,A)_{n+1}Mn_nO_{3n+1}$] has not received as much attention as the corresponding state in 3D compounds. There are a few reasons for this. In the first place, single-crystal samples are difficult to grow and multiple phases are

common (Berger *et al.*, 2000); second, the thermal and electric transport properties are strongly anisotropic and results obtained in ceramic polycrystalline samples mix up conductivity tensor components. Because of the structural similarities between 3D and layered manganites (see Fig. 10) it is expected that charge-lattice correlations play an important role in both of them. However, the tetragonal crystal field in $n=2$ compounds can split the degenerate Mn e_g orbitals, a condition that precludes the Jahn-Teller effect as the mechanism that drives small polaron formation in the paramagnetic insulator phase of the $n=\infty$ materials. Nonetheless, measurements in single-crystal samples of $La_{1.2}Sr_{1.8}Mn_2O_7$ (Zhou *et al.*, 1998) support the existence of charge localization effects due to small polaron formation. Anisotropic behavior is found in the electrical resistivity and thermopower that indicate conduction by Holstein small polarons in the c crystallographic direction (perpendicular to the La-Sr-Mn-O planes) and by "Zener-pair" polarons in the ab crystallographic direction (along La-Sr-Mn-O planes) that condense into clusters as the temperature is reduced. In a recent report, Liu *et al.* show that electrical transport in polycrystalline samples of $La_{1.4}Sr_{1.6}Mn_2O_{7+\delta}$ also behave as predicted by the small polaron Eqs. (14) and (15), with a thermal activation energy in the electrical conductivity close to 100 meV and a characteristic energy in the thermopower roughly 15–20 times smaller (Liu *et al.*, 2000). These numbers are quite close to those found in the 3D compounds, implying similar small polaron formation energies W_H are involved. The authors also report that N_2 annealing of the samples reduces the sample resistivity and thermopower and increases the Curie temperature and magnetoresistance. Similar results are reported by Jung in polycrystalline samples of $La_{1.6}Ca_{1.4}Mn_2O_7$ where $E_\sigma \simeq 100$ meV is substantially larger than $E_S = 13$ meV (Jung, 2000). A common feature in many layered manganites, the magnetic transition and a maximum in the thermoelectric power occur well above the temperature at which the electrical resistivity peaks (Hur *et al.*, 1998). This has been interpreted by several authors as indicative of small polaron cluster formation.

Thermal-conductivity measurements were carried out in $La_{1.2}Sr_{1.8}Mn_2O_7$ crystals (Matsukawa *et al.*, 2000). The thermal conductivity is anisotropic, being between three and five times larger in the ab direction. The thermal conduction in the ab direction resembles that of the cubic samples [Fig. 29(d)] with a positive slope above T_C and a feature at the onset of the ferromagnetic transition. Along the c direction the thermal conductivity increases as the temperature decreases, in agreement with what one would expect for most solids as the phonon mean free path increases, with no feature at the Curie temperature.

V. FERROMAGNETIC/PARAMAGNETIC PHASE TRANSITIONS

A. Theoretical background

The transition between the ferromagnetic state described in Sec. III.C and the high-temperature polaron-like behavior discussed in Sec. IV motivated the current resurgence of interest in these materials. The extreme sensitivity of the transport properties, the resistivity in particular, to applied magnetic field is, of course, the essence of colossal magnetoresistance. As discussed in Sec. II.C, the dependence of T_C on the charge-carrier bandwidth in a double exchange system, and the dependence of the bandwidth on temperature, led Kubo and Ohata (1972) to the conclusion that the nature of the phase transition would differ from the behavior expected for a 3D Heisenberg ferromagnet. More recently, Furukawa (1995a) used the ferromagnetic Kondo lattice model Hamiltonian for infinite spin and dimension,

$$\mathcal{H} = -t \sum_{\langle ij \rangle, \sigma} (c_{i\sigma}^\dagger c_{j\sigma} + \text{H.c.}) - J \sum_i \sigma_i \cdot m_i, \qquad (18)$$

to model the double exchange system and confirmed the linear dependence of T_c on the bandwidth.

Within the context of the Kubo-Ohata and Kondo lattice-model approaches (Furukawa, 1994, 1995b) the resistivity below the magnetic transition decreases as

$$\rho(M) = \rho(M=0)(1-CM^2), \qquad (19)$$

and is therefore constant above T_C. However, materials that exhibit colossal magnetoresistance are characterized by exponentially increasing resistivity as the temperature is reduced toward T_c.

The failure of earlier models to produce semiconductive behavior was remedied in a calculation by Millis *et al.* (1995) that takes into account fluctuations in the angle $\theta_{ij} = \cos^{-1}(\vec{S}_i \cdot \vec{S}_j / S^2)$, where i and j are neighboring sites on the lattice. The resistivity involves the correlation function $\langle \theta_{0\delta_1} \theta_{R\delta_2} \rangle$, where δ_1 and δ_2 are nearest neighbors of sites labeled 0 and R. Millis *et al.* point out that this differs from the usual Fisher-Langer resistivity, which involves only $\langle \theta_{0\delta_1} \rangle$ correlations and that, because static mean-field theory ignores fluctuations, it misses the upturn in resistivity. The resistivity calculated in the dynamic mean-field model is shown in Fig. 40 along with data from Tokura *et al.* (1994). The calculated resistivity is several orders of magnitude smaller than observed and requires an unreasonably large field to produce significant magnetoresistance. The conclusion is that a major element is missing from the model, namely, the Jahn-Teller interaction that characterizes the parent compound. In fact, each Mn^{4+} site, lacking an e_g electron, does not gain energy from a Jahn-Teller distortion of its local environment. It is likely, then, that hole motion is correlated with an "anti-Jahn-Teller" distortion, by which we mean an empty e_g site that is undistorted relative to neighboring occupied e_g orbitals and that takes the form of the polarons discussed in Sec. IV.

The effect of Jahn-Teller coupling was first treated by Röder, Zang, and Bishop (1996), who added it to Eq. (18) and demonstrated the tendency of carriers to become self-trapped once the effective Jahn-Teller coupling is sufficiently large. A subsequent calculation by Millis and co-workers (Millis, Shraiman, and Mueller, 1996; Millis, Mueller, and Shraiman, 1996) reproduced
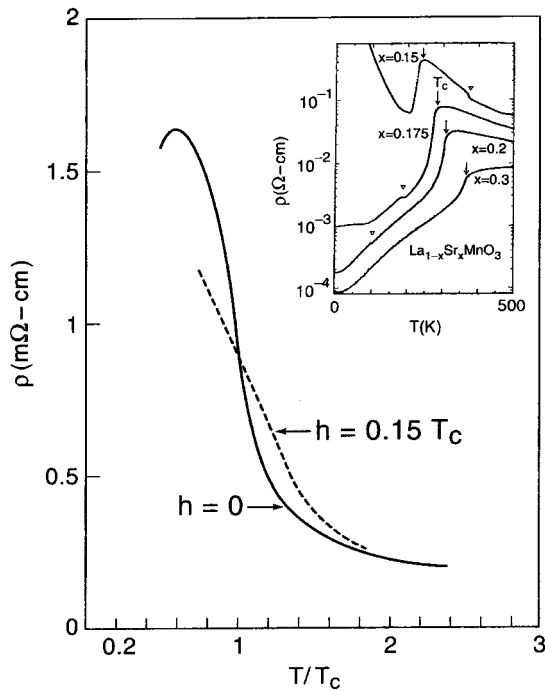
FIG. 40. Resistivity calculated from the double exchange model without electron-phonon interaction: solid line, the resistivity in zero field; dashed line, the resistivity in a field of $0.15T_C$, corresponding to 200 T. The inset displays data from Tokura *et al.* Both the clculated absolute change in resistivity and the magnetoresistance are much smaller than experiment. From Millis *et al.*, 1995.

the qualitative behavior observed in manganites near optimal doping. Figure 41 shows the magnetoresistance in this model for values of the effective Jahn-Teller coupling constant just below (upper panel) and just above (lower panel) the critical value for self-trapping. The effective coupling parameter $\lambda = g^2/tk$ depends not only the Jahn-Teller coupling strength g, but also inversely on the bandwidth through t and the lattice stiffness via k. As the dopant atom M changes from Ca to Pb to Sr in $La_{2/3}M_{1/3}MnO_3$, the bandwidth increases as the Mn-O-Mn bond angle tends toward 180°. Concomitantly, λ decreases such that Ca- and Pb-doped samples are above the critical value and Sr-doped samples, below. Substitution of Nd for La also affects the bond angle, and makes the system more prone to polaron formation. Typically, tabulated values of ionic sizes are used to estimate the deviation of the crystal structure from ideal perovskite structure through the tolerance factor f. As in the original Kubo-Ohata calculation and as shown in Fig. 42, the transition temperature depends on λ, which depends on the effective hopping matrix element t which, in turn, depends on the short-range spin order. This bootstrap mechanism was treated by Millis, Mueller, and Shraiman (1996) by means of a dynamical mean-field method which yields sharp, but continuous (second-order) transitions.

B. Nature of the phase transition

Despite the enormous body of literature in this field, relatively little effort has focused on the nature of the
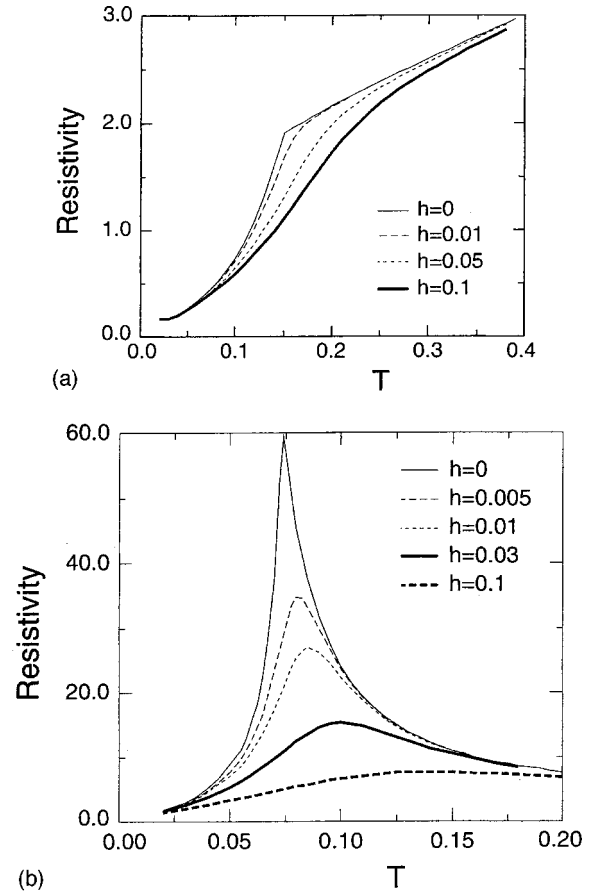

FIG. 41. The effect of including Jahn-Teller effects, characterized by an effective coupling parameter λ in the double exchange model. The temperature dependence of the resistivity is shown for different values of magnetic field h for (a) $\lambda = 0.7$ and (b) $\lambda = 1.12$. The parameter h is related to the physical field through $h = g\mu_B S_c H_{phys}/t$. Using $g = 2$, $t = 0.6$ eV, and $S_c = 3/2$, we find that $h = 0.01$ corresponds to $H_{phys} = 15$ T. From Millis, Mueller, and Shraiman, 1996.

phase transition beyond the obvious changes in resistivity. As the transition temperature is decreased, whether by doping or ion-size substitution, self-trapping becomes more evident through the activated behavior of the conductivity. Once T_C is reduced to 200 K or so, the transition becomes hysteretic and clearly first order. This is readily seen in the data of Fig. 43 (Hwang *et al.*, 1995), where the tolerance factor (and along with it, T_C) is reduced by substitution of Pr for La. Hysteresis on cooling and heating becomes increasingly significant as the transition temperature decreases (and the CMR effect increases). Even above that temperature, where there is no strong hysteresis, the transition differs markedly from that of a conventional Heisenberg ferromagnet. Clear evidence for this is seen in the heat-capacity data on polycrystalline $La_{0.7}Ca_{0.3}MnO_3$(LCMO) by Park, Jeong, and Lee (1997). Rather than broadening with increasing field, the specific-heat peak shifts to higher temperature with little change in shape. This has been confirmed in single crystals of the same composition ($T_C = 216$ K) by Lin *et al.* (2000) as seen in Fig. 44. The heat capacity peak is very sharp, suggesting a nearly first-
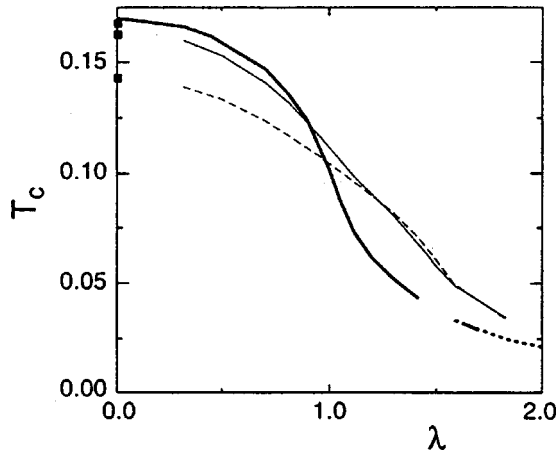
FIG. 42. The dependence of the Curie temperature T_C on the effective Jahn-Teller parameter λ. Because it is inversely proportional to the bandwidth, λ decreases as magnetic order sets in, causing the Curie temperature to increase with decreasing temperature. Millis, Mueller, and Shraiman, 1996.

order transition. This contrasts with the heat-capacity peak of $La_{0.7}Sr_{0.3}MnO_3$ ($T_C=359$ K) which is much more lambda like (Lin *et al.*, 2000) and which shifts relatively little in applied fields up to 1 T. A small-angle neutron study (Ibarra *et al.*, 1998) of a nominal $La_{2/3}Ca_{1/3}MnO_3$ sample ($T_C\approx250$ K) also showed unusual characteristics associated with the transition. While the quasielastic line shape is Lorentzian as expected, the inverse of its width, which measures the ferromagnetic correlation length, shows no power-law increase over the range $1.02T_C\lesssim T\lesssim1.15T_C$. Rather, the intensity of the quasielastic peak increases as T_C is approached then drops abruptly, following closely the anharmonic contribution to the volume thermal expansion (Ibarra *et al.*, 1998). Inelastic neutron scattering on a comparable sample finds that the spin-wave stiffness coefficient D does not tend toward zero as for a conventional ferromagnet, but rather retains 50% of its low temperature value at T_C [see Fig. 23(c)]. In place of the collapse of spin-wave groups toward zero energy, a strong diffusive peak appears which grows in intensity as T_C is approached from below and persists to at least $1.1T_C$ (Lynn *et al.*, 1996). A subsequent neutron-scattering study by Fernandez-Baca *et al.* (1998) found very similar behavior in $Nd_{0.7}Sr_{0.3}MnO_3$ ($T_C=198$ K) but more conventional behavior in $Pr_{0.63}Sr_{0.37}MnO_3$ ($T_C=301$ K).

Relatively little attention has been paid to the critical point properties of CMR manganites. This is not surprising considering the evidence presented above that the transition is percolative in nature. As the transition temperature is increased, either by doping or by changes in tolerance factor, the tendency for polaron formation decreases and the resistive behavior is metallic over the entire temperature range. Referring to Fig. 45, we see that the innermost contour of the ferromagnetic metal regime represents the most metallic, and possibly the most "normal" ferromagnetic transition. Indeed, a scaling analysis of a single crystal of $La_{0.7}Sr_{0.3}MnO_3$ (T_C
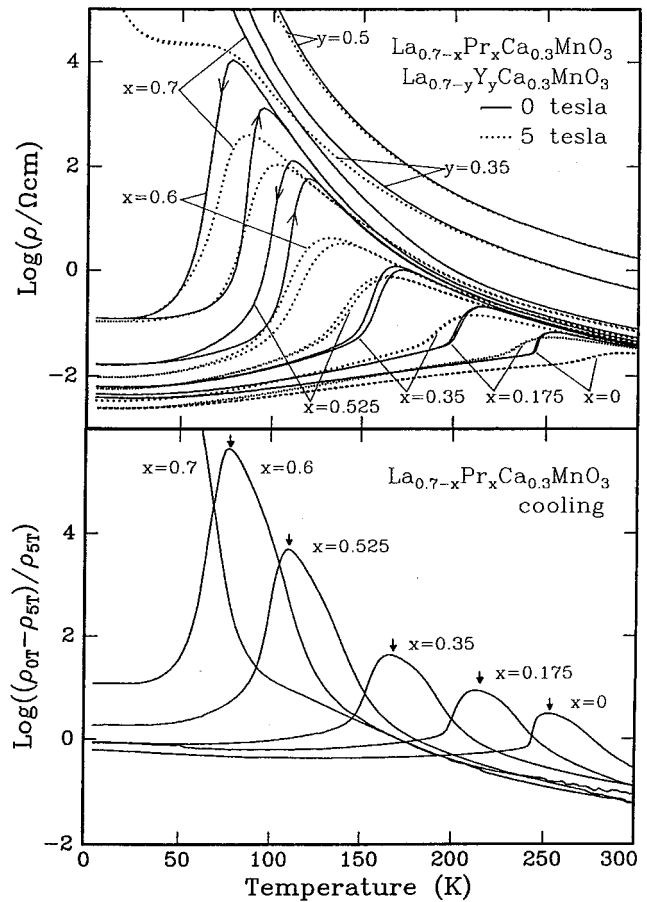

FIG. 43. Progression of the resistivity and magnetoresistance with changes in trivalent ion: top panel; $\ln\rho(T)$ in 0 and 5 T for a series of samples of $La_{0.7-x}Pr_xCa_{0.3}MnO_3$ ($x=0$, 0.175, 0.35, 0.525, 0.6, 0.7) and $La_{0.7-y}Y_yCa_{0.3}MnO_3$ ($y=0.35$ and 0.5). Bottom panel, magnetoresistance (cooling data) for $x=0$, 0.175, 0.35, 0.525, 0.6, 0.7 specified as $\ln(\rho_{0T}-\rho_{5T})/\rho_{5T}$, with the maximum in ρ_{0T} indicated by arrows. The interpretation is that increasing the Pr content increases the effective Jahn-Teller coupling constant by reducing the hopping matrix element. From Hwang *et al.*, 1995.

$=354$ K) by Ghosh *et al.* (1998) gives critical exponents $\beta=0.37$, $\gamma=1.22$, and $\delta=4.25$, as shown by the data collapsing shown in Fig. 46. These values differ from 3D Heisenberg values by amounts outside experimental uncertainty, and must be regarded as effective exponents that reflect some residual tendency for mixed-phase behavior. As expected, samples with 20% Sr doping ($T_C\approx310$ K) exhibit quite different effective critical exponents that are far from Heisenberg values (Mohan *et al.*, 1998; Schwartz, 2000). The pyrochlore CMR compound $Tl_2Mn_2O_7$, which has no indication of polaron formation, exhibits critical exponents that are very close to theoretical values for the 3D Heisenberg model (Zhao *et al.*, 1999). These results support the idea that the critical temperature, reflecting the combined effects of Jahn-Teller coupling, bandwidth, and lattice stiffness, serves as a measure of the degree to which polaron formation drives the material toward a first-order phase transition.
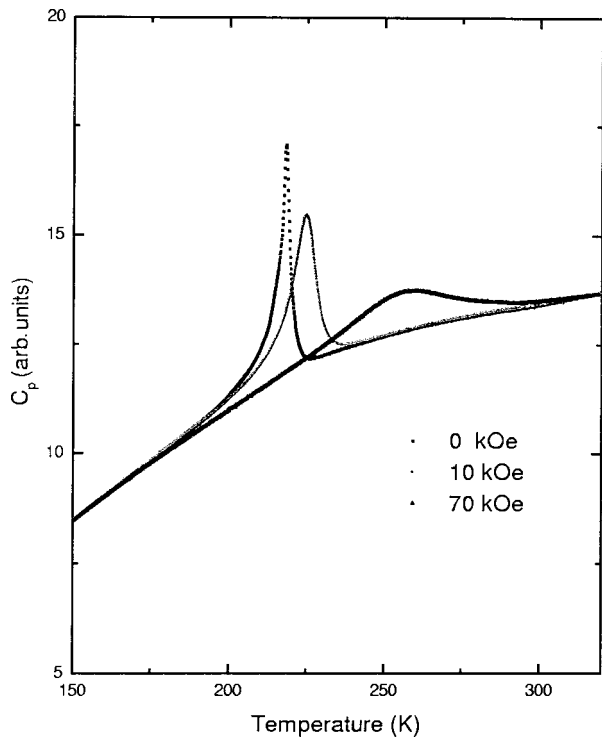
FIG. 44. Heat capacity of $La_{0.7}Ca_{0.3}MnO_3$ plotted vs temperature in external fields of 0, 10, and 70 kOe. Unlike conventional ferromagnetic transitions, the peak moves to significantly higher temperatures with applied field. The peaks do not obey the usual critical-point scaling behavior. From Lin *et al.*, 2000.

FIG. 45. Phase diagram in the plane defined by the average A-site covalent radius $\langle r_{cov} \rangle$ and divalent ion concentration x, showing the various antiferromagnetic insulating (AFI), ferromagnetic metal (FMM), ferromagnetic insulator (FMI), and charge ordered insulating (COI) phases. Inside the region labeled FMM, contours of T_C are shown. The dotted lines show the effect of Sr, Ca, and Ba substitution. The bold arrow indicates that the effective Jahn-Teller coupling, λ, increases as T_C decreases. Charge order is most stable near $x=0.5$ and $x=0.6$–0.67. From Ramirez, 1997.

Further evidence for an unconventional phase transition in LCMO is found in muon relaxation data (Heffner *et al.*, 1996). The muon precession frequency decreases with increasing temperature, but tends to zero at a temperature above the T_C deduced from the magnetization. In addition to the precessing component, which relaxes at a rate comparable to the precession frequency, a second contribution is found that relaxes at a rate several orders of magnitude slower. Initial studies of the slow component showed a peak in the relaxation rate at the magnetization value of T_C, but with nonexponential shape. Below T_C the relaxation function is a stretched exponential of form $\exp[-(\Lambda t)^{1/2}]$, slowly evolving into a simple exponential by $1.2 T_C$. The authors suggest a glassy state in which fast-relaxing and slow-relaxing components coexist for times on the order of ~ 1 μs. More recently, Heffner *et al.* (2000) have combined neutron spin-echo and muon relaxation data to identify two distinct components to the relaxation rate in LCMO, in place of a stretched exponential. One component is identified with an extended cluster and exhibits fast spin dynamics and critical slowing down, which translates into slower muon relaxation, and an increasing volume fraction as temperature is reduced. This component is observed only at small momentum transfer (large length scales) in the spin-echo data. The second component is characterized by slowly fluctuating Mn spins (rapid muon relaxation), and a decreasing volume fraction. These results strongly suggest that the ferromagnetic
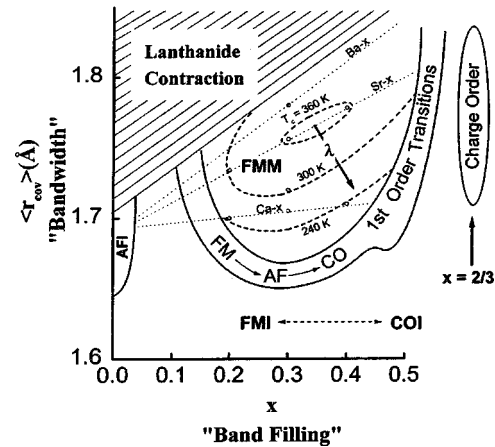
transition proceeds by means of changing volume fractions of rapidly and slowly relaxing local magnetization.

C. Two-phase behavior

An early suggestion that two-phase separation might govern the colossal magnetoresistive regime was made by Gor'kov (1998). Monte Carlo simulations of the double-exchange model with Jahn-Teller coupling also suggested phase segregation of ferromagnetic metal from antiferromagnetic insulator regimes. It is necessary to make a distinction here between *phase separation*, by which is meant coexistence of ferromagnetic/conducting and paramagnetic/insulating regions with constant carrier density, and *charge segregation* as suggested by Yunoki, Moreo, and Dagotto (1998). An experimental test of these ideas was carried out by Jaime *et al.* (1999) using an effective-medium approach. The resistivity data were analyzed in terms of a temperature and magnetic-field-dependent concentration $c(H,T)$ of the metallic phase. The power-law resistivity of the metallic regime and the activated conductivity of the polaronic regimes were assumed to persist into the mixed phase regime near the metal-insulator transition. Combining these with the measured resistivity, Jaime *et al.* extracted the metallic concentration using data from a thin-film sample of $La_{2/3}Ca_{1/3}MnO_3$ using effective-medium expressions. Because the film thermal conductivity is dominated by that of the substrate, the thermal conductivity can be eliminated from the transport equation to give a very simple expression for the thermoelectric power,
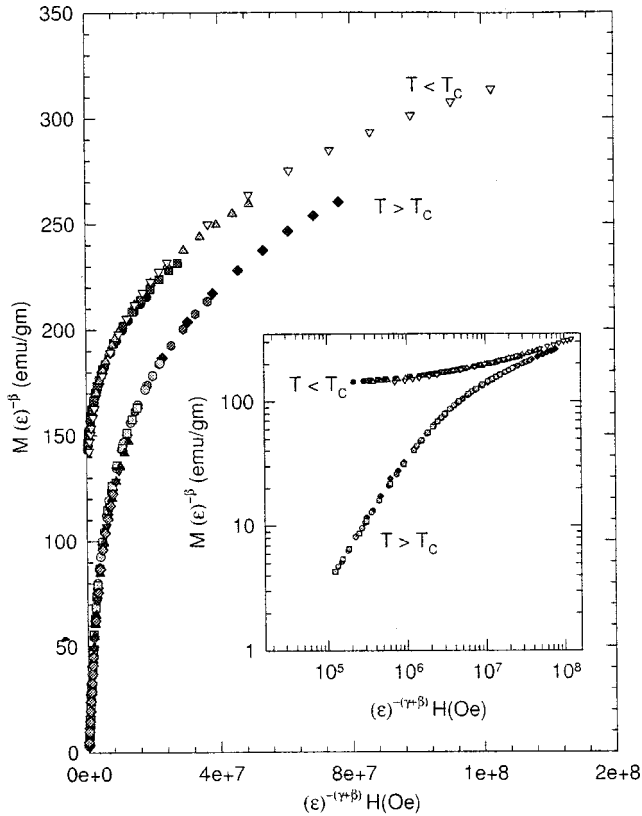
FIG. 46. Critical-scaling plots of $La_{0.7}Sr_{0.3}MnO_3$ below and above the Curie temperature ($T_C = 354.0 \, K$), using β and γ as noted in the text. Inset shows the same plot on a log scale. ϵ is equal to $|T - T_C|/T_C$. From Ghosh et al., 1998.

$$S(H,T) = \frac{1}{\rho_{pol} - \rho_{met}} [\rho_{pol} S_{met} - \rho_{met} S_{pol}$$
$$+ \rho_{exp}(H,T)(S_{pol} - S_{met})], \tag{20}$$

where the subscripts refer to polaron, metallic, and experimental values. As with the resistivity, the thermoelectric powers are fit in the two regimes and assumed to characterize the two phase region. The extracted values of $c(H,T)$ and the fits to the thermopower are shown in Fig. 47.

A number of other experimental probes provide further evidence for the mixed nature of the transition in the CMR regime. EXAFS studies of a series of $La_{1-x}Ca_xMnO_3$ samples, with $x = 0.21$, 0.25, and 0.30 were performed by Booth et al. (1998). The mean-square width of the Mn-O bond-length distribution decreases as the temperature is reduced, approaching at low temperatures the values for $x = 1$, for which there is no Jahn-Teller distortion. Similar results were found from neutron pair-distribution-function data for $La_{0.8}Sr_{0.2}MnO_3$ by Louca and Egami (1999). As seen in Fig. 48, the number of short Mn-O bond lengths changes from approximately four (indicating polaronic elongation of the oxygen octahedra) at high temperatures toward six (no average distortion) at low temperatures. Similar results for $La_{1-x}Ca_xMnO_3$ have been reported by Billinge et al. in which the two-phase coexistence re-
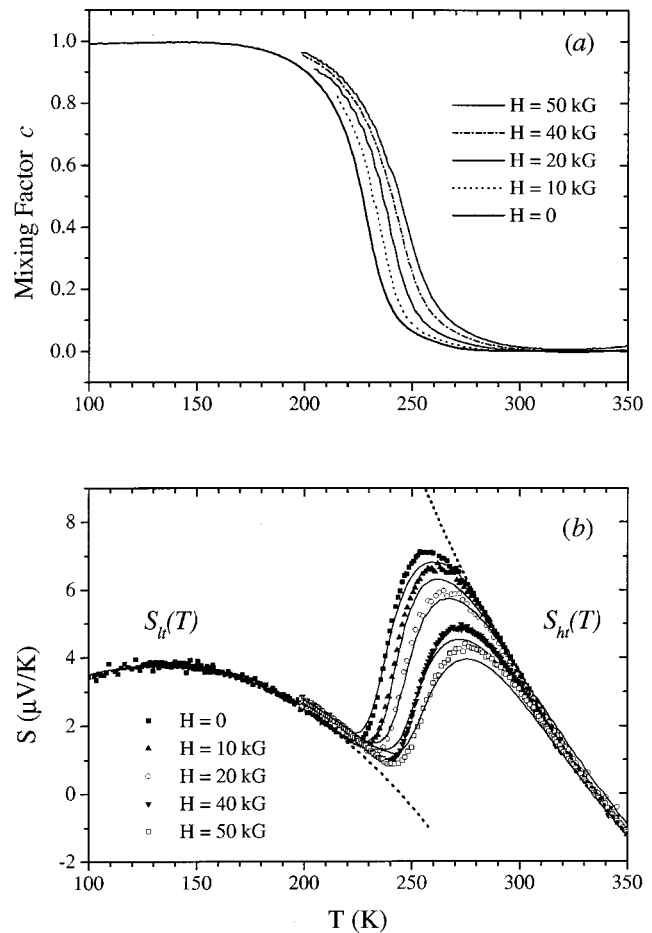

FIG. 47. Two-phase analysis of resistivity and thermopower: (a) The concentration of metallic regions $c(H,T)$ extracted from the resistivity data using the effective-medium approximation and assuming elongated conducting regions with length-to-width ratio $a/b = 50$; (b) Seebeck coefficient data and results of a computation using the measured resistivity $\rho_{exp}(H,T)$ and an effective-medium approximation as described in the text. Dotted lines show the low- and high-temperature fits. From Jaime et al., 1999.

gion is mapped out via pair-distribution-function analysis (Billinge et al., 2000). Particularly convincing evidence of two-phase coexistence is found in the Raman data of Yoon (1998). The spectrum for a sample of $Pr_{0.7}Pb_{0.21}Ca_{0.09}MnO_3$ exhibits, above its Curie temperature $T_C = 145 \, K$, two features in addition to phonons: a broad peak centered near $1100 \, cm^{-1}$ and a low-frequency diffusive response. The peak is attributed to the photoionization energy of small polarons and the diffusive signal, to their hopping motion. As the temperature is reduced, the diffusive signal evolves into a flat continuum response characteristic of metallic behavior. Figure 49 shows the temperature dependence of the integrated Raman intensities for the diffusive (polaronic) and continuum (electronic) contributions. Their coexistence in the vicinity of T_C is readily apparent.

Quite recently, diffuse neutron-scattering peaks have been detected (Dai, Fernandez-Baca et al., 2000) that indicate polaron-polaron correlations exist over a wide
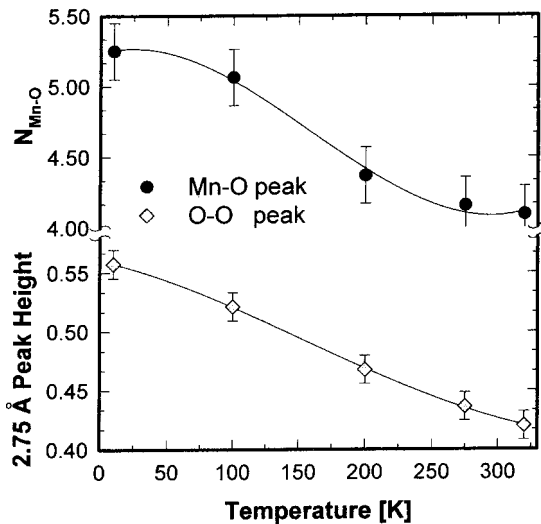
FIG. 48. Bond-length distribution: Top, the number N_{Mn-O} of short Mn-O bonds as a function of temperature for $La_{0.8}Sr_{0.2}MnO_3$, as determined by neutron pair-distribution-function analysis. The presence of four short bonds at high temperatures is indicative of the existence of Jahn-Teller polarons. The bond lengths tend to equalize with decreasing temperature, but some residual distortion of the oxygen octahedra remains at low temperatures. Bottom, the height of the pair-distribution function peak at 2.75 Å which includes the O-O pair. Its relation to temperature is similar to that of the N_{Mn-O} value. From Louca and Egami, 1999.

temperature range above T_C, but collapse below. The position of the peak suggests short-range charge ordering with a correlation length of ~ 1.4 nm at room temperature, increasing to ~ 2.8 nm at the transition. There is no sign of long-range charge ordering. Further evidence for mixed phases comes from a Mossbauer study of LCMO doped with ^{57}Co (Chechersky et al., 2000). Coexisting ferromagnetic and paramagnetic sites are

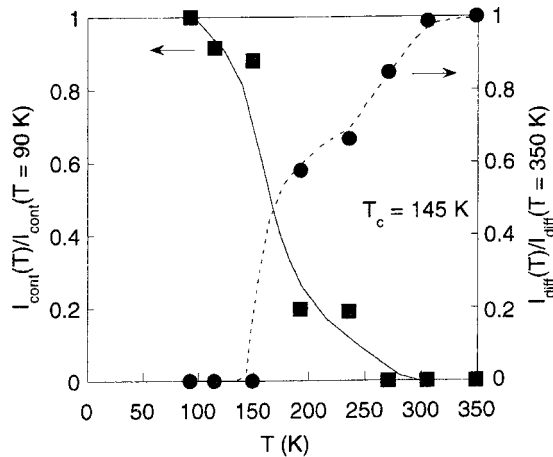FIG. 49. Raman-scattering data showing the temperature dependence of the integrated scattering strength ratio for ●, the diffusive response, $I_{diff}(T)/I_{diff}$ ($T=350$ K) indicative of polarons, and ■, the flat continuum response, $I_{cont}(T)/I_{cont}$ ($T=90$ K) indicative of band electrons, for a $T_C=145$ K sample. From Yoon et al., 1998.

found in the vicinity of the phase transition, as might be expected from the conducting/insulating mixture postulated by Jaime et al. (1999).

Additional evidence for inhomogeneous conductivity in the vicinity of the phase transition is found on the noise characteristics of film and single-crystal samples. Early work (Hardner et al., 1997) on a partially annealed $La_{2/3}Ca_{1/3}MnO_3$ film ($T_C \approx 100$ K) revealed presence of significant non-Gaussian noise in the form of discrete resistance switching that is largely absent well below the transition, but predominant at T_C. Anomalously large $1/f$ noise is also found in LCMO films (Alers et al., 1996; Raquet et al., 2000), and it has been found that the magnitude in epitaxial films is sensitive to oxygen content (and therefore T_C) (Rajeswari et al., 1998). Samples that are in the first-order transition regime show very large $1/f$ noise which is taken as evidence for a percolation transition (Podzorov et al., 2000). Recent noise measurements on single crystals also finds a large $1/f$ contribution in LCMO with evidence for two-state switching in a narrow temperature range near $T_C=218$ K. From the field and temperature characteristics of the switchers, the authors conclude that regions as large as 10^4 unit cells are fluctuating between high and low resistance states, providing strong evidence for inhomogeneous conducting paths as expected for a percolationlike transition (Merithew et al., 2000).

When the transition is fully first-order in character, the phase separated regions are mesoscopic (micrometer range) and have been observed by electron microscopy (Uehara et al., 1999). Static images of conducting and insulating regions have also been captured using scanning-tunneling microscopy (Tath et al., 1999). In this study, coexisting insulating and conducting regions on the 100-nm scale were imaged, and the growth of metallic regions was monitored as a magnetic field was applied near the transition temperature. Such quasistatic objects may be related to the slow-switchers observed in noise studies, but are larger in scale that those detected by neutron scattering. A recent calculation has indicated that these giant clusters have equal electronic density and result from disorder in the exchange and hopping amplitudes in the vicinity of a first-order transition (Moreo et al., 2000).

D. Phase-separation models

The effective-medium approach suggests that metallic and insulating regions coexist as interpenetrating clusters, also suggesting a percolation picture of the insulator-metal transition. One such percolative model was proposed by Bastiaansen and Knops (1998) based on a random resistor network. A Monte Carlo simulation of a 2D Ising model formed the basis of the calculation, with unit resistors connecting aligned nearest- and next-nearest-neighbor sites and infinite resistance linking unaligned sites. The resistance of the network is qualitatively similar to experiment. For a system of Heisenberg spins, of course, resistance of each link can vary continuously between 1 (linked spins parallel) and
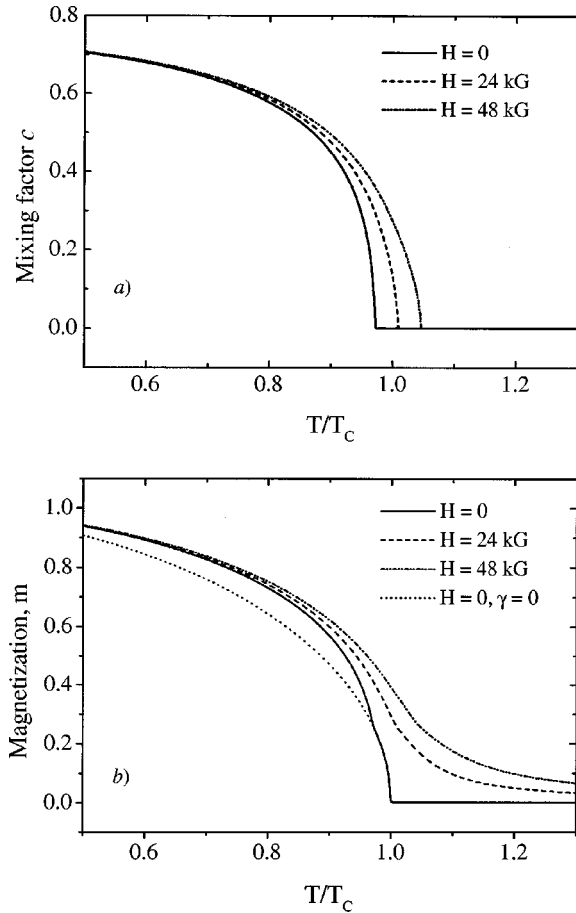
FIG. 50. Results of a coupled-order parameter model: (a) the conducting concentration $c(H,T)$ calculated in the mean-field model with $\alpha=0.02$ and $\gamma=0.3$; (b) the magnetization calculated with the same parameters. The dotted line shows the noninteractive case for comparison. From Jaime and Salamon, 1999.

FIG. 51. Inverse magnetic susceptibility H/m vs temperature near the M-I transition for $H=24$ kOe. Dashed line, the zero-field extrapolated behavior. The appearance of free carriers induces an increase in the effective T_C, leading to a kink in the susceptibility. Inset: inverse susceptibility of a single-crystal sample of $La_{0.7}Ca_{0.3}MnO_3$, measured in a field of 1 kG. From Jaime *et al.*, 1999.

infinity (linked spins antiparallel), greatly reducing the size of the resistance peak just at T_C. Quite similar results have been reported recently by Mayr *et al.* (2001). A more realistic model was proposed by Lyukyutov and Pokrovsky (1999) which is based on Varma's theory (Varma, 1996) of magnetic polaron formation, modified to include Jahn-Teller effects. Magnetic polarons, which coexist with small lattice polarons, are assumed to be large, basically comprising magnetically correlated regions. As the temperature is lowered, the magnetic polaron density increases until the magnetic polarons overlap, which defines the percolation point. The authors argue that long-range Coulomb effects render implausible suggestions that macroscopic charge separation underlies the CMR effect (Yunoki *et al.*, 1998; Moreo *et al.*, 1999). Similar ideas have been discussed by Gor'kov (Gor'kov, 1998; Gor'kov and Kresin, 1998).

A simple mean-field model has been proposed by Jaime *et al.* (1999) that gives a qualitative description of the conducting fraction $c(H,T)$. A simplification of the dynamic mean-field theory of Millis, Mueller, and Shraiman (1996), it recognizes that the fully metallic state $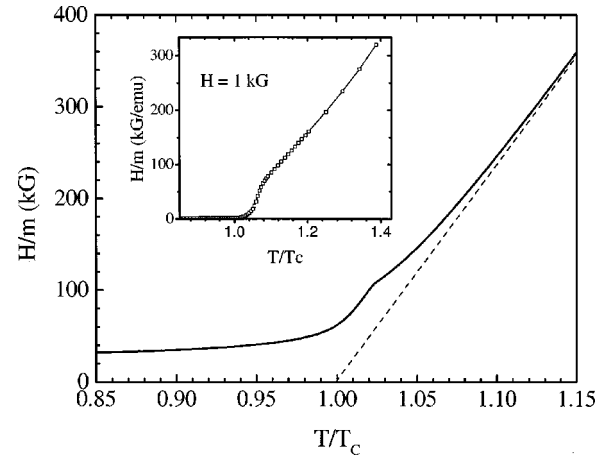c(0,T\rightarrow 0)$ is achieved only if the effective Jahn-Teller coupling constant λ_{eff} is smaller than the critical value λ_c. Because λ_{eff} is, in turn, inversely proportional to the bandwidth, the double exchange mechanism causes λ_{eff} to decrease as magnetic order sets in. In the CMR regime, where λ_{eff} is presumed to be near λ_c, it can be expanded as

$$\lambda_{eff}\simeq\lambda_c+\alpha-\gamma m^2, \tag{21}$$

where α is a small positive constant that assures that polarons will form once the magnetization $m=M(H,T)/M_{sat}$ becomes smaller than α/γ. The conducting fraction is then taken to be an order parameter satisfying

$$c=\tanh[(1-\alpha+\gamma m^2)c]. \tag{22}$$

The coupling constant γ causes the Curie temperature to increase when c is finite, so that the magnetization in zero field rises more rapidly for $c\gtrsim 0$. Figure 50 shows the conducting fraction and magnetization at several magnetic fields for $\alpha=0.02$ and $\gamma=0.4$, which compare well with $c(H,T)$ seen in Fig. 47(a). There is a kink in the magnetization at the point at which the mixing factor begins to increase; such kinks are frequently observed experimentally as seen in Fig. 51 (Jaime *et al.*, 1999). This model cannot, of course, capture the essential contributions of magnetic/conducting fluctuations.

E. Hall effect in the transition region

Even in the regime where the charge carriers are nominally "metallic," estimates based on free-electron ideas (electron density $n\approx10^{27}\,\mathrm{m}^{-3}$, effective mass $m\approx3m_e$) suggest that the mean free path approaches interatomic distances once the resistivity exceeds $1\,\mathrm{m\Omega\,cm}$. Therefore even the metallic portions of any percolation network must be considered to be localized
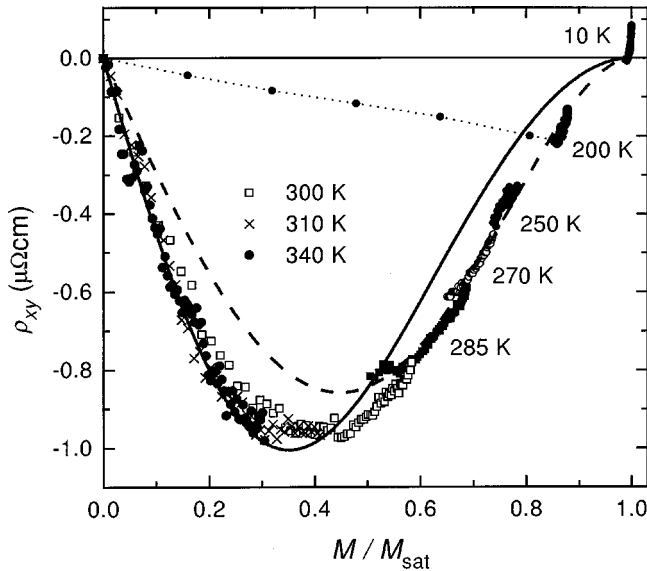
FIG. 52. Plot of the Hall resistivity ρ_{xy} vs reduced magnetization using the data shown in Fig. 27 showing scaling behavior: solid line, a fit to Eq. (23); dashed line, the numerator of Eq. (23) only. There are no fitting parameters except the amplitude. From Chun, Salamon, Lyanda-Geller et al., 2000.

(Gor'kov, 1998; Lyanda-Geller et al., 2000). The degree to which the localization length shrinks to permit self-trapping by Jahn-Teller processes determines the strength of the CMR effect. However, once the resistivity exceeds this Mott-Ioffe-Regel limit, all transport processes must be considered within a hopping framework. This point is made forcefully by the strongly anomalous behavior of the Hall effect which is very similar for a variety of manganites despite major differences in their resistive properties. Figure 27(a) shows the Hall resistivity of the single-crystal sample whose longitudinal resistivity was shown in Fig. 1. Despite the very large differences in ρ_{xx} among various samples, the ρ_{xy} data are remarkably similar, and deviate strongly from the behavior of conventional ferromagnets in the critical region. In conventional magnets, Eq. (13) permits the separation of ordinary and extraordinary components through the critical point, here the Hall resistivity becomes non-monotonic and strongly curved. Only at high temperatures, where the polaronic effects dominate, and at very low temperatures, can an ordinary Hall coefficient be defined, as seen in Figs. 27(a) and (b). The first suggestion that a mechanism beside skew scattering and side-jump processes was needed was made by Ye et al. (1999). Formulated for metallic conduction, this model predicted a maximum in ρ_{xy} above the Curie temperature, which is contrary to what is observed. Recognizing that the entire transition region is in the nonmetallic, hopping regime, Chun, Salamon, Lyanda-Geller et al. (2000) extended the classic Hall calculation of Holstein (1959) for the Hall constant of hopping charge carriers to take account of the Berry-like phase that is accumulated by charge carriers that are required by strong Hund's-rule coupling to follow the local spin texture. The model predicts that the Hall resistivity should de-

pend only on the magnetization, independent of the details of the hopping process, and is given by

$$\rho_{xy} = \rho_{xy}^0 \left(\frac{m(1-m^2)^2}{1+m^2} \right). \tag{23}$$

Figure 52 shows that this is obeyed by the data of Fig. 27(a) with values of ρ_{xy}^0 that are in reasonable agreement with estimates using atomic spin-orbit coupling constants. The boundary between this anomalous contribution and the ordinary (Holstein) contribution was found recently by Chun, Salamon, Jaime et al. (2000) as a minimum in the Hall mobility.

VI. CHARGE AND ORBITAL ORDERING TRANSITIONS

A. 3D manganites

Away from the ferromagnetic regime, and even overlapping it somewhat, is a variety of charge and orbitally ordered phases. The experimental situation has been reviewed in some detail recently by Rao and Raveau (Rao et al., 2000). It might be argued that charge ordering at doping levels that are rational fractions represent an order-disorder transition of Jahn-Teller polarons. This interpretation was favored by Cheong and Chen (1998) who found evidence for charge ordering in $La_{1/2}Ca_{1/2}MnO_3$ and $La_{1/3}Ca_{2/3}MnO_3$. Indeed, looking at Fig. 12 we would expect that approach to describe $Sm_{1/2}Ca_{1/2}MnO_3$, $Nd_{1/2}Ca_{1/2}MnO_3$, and $Pr_{1/2}Ca_{1/2}MnO_3$ and, for the last of these, direct evidence for it from high-resolution electron microscopy has been reported (Li et al., 1999). However, this picture cannot hold for $Nd_{1/2}Sr_{1/2}MnO_3$ or $Pr_{1/2}Sr_{1/2}MnO_3$, where the charge-ordered phase arises within the more metallic, ferromagnetic regime. Figure 53 shows the contrast between $Sm_{1/2}Ca_{1/2}MnO_3$ and $Nd_{1/2}Sr_{1/2}MnO_3$ (Tomioka et al., 1997). While the former shows a weak peak in magnetization and an insulator/insulator transition at the charge ordering temperature, the latter clearly becomes ferromagnetic and metallic near 250 K before undergoing a first-order metal/insulator transition to an antiferromagnetic phase near 160 K. That $Nd_{1/2}Sr_{1/2}MnO_3$ and $Pr_{1/2}Sr_{1/2}MnO_3$ both become antiferromagnetic at the charge ordering transition is shown by the neutron-diffraction data (Kawano et al., 1997) in Fig. 54. That figure also demonstrates the narrowness of the antiferromagnetic CE phase (see Fig. 11 for its structure) shown in Fig. 17. This has been explored in some detail by Kajimoto et al. (1999). At a Sr content of $x=0.55$ the ferromagnetic phase does not intercede between the paramagnetic state and the insulating, A-type antiferromagnetic phase. As was noted previously, the tendency toward stabilization of Jahn-Teller polarons is strongly correlated with the ionic size of the divalent dopant in the A site. This has been attributed to the intrinsic bandwidth to be expected in the fully metallic state, which in turn depends on the Mn-O-Mn bond angle. At $x=1/2$, as well, the primacy of the tendency toward charge ordering and an insulating state is closely tied to the tolerance
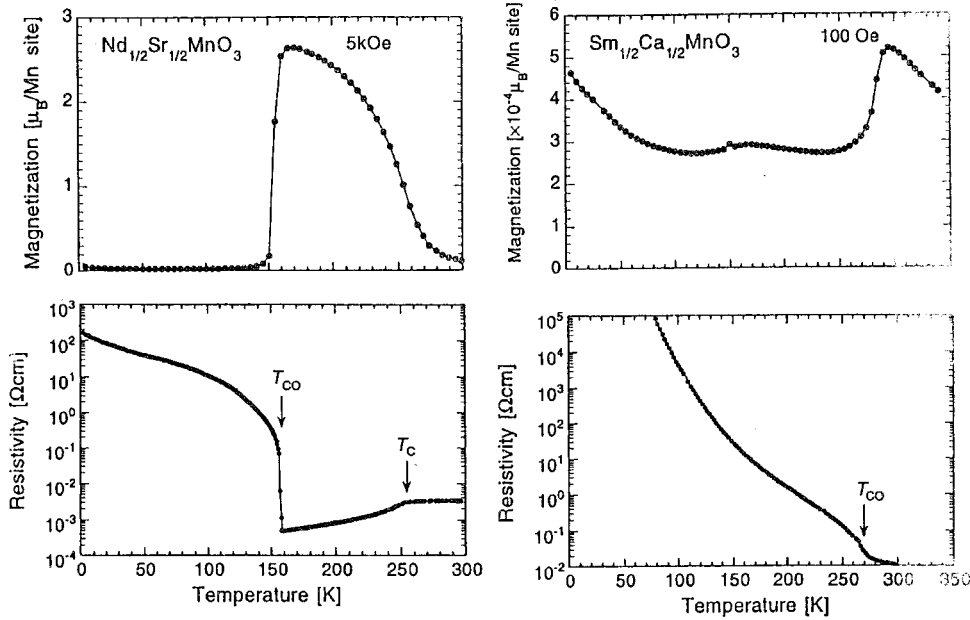
FIG. 53. Charge ordering transitions in $Sm_{1/2}Ca_{1/2}MnO_3$ and $Nd_{1/2}Sr_{1/2}MnO_3$. NSMO exhibits a ferromagnetic, metallic phase before undergoing a charge ordering transition. In contrast, SCMO makes a transition directly to the insulating, charge ordered state. From Tomioka et al., 1997.
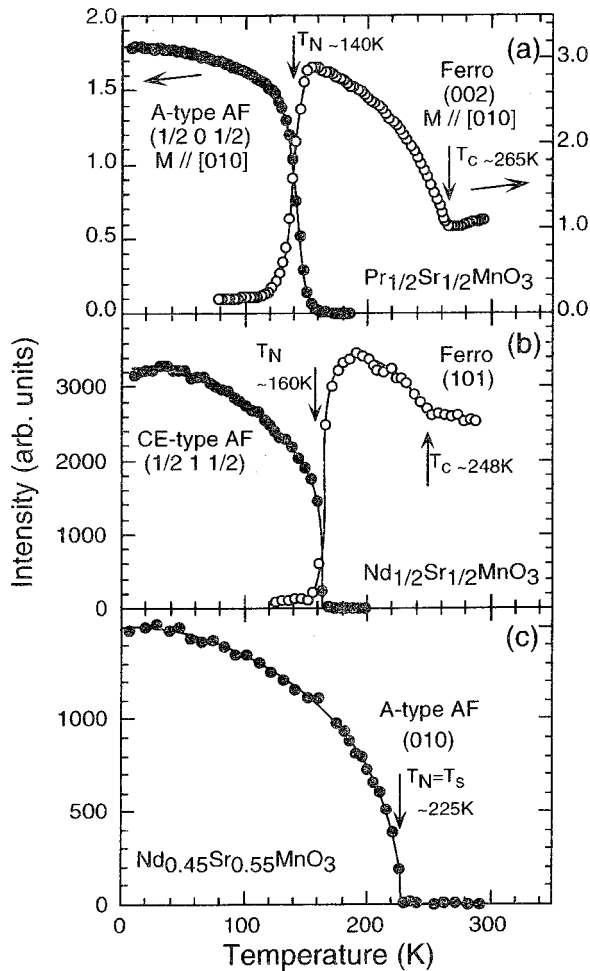

FIG. 54. Neutron-scattering results on the ferromagnetic-to-antiferromagnetic transitions in $x=1/2$ manganites showing A-type ($Pr_{1/2}Sr_{1/2}MnO_3$) and CE-type ($Nd_{1/2}Sr_{1/2}MnO_3$) order. The latter result on NSMO supports the data shown in Fig. 53. Off $x=1/2$ the ferromagnetic phase is absent and A-type order occurs. From Kawano et al., 1997.

factor. Figure 55 summarizes the sequence of transitions for various combinations of A-site atoms at $x=1/2$.

A dramatic feature of the charge ordered state is that it can be "melted" by a magnetic field, as first reported by Kuwahara et al. (1995). The transition, which is hysteretic in temperature at zero field, becomes strongly hysteretic in applied fields, as may be seen in Fig. 12. The melting transition is clearly observed in the resistivity, as is shown in Fig. 56 for $Pr_{1/2}Ca_{1/2}MnO_3$. The changes are even more dramatic (Tokura et al., 1996) for $Nd_{1/2}Sr_{1/2}MnO_3$, as seen in Fig. 57(a). At low temperatures, there is a resistive change of six orders of magnitude in a field of 7 T. Kuwahara and co-workers (Kuwahara et al., 1995; Kuwahara and Tokura, 1998) have mapped out the field-temperature phase diagram for this compound by cycling the field at fixed temperature. As seen in Fig. 57(b), the region of bistability grows dramatically as the temperature is reduced, with the metallic state tending toward metastability. Kuwahara and Tokura (1998) suggest that there exist two local minima in the free energy of the system, one corresponding to a large-M, charge liquid state and the other a small-M, charge ordered one, separated by a barrier U. At a critical value of the field, the Zeeman energy favors the metastable, large-M state and the system becomes metallic. As the field is removed, the barrier prevents the return of the system to its stable state, tending to trap it in the metastable, conducting state.

When the hole concentration is not exactly 1/2 or 2/3 and, in the case of $La_{1/2}Ca_{1/2}MnO_3$, possibly even at $x=1/2$ (Cheong and Chen, 1998), charge order is found to be incommensurate. There is evidence for coexistence of the $x=1/2$ and 2/3 structures as well as discommensurations. As a consequence of the discommensurations, there is a spin slip associated with the Mn^{3+} sites that results in a shorter correlation length for Mn^{3+} sublattice (Cheong and Chen, 1998). Figure 58 is a schematic
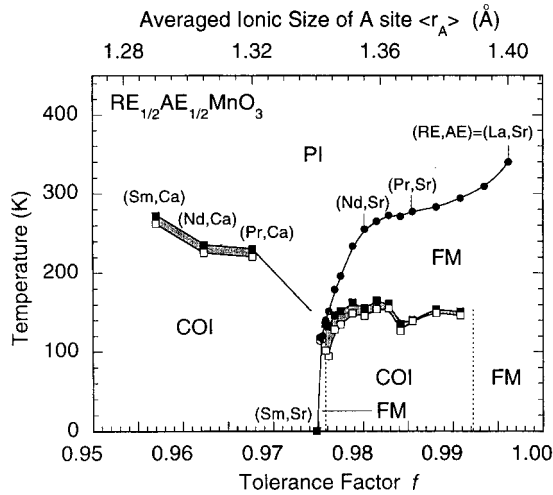
FIG. 55. Dependence of charge-ordering transition on ionic size or tolerance factor for various manganites. Phases include paramagnetic insulator (PI), a charge-ordered insulator (COI), and a ferromagnetic metal (FM), respectively. From Kuwahara and Tokura, 1998.

sketch of a discommensuration that results from a spin (and orbital) slip along a line of Mn^{4+} ions.

There have been several theoretical efforts to understand the charge ordering mechanism and the emergence of the CE antiferromagnetic state. A general study of charge ordering in the context of the Holstein model was carried out by Chiuchi and de Pasquale using dynamical mean-field theory (Chiuchi and de Pasquale, 1999). They identify a phase boundary between a randomly distorted, charge ordered state and a polaronic ordered phase as a function of the effective electron-phonon coupling parameter λ (see Sec. IV). van Veenendal and Fedro argue that when polarons encompass two sites, the hopping of the electron between them

FIG. 57. Field-induced metastability at $x = (\frac{1}{2})$; (a) field-induced metal-insulator transition in $Nd_{1/2}Sr_{1/2}MnO_3$ taken from a series of Sm-doped samples From Tokura *et al.*, 1996; (b) field-temperature phase diagram for $Nd_{1/2}Sr_{1/2}MnO_3$. The hatched area corresponds to a region of metastability. From Kuwahara *et al.*, 1995.

"dresses" the polaron, and provides an explanation for the ferromagnet-CE phase transition (van Veenendaal and Fedro, 1999). Shen and Wang (1999) demonstrate that Wigner crystallization occurs within the double exchange model when processes that allow the possibility of S-1/2 states, where S is the spin of the t_{2g} core, even absent Jahn-Teller coupling. This may be relevant to the Wigner crystal ordering observed at 2/3 filling.

B. Layered manganites

As discussed in Sec. III.B.2, the bilayer manganites $RESr_2Mn_2O_7$ also show charge ordering effects. The situation is more complicated with the charge-ordered state exhibiting a competition between A-type and CE-type magnetic order. In a study of $(Nd_{1-x}La_x)Sr_2Mn_2O_7$, Moritomo *et al.* (1999) found a

FIG. 56. Field-induced metal-insulator transition in $Pr_{1/2}Ca_{1/2}MnO_3$. From Tomioka *et al.*, 1996.

up   down

$\oplus$ $\ominus$ Mn^{+4} ——— AFM
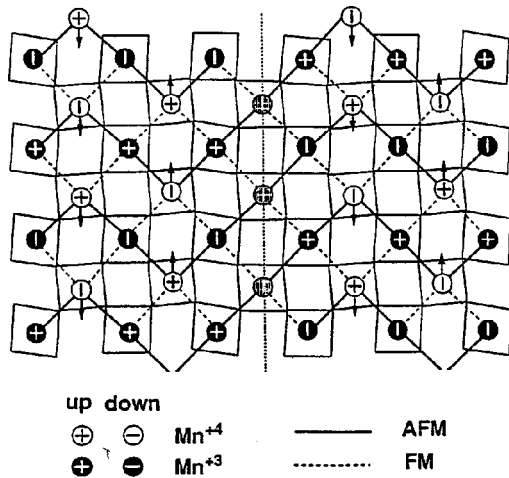
$\bullet$ $\bullet$ Mn^{+3} ········· FM

FIG. 58. Sketch of a discommensuration exhibiting a spin slip in the Mn^{3+} sublattice. From Cheong and Chen, 1998.

narrow, charge-order CE antiferromagnetic regime to exist on the La-rich end of the series, but to dominate in a narrow temperature range between 110 and 220 K. On cooling, the resistivity of LaSr$_2$Mn$_2$O$_7$ first increases sharply at the charge ordering transition, reaches a maximum, and then decreases to a minimum near 100 K. Single-crystal neutron-scattering data provide greater detail (Kubota, Fujioka *et al.*, 1999; Kubota, Yoshizawa *et al.*, 1999). As shown in Fig. 59, *A*-type antiferromagnetic order [Fig. 59(a)] and CE-type charge order [Fig. 59(b)] appear simultaneously at 210 K. This coincides with a decrease in diffuse magnetic scattering [Fig. 59(c)]. Near 120 K, the CE-type charge ordering disappears and a weak, CE-type antiferromagnetic peak [Fig. 59(d)] appears. A small volume fraction of CE antiferromagnetic order persists to low temperature, but the
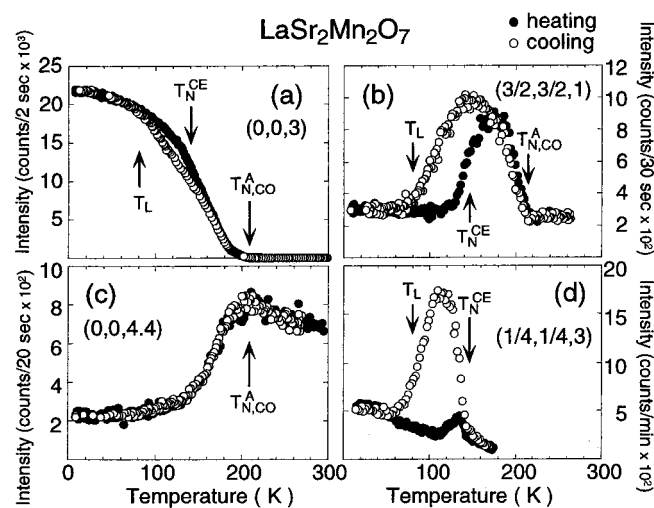

FIG. 59. Neutron-diffraction results for NdSr$_2$Mn$_2$O$_7$. (a) Antiferromagnetism and (b) charge ordering appear at 210 K, while (c) diffuse magnetic scattering decreases below that temperature. (d). Near 120 K, the antiferromagnetic order changes to CE type over a narrow temperature range. From Kubota, Fujioka *et al.*, 1999b.

main contribution disappears at the temperature at which CE charge order vanishes. The authors conclude that this "melting" of the charge ordered state reflects the competition between *A*-type $d_{x^2-y^2}$ and CE-type $d_{3x^2-r^2}$ and $d_{3y^2-r^2}$ orbitals. Substitution of Nd for La lowers and reduces the resistivity peak, but leaves some remanence of the charge ordered state in the temperature range between 100 and 200 K.

The resistivity of the single-layered compound La$_{1/2}$Sr$_{3/2}$MnO$_4$ increases slowly with decreasing temperature to approximately 240 K, below which it increases rapidly (Moritomo *et al.*, 1995). Electron diffraction showed this temperature to mark the onset of charge ordering. Subsequent work by Bao *et al.* (1996) found the charge order superlattice spots to be consistent with 3D ordering, and to lie at 1/4 positions. However, neutron-scattering data (Sternlieb *et al.*, 1996) showed that charge order to set in near 220 K in the pattern shown in Fig. 14, with spin ordering occurring at 110 K. Peaks at the 1/4 position were observed by x-ray diffraction at the Mn *K* edge, and were attributed to orbital ordering in the pattern shown in Fig. 14 (Murakami, Kawada *et al.*, 1998).

VII. IMPLICATIONS

Between the time of early experiments (Jonker, and van Santen, 1950; van Santen and Jonker, 1950; Volger, 1954) and subsequent theoretical treatments (Zener, 1951; Anderson and Hasegawa, 1955; Goodenough, 1955; de Gennes, 1960) in the 1950s and the work of Jin and co-workers in the 1990s (Jin, McCormack *et al.*, 1994; Jin, Tiefely *et al.*, 1994) this field lay dormant. The double exchange mechanism was partly at fault, lulling researchers into believing that it contained the essential elements needed to understand these materials. The reawakening of the field came as a consequence of the large increases in magnetoresistance discovered in ferromagnetic/nonmagnetic metallic multilayers, and their ability to increase dramatically the areal bit density in magnetic recording. However, we have seen the CMR effect is only one manifestation of a competition between double exchange, that favors ferromagnetic order, and a combination of Jahn-Teller coupling, Coulomb interactions, and antiferromagnetic superexchange, which favor various flavors of charge/orbital/antiferromagnetic order. The main impact of the double exchange mechanism is to serve as an amplifier of the magnetic field in that alignment of neighboring spins serves as a valve that controls the flow of doped-in holes through the double exchange transfer matrix element t_{ij}^{eff} $=t\cos(\theta/2)$. The amplification can be readily seen in the heat capacity of La$_{0.7}$Ca$_{0.3}$MnO$_3$ near the ferromagnetic transition, Fig. 44 where a field of 7 T, corresponding to 12 K for $S=2$, gives rise to a shift in the transition temperature more than three times larger. This even more dramatically demonstrated in Fig. 57(a), where a 7-T field drives the charge ordering transition from 150 K to zero, a tenfold amplification of the field energy. Here again, aligning spins delocalizes the doped-in hole, re-

duces its kinetic energy, and in turn reinforces the effect of the field. In that way, a relatively small magnetic field creates a band and with it, an energy gain of 3/5 of the Fermi energy which, at half filling, is 3/10 of the bandwidth. Taking the bandwidth to be of order $(10^4\,\mathrm{K})k_B$ (Coey *et al.*, 1999) this yields more than the 150 K required to balance the charge ordering energy of $\mathrm{Nd}_{1/2}\mathrm{Sr}_{1/2}\mathrm{MnO}_3$.

The amplification of magnetic order described above tends to overcome the tendency for charge/orbital ordering and to drive, thereby, the colossal magnetoresistance. How this comes about has been clarified by recent neutron-scattering (Dai, Fernandez-Baca *et al.*, 2000) and electron-diffraction results (Zuo and Tao, 2001), on $\mathrm{La}_{2/3}\mathrm{Ca}_{1/3}\mathrm{MnO}_3$. Diffuse, nonmagnetic, quasielastic peaks are observed in neutron scattering at (1/4, 1/4, 0) positions, indicating the presence of short-range (1–2 nm) CE-type antiferromagnetic orbital ordering. Confirming data from electron diffraction reveals the presence of 1/2-order diffuse charge peaks of comparable correlation length. The CE-type diffuse intensity increases with decreasing temperature, reaching a maximum near the temperature of the resistivity maximum. At the same time, underlying diffuse scattering attributed to uncorrelated polarons, relatively constant above T_C, drops gradually below. To achieve such large volumes of fully charge ordered regions with alternating Mn^{3+} and Mn^{4+} sites in a sample with only 1/3 of the sites doped to Mn^{4+} would require excessive Coulomb energy. Rather, there must be slightly hole-rich regions, exhibiting CE-type antiferromagnetic charge modulations, surrounded by hole-poor regions. Because CE-type antiferromagnetic charge order is stripelike, the manganites in this regime resemble, to some extent, the "electronic liquid crystal phases" that have been proposed for cuprates doped to comparable levels. As the temperature is reduced, the hole-rich regions find themselves above the global Curie temperature, and develop ferromagnetic correlations. These correlations then suppress the tendency toward charge/orbital order, cause the diffuse CE-type peaks to lose intensity, and produce local conducting regions, exactly as postulated by the two-fluid model. This picture is also consistent with the observation that ferromagnetic correlations do not grow critically as the phase transition is approached, but rather saturate at roughly the same 1–2-nm scale observed for the size of CE-correlated regions.

The competition between charge/orbital ordering and ferromagnetism raises fundamental questions about the nature of the transitions. Away from the ferromagnetic concentration regime, the charge ordering transitions are clearly first order in both field and temperature. However, the ferromagnetic transitions in the "nominal" concentration regime are not obviously first order, as is suggested by Fig. 45. However, as the heat-capacity data show, they do not behave as expected for conventional second-order transitions, either. As the bandwidth/band filling point in Fig. 45 moves into the 360-K contour, the nature of the phase transition becomes much closer to that of a conventional ferromagnetic transition, as seen

in the scaling curve of Fig. 46. This suggests that the tendency to localize charge carriers into insulating and ferromagnetic regimes causes the material to act like a ferromagnet with quenched in disorder, and therefore opens the possibility that the critical behavior is influenced by Griffiths singularities (Griffiths, 1969; Bray, 1987). Indeed, the spin dynamics in the region between the observed ordering temperature ($\approx 250\,\mathrm{K}$ for $\mathrm{La}_{2/3}\mathrm{Ca}_{1/3}\mathrm{MnO}_3$) and the highest temperature when all double exchange bonds are active ($\approx 360\,\mathrm{K}$ for $\mathrm{La}_{2/3}\mathrm{Sr}_{1/3}\mathrm{MnO}_3$) have been found to exhibit the nonexponential relaxation (Heffner *et al.*, 1997, 2000) expected for Griffiths phases. As deduced from the resistivity, the magnetic transition occurs as regions with an excess of active bonds percolate to develop long-range order.

Important theoretical challenges also remain in understanding the low-temperature properties. Despite differences in Curie temperature and doping, the underlying exchange interactions in the ferromagnetic state appear to be robust, at least as revealed by the behavior of long-wavelength ferromagnetic spin waves seen in Fig. 14. It remains to be understood how the exchange interaction can be insensitive to the number of possible Mn^{3+}-Mn^{4+} pairs. As pointed out in Sec. III.C.2, the resistivity in the ferromagnetic regime loses its temperature dependence at low temperatures, in violation of Mathiesson's rule. Weak temperature dependence is expected in a half-metallic ferromagnet, due to the suppression of spin-flip scattering. However, the very excitation of spin waves eventually restores a down-spin band and with it, the possibility of spin-flip scattering. Just how the down-spin band develops and when spin-wave scattering returns remains an open question, although a first attempt to address this has been made (Furukawa, 2000). The nature of the orbital degrees of freedom in the ferromagnetic regime also remains an open question. It has generally be thought of (Tokura and Nagaosa, 2000) as an "orbital liquid," but there have been some recent suggestions that a chiral orbital liquid might be possible (Maezono and Nagaosa, 2000).

From a condensed-matter perspective the tendency for stripe order to occur in both electron doped (e.g., Ca-rich) and hole-doped (e.g., La-rich) ends of the phase diagram make these materials interesting testing grounds for understanding the nature of liquid-crystal-like phases in dilute electronic systems. The strong core magnetism and its partner, strong Hund-rule coupling, prevent the itinerant electrons from developing superconducting fluctuations such as is the case in cuprates. However, these materials represent one end of a continuum of transition-metal oxides with perovskite-type structures. All of them exhibit competition among charge, magnetic, and orbital order. When these are present, of equal strength, but not strong, as in the copper end point, superconductivity can occur. The manganites, along with cobaltates and nickelates, and probably ruthenates, must be fully understood before the unusual metallic behavior of the cuprates can be comprehended. It may well be that the metallic state of all these oxides

represents a new, non-Fermi-liquid state of dense electron systems and that new theory of metals will be required.

As noted above, the initial motivation for reexamining this materials was to explore their possible applications to magnetic recording, sensing, and memory. The half-metallic ground state suggested that very large magnetoresistance could be attained by fabricating tunnel junctions. These efforts have been reviewed elsewhere. (Ramesh *et al.*, 1998). In a similar regard, there are numerous reviews whose focus has been on the role of crystal chemistry and the microstructure of films grown by various methods. Our focus here has been on the variety of possible states and the transitions among them. Whether or not these materials eventually find useful applications, they have already expanded our understanding of what is a metal or an insulator, and what characterizes the transitions between these states. The lesson is that strong, but evenly balanced, interactions lead to dramatic changes in physical properties and that an understanding of how to treat such situations remains to be found.

ACKNOWLEDGMENTS

REFERENCES

Alers, G. P., A. P. Ramirez, and S. Jin, 1996, Appl. Phys. Lett. **68**, 3644.

Alexandrov, A., and A. Bratkovsky, 1999, J. Appl. Phys. **85**, 4349.

Anderson, P., and H. Hasegawa, 1955, Phys. Rev. **100**, 675.

Argyriou, D. N., J. F. Mitchell, P. G. Radaelli, H. N. Bordallo, D. E. Cox, M. Medarde, and J. D. Jorgensen, 1999, Phys. Rev. B **59**, 8695.

Ashcroft, N., and N. Mermin, 1976, *Solid State Physics* (Saunders College Publishing, Philadelphia).

Babushkina, N. A., L. M. Belova, A. N. Taldenkov, E. A. Chistotina, D. I. Khomskii, K. I. Kugel, O. Yu. Gorbenko, and A. R. Kaul, 1999, J. Phys.: Condens. Matter **11**, 5865.

Balcells, L., J. Fontcuberta, B. Martinez, and X. Obradors, 1998, Phys. Rev. B **58**, R14697.

Bao, W., C. H. Chen, S. A. Carter, and S.-W. Cheong, 1996, Solid State Commun. **98**, 55.

Bastiaansen, P. J. M., and H. J. F. Knops, 1998, J. Phys. Chem. Solids **59**, 297.

Battle, P., 1996, J. Phys.: Condens. Matter **8**, L427.

Battle, P., M. Green, N. Laskey, J. Millburn, P. Radaelli, M. Rosseinsky, S. Sullivan, and J. Vente, 1996, Phys. Rev. B **54**, 15967.

Benfatto, M., Y. Joly, and C. R. Natoli, 1999, Phys. Rev. Lett. **83**, 636.

Berger, A., J. Mitchell, D. Miller, J. Jiang, and S. Bader, 2000, J. Vac. Sci. Technol. A **18**, 1239.

Berman, R., 1976, *Thermal Conduction in Solids*, Oxford Studies in Physics (Clarendon Press, Oxford).

Billinge, S. J. L., T. Proffen, V. Petkov, J. L. Serrao, and S. Kycia, 2000, Phys. Rev. B **62**, 1203.

Booth, C. H., F. Bridges, G. Kwei, J. Lawrence, A. Cornelius, and J. Neumeier, 1998, Phys. Rev. Lett. **80**, 853.

Bouloux, J., J. Soubeyroux, A. Daoudi, and G. Leflem, 1981, Mater. Res. Bull. **16**, 855.

Bray, A. J., 1987, Phys. Rev. Lett. **59**, 586.

Broussard, P., S. Qadri, V. Browning, and V. Cestone, 1999, J. Appl. Phys. **85**, 6563.

Causa, M., M. Tovar, A. Caneiro, F. Prado, G. Ibanez, C. Ramos, A. Butera, B. Alascio, X. Obradors, S. Pinol, F. Rivadulla, C. Vazquez-Vazquez, M. Lopez-Quintela, J. Rivas, Y. Tokura, and S. Oseroff, 1998, Phys. Rev. B **58**, 3233.

Chaikin, P., and G. Beni, 1976, Phys. Rev. B **13**, 647.

Chechersky, V., A. Nath, C. Michel, M. Hervieu, K. Ghosh, and R. L. Greene, 2000, Phys. Rev. B **62**, 5316.

Chen, B., A. Rojo, C. Uher, H. Ju, and R. Greene, 1997, Phys. Rev. B **55**, 15471.

Chen, C. H., and S. W. Cheong, 1996, Phys. Rev. B **76**, 4042.

Cheong, S.-W., and C. H. Chen, 1998, Striped charge and orbital ordering in perovskite manganites, in *Colossal Magnetoresistance, Charge Ordering and Related Properties*, edited by B. Raveau and C. N. R. Rao (World Scientific, Singapore).

Cheong, S.-W., and H. Y. Hwang, 2000, Ferromagnetism vs charge/orbital ordering in mixed-valence manganites, in *Colossal Magnetoresistive Oxides*, edited by Y. Tokura (Gordon and Breach, New York).

Chiuchi, S., and F. de Pasquale, 1999, Phys. Rev. B **59**, 5431.

Chun, S., M. Salamon, and P. Han, 1999, J. Appl. Phys. **85**, 5573.

Chun, S., M. Salamon, M. Jaime, R. Suryanarayanan, G. Dhalenne, and A. Recolevschi, 2000, Physica B **284-288**, 1442.

Chun, S., M. Salamon, Y. Lyanda-Geller, P. Goldbart, and P. Han, 2000, Phys. Rev. Lett. **84**, 757.

Chun, S., M. Salamon, Y. Tomioka, and Y. Tokura, 2000, Phys. Rev. B **61**, R9225.

Coey, J., A. Berkowitz, L. Balcells, F. Putris, and A. Barry, 1998, Phys. Rev. Lett. **80**, 3815.

Coey, J., M. Viret, L. Ranno, and K. Ounadjela, 1995, Phys. Rev. Lett. **75**, 3910.

Coey, J., M. Viret, and S. von Molnar, 1999, Adv. Phys. **48**, 167.

Cohn, J., 2000, J. Supercond. **13**, 291.

Cohn, J., J. Neumeier, C. Popoviciu, K. McClellan, and T. Leventouri, 1997, Phys. Rev. B **56**, R8495.

Cooper, S. L., 2001, Struct. Bonding (Berlin) **98**, 161.

Dai, P., J. A. Fernandez-Baca, N. Wakabayashi, E. W. Plummer, Y. Tomioka, and Y. Tokura, 2000, Phys. Rev. Lett. **85**, 2553.

Dai, P., H. Hwang, J. Zhang, J. Fernandez-Baca, S.-W. Cheong, C. Kloc, Y. Tomioka, and Y. Tokura, 2000, Phys. Rev. B **61**, 9553.

de Gennes, P., 1960, Phys. Rev. **118**, 141.

De Teresa, J. M., K. Dorr, K. Muller, L. Schultz, and R. Chakalova, 1998, Phys. Rev. B **58**, R5928.

Emin, D., 1973, in *Electronic Structure Properties of Amorphous Semiconductors*, edited by P. L. Comber and N. Mott (Academic Press, New York).

Emin, D., and T. Holstein, 1969, Ann. Phys. (N.Y.) **53**, 439.

Entin-Wohlman, O., A. G. Aronov, Y. Levinson, and Y. Imry, 1995, Phys. Rev. Lett. **75**, 4094.

Esaki, L., P. Stiles, and S. von Molnár, 1967, Phys. Rev. Lett. **19**, 852.

Fernandez-Baca, J., P. Dai, H. Hwang, C. Kloc, and S. Cheong, 1998, Phys. Rev. Lett. **80**, 4012.

Friedman, L., and T. Holstein, 1963, Ann. Phys. (N.Y.) **21**, 494.

Furukawa, N., 1994, J. Phys. Soc. Jpn. **63**, 3214.

Furukawa, N., 1995a, J. Phys. Soc. Jpn. **64**, 2754.

Furukawa, N., 1995b, J. Phys. Soc. Jpn. **64**, 3164.

Furukawa, N., 2000, J. Phys. Soc. Jpn. **69**, 1954.

Furukawa, N., Y. Y. Shimomura, T. Akimoto, and Y. Moritomo, 2000, cond-mat/0009036.

Ganguly, P., 1984, J. Solid State Chem. **53**, 193.

Ghivelder, L., I. Castillo, N. Alford, G. Tomka, P. Riedi, J. MacManus-Driscoll, A. Hossain, and L. Cohen, 1998, J. Magn. Magn. Mater. **189**, 274.

Ghivelder, L., I. Castillo, M. Gusmao, J. Alonso, and L. Cohen, 1999, Phys. Rev. B **60**, 12184.

Ghosh, K., C. Lobb, R. Greene, S. Karabashev, D. Shulyatev, A. Arsenov, and Y. Mukovskii, 1998, Phys. Rev. Lett. **81**, 4740.

Goodenough, J. B., 1955, Phys. Rev. **100**, 564.

Gordon, J., R. Fisher, X. Jia, N. Phillips, S. Reklis, D. Wright, and A. Zettl, 1999, Phys. Rev. B **59**, 127.

Gor'kov, L. P., 1998, Sov. Phys. Usp. **41**, 589.

Gor'kov, L. P., and V. Z. Kresin, 1998, JETP Lett. **67**, 985.

Gorter, E., 1963, J. Appl. Phys. **34**, 1253.

Griffiths, R. B., 1969, Phys. Rev. Lett. **23**, 17.

Hamilton, J., E. Keatley, H. Ju, A. Raychaudhuri, V. Smolyaninova, and R. Greene, 1996, Phys. Rev. B **54**, 14926.

Hardner, H., M. Weissman, M. Jaime, R. Treece, P. Dorsey, J. Horwitz, and D. Chrisey, 1997, J. Appl. Phys. **81**, 272.

Heffner, R., L. Le, M. Hundley, J. Neumeier, G. Luke, K. Kojima, B. Nachumi, Y. Uemura, D. MacLaughlin, and S.-W. Cheong, 1996, Phys. Rev. Lett. **77**, 1869.

Heffner, R., L. Le, D. MacLaughlin, G. Luke, K. Kojima, B. Nachumi, Y. Uemura, G. Nieuwenhuys, and S.-W. Cheong, 1997, Physica B **230**, 759.

Heffner, R., J. Sonier, D. MacLaughlin, G. Nieuwenhuys, G. Ehlers, F. Mezei, S. Cheong, J. Gardner, and H. Röder, 2000, Phys. Rev. Lett. **85**, 3285.

Heikes, R., 1965, in *Thermoelectricity*, edited by P. Egli (Wiley, New York).

Hejtmanek, J., Z. Jirak, S. Krupicka, C. Martin, C. Simon, A. Maignan, B. Raveau, E. Grivei, and J. Issi, 1997, J. Appl. Phys. **81**, 4975.

Hejtmanek, J., Z. Jirak, M. Marysko, C. Martin, A. Maigan, M. Hervieu, and B. Raveau, 1999, Phys. Rev. B **60**, 14057.

Hillery, M., D. Emin, and N. Liu, 1988, Phys. Rev. B **38**, 9771.

Holstein, T., 1959, Ann. Phys. (N.Y.) **8**, 343.

Holstein, T., 1973, Philos. Mag. **27**, 225.

Hotta, T., S. Yunoki, M. Mayr, and E. Dagotto, 1999, Phys. Rev. B **60**, R15009.

Huang, Q., A. Santoro, J. W. Lynn, R. W. Erwin, J. A. Borchers, J. L. Peng, and R. L. Greene, 1997, Phys. Rev. B **55**, 14987.

Hundley, M., M. Hawley, R. Heffner, Q. Jia, J. Neumeier, J. Tesmer, J. Thompson, and X. Wu, 1995, Appl. Phys. Lett. **67**, 860.

Hundley, M., and J. Neumeier, 1997, Phys. Rev. B **55**, 11511.

Hur, N. H., J. T. Kim, K. H. Yoo, Y. K. Park, and J. C. Park, 1998, Phys. Rev. B **57**, 10740.

Hwang, H., S.-W. Cheong, N. Ong, and B. Batlogg, 1996, Phys. Rev. Lett. **77**, 2041.

Hwang, H., S.-W. Cheong, P. Radaelli, M. Marezio, and B. Batlogg, 1995, Phys. Rev. Lett. **75**, 914.

Ibarra, M., G. Zhao, J. de Teresa, B. Garcia-Landa, B. Arnold, C. Marquina, P. Algarabel, H. Keller, and C. Ritter, 1998, Phys. Rev. B **57**, 7446.

Inoue, J., and S. Maekawa, 1995, Phys. Rev. Lett. **74**, 3407.

Irkhin, V. Y., and M. I. Katsnel'son, 1994, Phys. Usp. **37**, 659.

Jaime, M., H. Hardner, M. Salamon, M. Rubinstein, P. Dorsey, and D. Emin, 1997, Phys. Rev. Lett. **78**, 951.

Jaime, M., P. Lin, S. Chun, and M. Salamon, 1999, Phys. Rev. B **60**, 1028.

Jaime, M., P. Lin, M. Salamon, and P. Han, 1998, Phys. Rev. B **58**, R5901.

Jaime, M., R. Movshovich, G. Stewart, W. Beyermann, M. G. Berisso, M. Hundley, P. Canfield, and J. Sarrao, 2000, Nature (London) **405**, 160.

Jaime, M., and M. Salamon, 1999, Transport properties of Ca manganites, in *Physics of Manganites* (Kluwer Academic/ Plenum Publishers, New York), p. 243.

Jaime, M., M. B. Salamon, K. Pettit, M. Rubinstein, R. Treece, J. Horwitz, and D. Chrisey, 1996, Appl. Phys. Lett. **68**, 1576.

Jaime, M., M. Salamon, M. Rubinstein, R. Trece, J. Horwitz, and D. Chrisey, 1996, Phys. Rev. B **54**, 11914.

Jakob, G., F. Martin, W. Westerburg, and H. Adrian, 1998, Phys. Rev. B **57**, 10252.

Jakob, G., W. Westerburg, F. Martin, and H. Adrian, 1998, Phys. Rev. B **58**, 14966.

Jin, S., M. McCormack, T. Tiefel, and R. Ramesh, 1994, J. Appl. Phys. **76**, 6929.

Jin, S., T. Tiefel, M. McCormack, R. Fastnacht, R. Ramesh, and L. Chen, 1994, Science **264**, 413.

Jonker, G., 1954, Physica (Amsterdam) **20**, 1118.

Jonker, G., 1956, Physica (Amsterdam) **22**, 707.

Jonker, G., and J. van Santen, 1950, Physica (Amsterdam) **16**, 337.

Jonker, G., and J. van Santen, 1953, Physica (Amsterdam) **19**, 120.

Jung, W. H., 2000, J. Mater. Sci. Lett. **19**, 1307.

Kadowaki, K., and S. Woods, 1986, Solid State Commun. **58**, 507.

Kajimoto, R., H. Yoshizawa, H. Kawano, H. Kuwahara, Y. Tokura, K. Ohovama, and M. Ohashi, 1999, Phys. Rev. B **60**, 9506.

Kanamori, J., 1960, J. Appl. Phys. **31**, 145.

Kasuya, T., 1959, Prog. Theor. Phys. **22**, 227.

Kasuya, T., 1970a, Solid State Commun. **8**, 1635.

Kasuya, T., 1970b, in *Proceedings of the Tenth International Conference on the Physics of Semiconductors*, p. 243.

Kasuya, T., and A. Yanase, 1968, Rev. Mod. Phys. **40**, 684.

Kasuya, T., A. Yanase, and T. Takeda, 1970, Solid State Commun. **8**, 1543.

Kawano, H., R. Kajimoto, Y. Yoshizawa, Y. Tomioka, H. Kuwahara, and Y. Tokura, 1997, Phys. Rev. Lett. **78**, 4253.

Kimura, T., R. Kumai, Y. Tokura, J. Q. Li, and Y. Matsue, 1998, Phys. Rev. B **58**, 11081.

Kubo, K., and N. Ohata, 1972, J. Phys. Soc. Jpn. **33**, 21.

Kubota, M., H. Yoshizawa, Y. Moritomo, H. Fujioka, K. Hirota, and Y. Endoh, 1999, J. Phys. Soc. Jpn. **68**, 2202.

Kubota, M., H. Fujioka, K. Ohoyama, K. Hirota, Y. Moritomo, H. Yoshizawa, and Y. Endoh, 1999, J. Phys. Chem. Solids **60**, 1161.

Kuwahara, H., and Y. Tokura, 1998, in *Colossal Magnetoresistance, Charge Ordering and Related Properties of Manganese Oxides*, edited by C. N. R. Rao and B. Raveau (World Scientific, Singapore), p. 217.

Kuwahara, H., Y. Tomioka, A. Asamitsu, Y. Moritomo, and Y. Tokura, 1995, Science **270**, 961.

Lees, M. R., O. Petrenko, G. Balakrishnan, and D. Paul, 1999, Phys. Rev. B **59**, 12298.

Leung, L., A. Morrish, and C. Searle, 1969, Can. J. Phys. **47**, 2697.

Li, J. Q., Y. Matsui, T. Kimura, Y. Moritomo, and Y. Tokura, 1997, in *Electron Microscopy and Analysis Group Conference*, edited by J. M. Rodenburg (Institute of Physics, Institute of Physics Publishing, Bristol, U.K.).

Li, J. Q., M. Uehara, C. Tsuruta, Y. Matsui, and Z. X. Zhao, 1999, Phys. Rev. Lett. **82**, 2386.

Li, X., A. Gupta, G. Xiao, and G. Gong, 1997, Appl. Phys. Lett. **71**, 1124.

Lin, P., S. H. Chun, M. B. Salamon, Y. Tomioka, and Y. Tokura, 2000, J. Appl. Phys. **87**, 5825.

Liu, C. J., C. S. Sheu, and M. S. Huang, 2000, Phys. Rev. B **61**, 14323.

Loktov, V. M., and Y. G. Pogoretov, 2000, Low Temp. Phys. **26**, 171.

Louca, D., and T. Egami, 1999, Phys. Rev. B **59**, 6193.

Louca, D., T. Egami, E. Brosha, H. Röder, and A. Bishop, 1997, Phys. Rev. B **56**, R8475.

Lyanda-Geller, Y., S. H. Chun, P. M. Goldbart, P. D. Han, Y. Tomioka, A. Asamitsu, and Y. Tokura, 2001, Phys. Rev. B **63**, 184426.

Lynn, J., R. Erwin, J. Borchers, Q. Huang, A. Santoro, J. Peng, and Z. Li, 1996, Phys. Rev. Lett. **76**, 4046.

Lynn, J., R. Erwin, J. Borchers, A. Santoro, Q. Huang, J. Peng, and R. Greene, 1997, J. Appl. Phys. **81**, 5488.

Lyuksyutov, I. F., and V. L. Pokrovsky, 1999, Mod. Phys. Lett. B **13**, 379.

Maezono, R., S. Ishihara, and N. Nagaosa, 1998a, Phys. Rev. B **57**, 13993.

Maezono, R., S. Ishihara, and N. Nagaosa, 1998b, Phys. Rev. B **58**, 11583.

Maezono, R., and N. Nagaosa, 2000a, Phys. Rev. B **61**, 1825.

Maezono, R., and N. Nagaosa, 2000b, Phys. Rev. B **62**, 11576.

Mannari, T., 1959, Prog. Theor. Phys. **22**, 325.

Martin, M., G. Shirane, Y. Endoh, K. Hirota, Y. Moritomo, and Y. Tokura, 1996, Phys. Rev. B **53**, 14285.

Matl, P., N. P. Ong, Y. Yan, Y. Li, D. Studebaker, T. Baum, and G. Doubinira, 1998, Phys. Rev. B **57**, 10248.

Matsukawa, M., R. Sato, H. Ogasawara, M. Yoshizawa, R. Suryanarayanan, G. Dhalenne, A. Revcolevschi, and K. Itoh, 2000, Physica B **281-282**, 505.

Mattis, D., 1981, *The Theory of Magnetism* (Springer, Heidelberg).

Mayr, M., A. Moreo, J. A. Vargas, J. Arispe, A. Geiguin, and E. Dagotto, 2001, Phys. Rev. Lett. **86**, 135.

McCormack, M., S. Jin, T. Tiefel, R. Fleming, J. Phillips, and R. Ramesh, 1994, Appl. Phys. Lett. **64**, 3045.

Merithew, R., M. Weissman, F. Hess, P. Spradling, E. Nowak, J. ODonnell, J. Eckstein, Y. Tokura, and Y. Tomioka, 2000, Phys. Rev. Lett. **84**, 3442.

Millis, A., P. Littlewood, and B. I. Shraiman, 1995, Phys. Rev. Lett. **74**, 5144.

Millis, A., B. Shraiman, and R. Mueller, 1996, Phys. Rev. Lett. **77**, 175.

Millis, A. J., R. Mueller, and B. I. Shraiman, 1996, Phys. Rev. B **54**, 5405.

Mishra, S. K., S. Satpathy, F. Aryasetiawan, and O. Gunnersson, 1997, Phys. Rev. B **55**, 2725.

Mishra, S. K., R. Pandit, and S. Satpathy, 1997, Phys. Rev. B **56**, 2316.

Mohan, C. V., M. Seeger, H. Kronmuller, P. Murugarag, and J. Maier, 1998, J. Magn. Magn. Mater. **183**, 348.

Moreo, A., M. Mayr, A. Geiguin, S. Yunoki, and E. Dagotto, 2000, Phys. Rev. Lett. **84**, 5568.

Moreo, A., S. Yunoki, and E. Dagotto, 1999, Science **283**, 2034.

Moritomo, Y., A. Asamitsu, H. Kuwahara, and Y. Tokura, 1996, Nature (London) **380**, 141.

Moritomo, Y., A. Nakamura, K. Ohoyama, M. Ohashi, and K. Hirota, 1999, J. Phys. Soc. Jpn. **68**, 631.

Moritomo, Y., Y. Tomioka, A. Asamitsu, Y. Tokura, and Y. Matsui, 1995, Phys. Rev. B **51**, 3297.

Morrish, A., B. Evans, J. Eaton, and L. Leung, 1969, Can. J. Phys. **47**, 2691.

Mott, N., and E. Davis, 1971, *Electronic Processes in Non-Crystalline Materials* (Clarendon Press, Oxford).

Murakami, Y., J. P. Hill, D. Gibbs, M. Blume, I. Koyama, M. Tanaka, H. Kawata, T. Arima, Y. Tokura, K. Hirota, and Y. Endoh, 1998, Phys. Rev. Lett. **81**, 582.

Murakami, Y., H. Kawada, H. Kawata, M. Tanaka, T. Arima, Y. Moritomo, and Y. Tokura, 1998, Phys. Rev. Lett. **80**, 1932.

Nagel, S., 1977, Phys. Rev. B **16**, 1694.

Nagels, P., 1980, in *The Hall Effect and its Applications*, edited by C. Chien and C. Westgate (Plenum, New York), p. 253.

Ohtaki, M., H. Koga, T. Tokunaga, K. Eguchi, and H. Arai, 1995, J. Solid State Chem. **120**, 105.

Okuda, T., A. Asamitsu, Y. Tomioka, T. Kimura, Y. Taguchi, and Y. Tokura, 1998, Phys. Rev. Lett. **81**, 3203.

Okuda, T., T. Kimura, H. Kuwahara, Y. Tomioka, A. Asamitsu, Y. Okimoto, E. Saito, and Y. Tokura, 1999, Mater. Sci. Eng., B **B56**, 186.

Okuda, T., T. Kimura, and Y. Tokura, 1999, Phys. Rev. B **60**, 3370.

Oretzki, M., and P. Gaunt, 1970, Can. J. Phys. **48**, 346.

Palstra, T., A. Ramirez, S.-W. Cheong, B. Zegarski, P. Schiffer, and J. Zaanen, 1997, Phys. Rev. B **56**, 5104.

Park, J.-H., E. Vescovo, H. Kim, C. Kwon, R. Ramesh, and T. Venkatesan, 1998, Nature (London) **392**, 794.

Park, S. H., Y.-H. Jeong, and K.-B. Lee, 1993, Phys. Rev. B **56**, 67.

Peacor, S., J. Cohn, and C. Uher, 1991, Phys. Rev. B **43**, 8721.

Penney, T., M. Shafter, and J. Torrance, 1972, Phys. Rev. B **5**, 3669.

Pickett, W., and D. Singh, 1996, Phys. Rev. B **53**, 1146.

Pickett, W., and D. Singh, 1997, Phys. Rev. B **55**, R8642.

Pickett, W. E., and D. J. Singh, 1997, J. Magn. Magn. Mater. **172**, 237.

Podzorov, V., M. Uehara, M. E. Gershenson, T. Y. Koo, and S.-W. Cheong, 2000, Phys. Rev. B **61**, 3784.

Popovic, Z., and S. Satpathy, 2000, Phys. Rev. Lett. **84**, 1603.

Radaelli, P. G., D. E. Cox, L. Capogna, S.-W. Cheong, and M. Marezio, 1999, Phys. Rev. B **59**, 14440.

Rajeswari, M., R. Shreekala, A. Goyal, S. E. Lofland, S. M. Bhagat, K. Ghosh, R. P. Sharma, R. L. Greene, R. Ramesh, and T. Venkatesan, 1998, Appl. Phys. Lett. **73**, 2672.

Ramesh, R., S. B. Ogale, M. Rajeswari, R. L. Greene, and T. Venkatesan, 1998, in *Colossal Magnetoresistance, Charge Or-*

dering and Related Properties of Manganese Oxides, edited by C. N. R. Rao and R. Raveau (World Scientific, Singapore), p. 155.

Ramirez, A., 1997, J. Phys.: Condens. Matter **9**, 8171.

Rao, C., A. Arulraj, A. Cheetham, and B. Raveau, 2000, J. Phys.: Condens. Matter **12**, R83.

Rao, C. N. R., and B. Raveau, 1998, Eds., *Colossal Magnetoresistance, Charge Ordering and Related Properties of Manganese Oxides* (World Scientific, Singapore).

Raquet, B., A. Anane, S. Wirth, P. Xiong, and S. von Molnar, 2000, Phys. Rev. Lett. **84**, 4485.

Raychaudhuri, P., C. Mitra, A. Paramekanti, R. Pinto, A. K. Nigam, and S. K. Dhar, 1998, J. Phys. Condens. Matter **10**, L191.

Reinen, D., 1979, J. Solid State Chem. **27**, 71.

Röder, H., J. Zang, and A. Bishop, 1996, Phys. Rev. Lett. **76**, 1356.

Ruddlesden, S., and P. Popper, 1958, Acta Crystallogr. **11**, 541.

Satpathy, S., Z. Popovic, and F. R. Vukajlovic, 1996, Phys. Rev. Lett. **76**, 960.

Satpathy, S., Z. S. Popovic, and F. R. Vukajlovic, 1996, J. Appl. Phys. **79**, 4555.

Schiffer, P., A. Ramirez, W. Bao, and S.-W. Cheong, 1995, Phys. Rev. Lett. **75**, 3336.

Schwartz, A., M. Scheffer, and S. M. Anlage, 2000, Phys. Rev. B **61**, R870.

Searle, C., and S. Wang, 1969, Can. J. Phys. **47**, 2703.

Shen, S.-Q., and Z. D. Wang, 1999, Phys. Rev. B **59**, 14484.

Singh, D., and W. Pickett, 1998, Phys. Rev. B **57**, 88.

Smolyaninova, V. N., A. Biswas, X. Zhang, K. H. Kim, B-G. Kim, S-W. Cheong, and R. L. Greene, 2000, Phys. Rev. B **62**, R6093.

Smolyaninova, V., J. Hamilton, R. Green, Y. Mukovskii, S. Karabashev, and A. Balbashov, 1997, Phys. Rev. B **55**, 5640.

Snyder, G., R. Hiskes, S. Dicarolis, M. Beasley, and T. Geballe, 1996, Phys. Rev. B **53**, 14434.

Sternlieb, B. J., J. P. Hill, U. C. Wildgruber, G. M. Luke, B. Nachumi, Y. Moritomo, and Y. Tokura, 1996, Phys. Rev. Lett. **76**, 2169.

Takata, M., E. Nishibori, K. Kato, M. Sakata, and Y. Moritomo, 1999, J. Phys. Soc. Jpn. **68**, 2190.

Tanaka, J., M. Umehara, S. Tamura, M. Tsukioka, and S. Ehara, 1982, J. Phys. Soc. Jpn. **51**, 1236.

Tath, M., S. Reisem, A. A. Menovsky, Y. Tomioka, J. Aarts, and J. A. Mydosh, 1999, Science **285**, 1540.

Tokunaga, M., N. Miura, Y. Tomioka, and Y. Tokura, 1998, Phys. Rev. B **57**, 5259.

Tokura, Y., 2000, Ed., *Colossal Magnetoresistive Oxides* (Gordon and Breach, New York).

Tokura, Y., H. Kuwahara, Y. Moritomo, Y. Tomioka, and A. Asamitsu, 1996, Phys. Rev. Lett. **76**, 3184.

Tokura, Y., and N. Nagaosa, 2000, Science **288**, 462.

Tokura, Y., and Y. Tomioka, 1999, J. Magn. Magn. Mater. **200**, 1.

Tokura, Y., A. Urushibara, Y. Moritomo, T. Arima, A. Asamitsu, G. Kido, and N. Furukawa, 1994, J. Phys. Soc. Jpn. **63**, 3931.

Tomioka, Y., A. Asamitsu, H. Kuwahara, Y. Moritomo, R. Kumai, and Y. Tokura, 1997, Physica B **237−238**, 6.

Tomioka, Y., A. Asamitsu, H. Kuwahara, Y. Moritomo, and Y. Tokura, 1996, Phys. Rev. B **53**, R1689.

Tomioka, Y., A. Asamitsu, Y. Moritomo, H. Kuwahara, and Y. Tokura, 1995, Phys. Rev. Lett. **74**, 5108.

Uehara, M., S. Mori, C. H. Chen, and S.-W. Cheong, 1999, Nature (London) **399**, 560.

Urushibara, A., Y. Moritomo, T. Arima, A. Asamitsu, G. Kido, and Y. Tokura, 1995, Phys. Rev. B **51**, 14103.

van Santen, J. H., and G. Jonker, 1950, Physica (Amsterdam) **16**, 599.

van Veenendaal, M., and A. J. Fedro, 1999, Phys. Rev. B **59**, 15056.

Varma, C., 1996, Phys. Rev. B **54**, 7328.

Vasiliu-Doloc, L., J. Lynn, Y. Mukovskii, A. Arsenov, and D. Shulyatev, 1998, J. Appl. Phys. **83**, 7342.

Verwey, E., P. Haaijman, F. Romeijn, and G. van Oosterhout, 1950, Philips Res. Rep. **5**, 173.

Visser, D., A. Ramirez, and M. Subramanian, 1997, Phys. Rev. Lett. **78**, 3947.

Volger, J., 1954, Physica (Amsterdam) **20**, 49.

von Molnar, S., and T. Kasuya, 1968, Phys. Rev. Lett. **21**, 1757.

Watts, S. M., 2000, private communication.

Watts, S. M., S. Wirth, S. von Molnar, A. Barry, and J. Coey, 2000, Phys. Rev. B **61**, 9621.

Wollan, E., and K. Koehler, 1955, Phys. Rev. **100**, 545.

Woodfield, B., M. Wilson, and J. Byers, 1997, Phys. Rev. Lett. **78**, 3201.

Worledge, D., L. Miéville, and T. Geballe, 1998, Phys. Rev. B **57**, 15267.

Worledge, D., G. Snyder, M. Beasley, and T. Geballe, 1996, J. Appl. Phys. **80**, 5158.

Yakel, H. L., 1955, Acta Crystallogr. **8**, 394.

Ye, J., Y. B. Kim, A. J. Millis, B. I. Shraiman, P. Majumdar, and Z. Tesanovic, 1999, Phys. Rev. Lett. **83**, 3737.

Yoon, S., H. Liu, G. Schollere, S. Cooper, P. Han, D. Payne, S. Cheong, and Z. Fisk, 1998, Phys. Rev. B **58**, 2795.

Yunoki, S., J. Hu, A. L. Malvezzi, A. Moreo, N. Furukawa, and E. Dagotto, 1998, Phys. Rev. Lett. **80**, 845.

Yunoki, S., A. Moreo, and E. Dagotto, 1998, Phys. Rev. Lett. **81**, 5612.

Zener, C., 1951, Phys. Rev. **2**, 403.

Zhao, G., K. Conder, H. Keller, and K. Müller, 1996, Nature (London) **381**, 676.

Zhao, G., V. Smolyaninova, W. Prellier, and H. Keller, 2000, Phys. Rev. Lett. **84**, 6086.

Zhao, J. H., H.-P. Kunkel, X. Z. Zhou, G. Williams, and M. A. Subramanian, 1999, Phys. Rev. Lett. **83**, 219.

Zhou, J. S., J. B. Goodenough, and J. F. Mitchell, 1998, Phys. Rev. B **58**, R579.

Ziese, M., and C. Srinitiwarawong, 1998, Phys. Rev. B **58**, 11519.

Zuo, J. M., and J. Tao, 2001, Phys. Rev. B **63**, 060407.